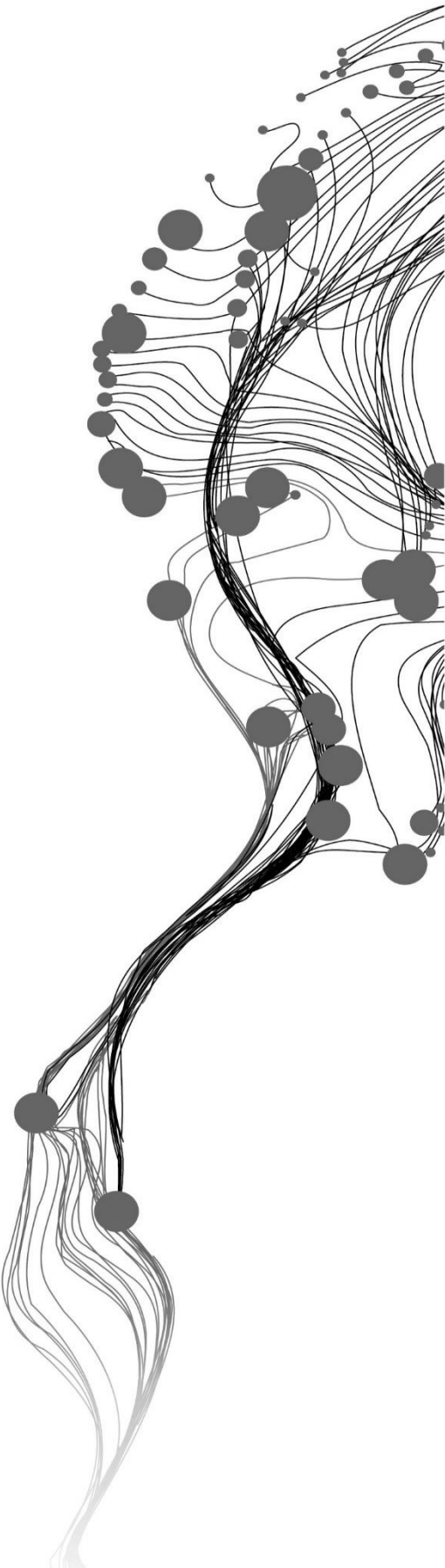


**INTERGRATING SENTINEL-2  
DERIVED VEGETATION INDICES  
AND TERRESTRIAL LASER  
SCANNER TO ESTIMATE ABOVE-  
GROUND BIOMASS/CARBON IN  
AYER HITAM TROPICAL FOREST  
MALAYSIA.**

MARIAM SALIM ADAN  
February, 2017

SUPERVISORS:  
Dr. Yousif A. Hussin  
Drs. E. H. Kloosterman



**INTERGRATING SENTINEL-2  
DERIVED VEGETATION INDICES  
AND TERRESTRIAL LASER  
SCANNER TO ESTIMATE ABOVE-  
GROUND BIOMASS/CARBON IN  
AYER HITAM TROPICAL FOREST  
MALAYSIA.**

MARIAM SALIM ADAN

Enschede, The Netherlands, February, 2017

Thesis submitted to the Faculty of Geo-Information Science and Earth Observation of the University of Twente in partial fulfilment of the requirements for the degree of Master of Science in Geo-information Science and Earth Observation.  
Specialization: Natural Resources Management

**SUPERVISORS:**

Dr. Yousif A. Hussin

Drs. E. H. Kloosterman

**THESIS ASSESSMENT BOARD:**

Dr. A. G. Toxopeus (Chair)

Dr. T. Kauranne (External Examiner, LUT school of Engineering Science, Finland)

#### DISCLAIMER

This document describes work undertaken as part of a programme of study at the Faculty of Geo-Information Science and Earth Observation of the University of Twente. All views and opinions expressed therein remain the sole responsibility of the author, and do not necessarily represent those of the Faculty.

## ABSTRACT

Carbon dioxide (CO<sub>2</sub>) emission together with other greenhouse gases has been increasing at a fast rate in recent years leading to global warming which has caused an upsurge in natural disasters. The solution to this problem is to conserve or protect tropical rainforest since they store up to 40% of terrestrial carbon. However, they are being depleted at a faster rate due to increase in anthropogenic activities. Thus, REDD+ came up with an initiative to reduce emissions from deforestation through carbon accounting, in which the developing countries Measure, Report and Verify (MRV) the amount of Above Ground Biomass (AGB)/carbon stored in a particular forest. Nonetheless, the major challenge for REDD+ is to find an accurate method for biomass estimation. Thus, this study managed to assess the potential of Vegetation Indices (VIs) derived from Sentinel-2 medium resolution images in estimating AGB. By studying the relationship between VIs and AGB including both upper canopy and total biomass (Combined upper and lower canopy biomass). The canopy separation was considered necessary, since Ayer Hitam tropical rain forest has a multi-layer forest structure which makes the extraction of accurate height measurement difficult. An allometric equation was applied by using field DBH and ALS height for the upper canopy biomass while TLS height and DBH were used for the lower canopy biomass. ALS height was preferred to the field height since it was more accurate. Furthermore, the upper and lower canopy biomass were combined to obtain a total biomass of 182 Mg and a carbon stock of 85Mg per plot. For this study seven VIs were selected. They were categorized into: canopy water content (NDWI and NDII), narrow red-edge (RERVI, RENDVI, and RE-EVI2), and broadband VIs (NDVI and EVI2). The study assessed the relationship between the VIs and upper canopy and total biomass using both linear and exponential regression models. The best VI model for the upper canopy biomass was combined with TLS lower canopy biomass. The study findings revealed that an exponential model best explains the relationship between VIs and AGB, since it had a higher  $r^2$  (of 0.66, 0.66, 0.63, 0.32, 0.26, 0.15 and 0.11 for RERVI, RE-EVI, NDWI, NDII, EVI2 and NDVI respectively) and a low Root Mean Square Error (RMSE) compared to a linear model ( $r^2$  of 0.63, 0.62, 0.59, 0.31, 0.23, 0.15 and 0.1 of the same VIs). The study also, revealed that there was insignificant variation in the performance of relationship between VIs with upper canopy and total biomass. However, the best model was obtained from total biomass estimated by combining upper canopy biomass estimated from VIs and the TLS biomass obtaining an  $r^2$  of 0.74 with a RMSE of 0.161 Mg. Moreover, all the models were significant at 95% confidence level, since all P-values were  $< 0.05$ . The red-edge VIs have a better relationship with AGB compared to the broadband and canopy water content VIs, while the broadband VIs had the poorest relationship with AGB due to saturation. Thus, the study suggests the use of the red-edge VIs in reducing saturation. Furthermore, the combination VIs and TLS improves the accuracy of AGB estimation.

**Keywords:** Vegetation Indices, Terrestrial Laser Scanner, Airborne Lidar, Red-edge, forest biomass.

## ACKNOWLEDGEMENTS

I give thanks to the faculty of geo-information science and earth observation (ITC), for giving me an opportunity to partake the MSc programme, since I have been able to acquire skills and knowledge that will have an impact on my career. A special thanks goes to my first supervisor Dr.Yousif Ali Hussin for his advice and continuous support, feedback and comments throughout my research period. Also, I am very grateful to my second supervisor Drs. E.Henk Kloosterman for his dedication and assistance throughout my research period, especially during field work, as we worked together in Ayer Hitam tropical rain forest.

I would like to thank Drs.RG.Nijmeijer, NRM course director for coordinating the course work from the beginning of my MSc programme to my thesis defence. He always made everything ran smoothly, am also grateful for the support he gave whenever we faced some challenges.

Also am, very grateful to the University Putra Malaysia (UPM) for their assistance and support during the field work. The staff including D.r Mohd. Hasmadi, Mr. Mohd Neam, Mr. Fazli Shariff, Mrs. Siti Zurina Zakari, Mr. Rizal and Mr.Mohd Fakhrollah played a huge role that made the completion of the fieldwork possible. They provided us with logistical and technical support, guiding us through the forest to identify suitable plots, clearing the forest to reduce occlusion and also identifying the tree species.

My sincere gratitude goes to my colleagues, Mr. John Hongoa, Mr. Muluken Nega, Mr. Yuvenal Pantaleo and Mr. Solomon Mulat for their cooperation, as we exchanged ideas in some aspects of my research, and, their dedication as we worked together during the field work. I would also like to thank Mr. Muluken Nega for assisting me with ALS height data. Moreover, I would like to thank Mr.Yvenal and Mr. John Hongoa for providing me with the UAV images.

Lastly, my deepest gratitude goes to my parent Salim Adan and Amina Hassan for always believing in me and providing me with the moral and financial support for me to achieve my dreams, I just can't thank them enough. Also, my heartfelt appreciation goes to the rest of my family and friends for putting me in their prayers.

Mariam Salim Adan  
Enschede, The Netherlands  
February 2017

# TABLE OF CONTENTS

---

List of figures .....	vii
List of tables .....	viii
List of Equations .....	i
List of Appendices.....	ii
List of Acronyms .....	iii
1. INTRODUCTION.....	1
1.1. Background.....	1
1.2. Problem statement .....	2
1.3. Research objectives .....	4
1.3.1. Main objective .....	4
1.3.2. Specific Objectives.....	4
1.3.3. Research Questions. ....	4
1.3.4. Hypothesis or anticipated results. ....	4
2. LITERATURE REVIEW.....	5
2.1. Tropical Rainforest.....	5
2.2. Biomass and Carbon .....	5
2.3. Overview of Terrestrial Laser Scanner .....	6
2.4. Sentinel-2 Optical Satellite image. ....	7
2.5. Vegetation Indices for biomass estimation.....	8
2.6. Integration of Remote Sensing Methods for biomass Estimation. ....	9
2.7. Allometric Equation.....	9
3. MATERIALS AND METHODS .....	10
3.1. Study Area.....	10
3.1.1. Geographic Location.....	10
3.1.2. Climate and Topography .....	10
3.1.3. Vegetation and Structure .....	10
3.2. Materials .....	11
3.2.1. Field instruments/images/Airborne laser scanner (ALS) height data. ....	11
3.2.2. Software and tools .....	11
3.3. Methods .....	11
3.3.1. Pre-field work .....	13
3.3.2. Plot size.....	13
3.3.3. Sampling-design .....	13
3.4. Data collection .....	14
3.4.1. Demarcation of the circular plot .....	14
3.4.2. Biometric Data collection .....	14
3.4.3. TLS data Collection.....	15
3.4.4. Sentinel-2 Image acquisition .....	16
3.5. Data Processing .....	16
3.5.1. TLS data processing .....	16
3.5.2. Processing/ radiometric correction of Sentinel-2 image.....	17
3.5.3. Deriving Vegetation Indices (VIs) from Sentinel-2 optical satellite image.....	18
3.5.4. Canopy separation. ....	20
3.5.5. Removal of outliers.....	20
3.6. Calculation of AGB and Carbon stock estimation .....	21
3.7. Statistical Analysis.....	22

4.	RESULTS .....	23
4.1.	Calculation of Vegetation Indices (VIs) .....	23
4.2.	Above ground biomass estimation (AGB) .....	24
4.2.1.	Upper canopy Biomass .....	24
4.2.2.	Lower canopy biomass .....	25
4.2.3.	Summary of the lower and upper canopy biomass .....	25
4.2.4.	Carbon stock estimation.....	26
4.3.	Statistical Analysis.....	26
4.3.1.	Linear relationship between upper canopy biomass and vegetation Indices.....	26
4.3.2.	Exponential relationship between VIs and upper canopy biomass.....	32
4.3.3.	Exponential relationship between VIs and total biomass.....	35
4.3.4.	Summary of the linear relationship and Exponential relationship with upper canopy biomass. .....	37
4.3.5.	Summary of the linear relationship and Exponential relationship and total biomass .....	37
4.3.6.	Combination of VIs with TLS.....	38
5.	DISCUSSION .....	39
5.1.	Above Ground Biomass Estimation.....	39
5.2.	Linear and exponential relationship between VIs and AGB. ....	41
5.3.	Relationship between VIs and AGB.....	42
5.3.1.	Relationship between Narrow red-edge VIs and AGB.....	42
5.3.2.	Relationship between canopy water content VIs and AGB .....	44
5.3.3.	Relationship between broadband VIs and AGB .....	44
5.4.	The combination of VIs with TLS.....	44
5.5.	Relevance of the Research for REDD+ .....	45
5.6.	Limitations of the study. ....	45
6.	CONCLUSION AND RECOMMENDATION .....	46
6.1.	Conclusion .....	46
6.2.	Recommendation .....	46
	LIST OF REFERENCES .....	47
	APPENDICES.....	54

# LIST OF FIGURES

---

Figure 2.1: Tropical Rainforest Structure .....	5
Figure 2.2: RIEGL V2- 400 TLS with its main feature.....	6
Figure 2.3: An example of how TLS sends and receives laser pulse.....	7
Figure 2.4: Comparison of Landsat 7 and 8 bands with Sentinel-2 sensors .....	8
Figure 3.1: Location of the study area.....	10
Figure 3.2: Flow chart of the research method.....	12
Figure 3.3: Circular plot of 500m <sup>2</sup> .....	13
Figure 3.4: Tagged sample trees .....	14
Figure 3.5: circular retroreflectors (1) and cylindrical retroreflectors (2).....	15
Figure 3.6: Multiple Scanning Positions.....	15
Figure 3.7: Sentinel-2 Multispectral image.....	16
Figure 3.8:a) DBH Measurement and b) Height Measurement using RiSCANPRO software .....	17
Figure 3.9: Comparison between the 15m (a) and the 10m (b) spatial resolution within the circular plot..	18
Figure 3.10: Pixels that were considered to be outliers .....	21
Figure 4.1: Three categories of VIs; Narrow red-edge, canopy water content and broad band VIs .....	23
Figure 4.2: Scatter plot a b and c for the relationship between Narrow Red-edge vegetation indices and upper canopy biomass. ....	27
Figure 4.3: Scatter plot a b and c for the relationship between Narrow Red-edge vegetation indices and total biomass.....	28
Figure 4.4: Scatter plot a, b showing the relationship between canopy water content VIs and upper canopy biomass.....	29
Figure 4.5: Scatter plot showing the relationship between canopy water content indices and total biomass .....	30
Figure 4.6: Scatter plot (a, b) showing the relationship between broad band indices and total biomass. ....	32
Figure 4.7: Scatter plot a b and c showing the exponential relationship between Narrow Red-edge vegetation indices and upper canopy biomass.....	33
Figure 4.8: Scatter plot a, b showing exponential relationship between canopy water content vegetation indices and upper canopy biomass. ....	34
Figure 4.9: Scatter plot a , b showing exponential relationship between broad band vegetation indices and upper canopy biomass. ....	34
Figure 4.10: Scatter plot a, b showing the exponential relationship between Narrow-edge vegetation indices and total biomass.....	35
Figure 4.11: Scatter plots a, b showing the exponential relationship between canopy water content indices and total biomass. ....	36
Figure 4.12: Scatter plots a, b showing exponential relationship between broadband indices and total biomass.....	36
Figure 4.13: Scatter plot showing the relationship between Predicted AGB combined VIs (upper canopy) and TLS (lower canopy) and Estimated AGB combined ALS (upper canopy) and TLS (lower canopy) in Mg per 10m pixel size. ....	38
Figure 5.1: Airborne Lidar and Terrestrial laser scanner data acquisition. ....	39
Figure 5.2: Comparison between upper and lower canopy average DBH per plot.....	40
Figure 5.3: Comparison between upper and lower canopy average height per plot.....	41
Figure 5.4: Comparison between upper and lower canopy biomass per plot.....	41
Figure 5.5: comparison between linear and exponential model: RERVI and AGB.....	42
Figure 5.6: The position of the Red-edge along the electromagnetic spectrum.....	43

# LIST OF TABLES

---

Table 2.1: Sentinel-2 spectral bands with its resolution.....	7
Table 3.1: the list of the field equipment and image with their purpose.....	11
Table 3.2: Software and tools for processing and analysis .....	11
Table 4.1: Descriptive statistics of upper canopy biomass .....	24
Table 4.2: Descriptive statistics of lower canopy biomass .....	25
Table 4.3: Descriptive statistic of lower and upper canopy Biomass.....	26
Table 4.4: Descriptive statistics of lower and upper canopy carbon stock.....	26
Table 4.5 : Regression statistics summary; Narrow Red-edge VIs and upper canopy biomass. ....	27
Table 4.6: Regression statistics summary; Narrow Red-edge VIs and total biomass.....	29
Table 4.7: Regression statistics summary; canopy water content VIs and upper canopy biomass. ....	30
Table 4.8: Regression statistics summary; canopy water content VIs and total biomass .....	30
Table 4.9: Regression statistics summary; Broad band VIs and upper canopy biomass .....	31
Table 4.10: Regression statistics summary; Broad band VIs and total biomass.....	32
Table 4.11: Comparison between linear and exponential relationship; VIs and upper canopy biomass.....	37
Table 4.12: Comparison between linear and exponential relationship; VIs and total biomass .....	37
Table 4.13: Regression statistics summary; Total biomass (VIs and TLS) and total biomass (ALS and TLS) .....	38

# LIST OF EQUATIONS

---

Equation 3-1: NDVI formula .....	18
Equation 3-2: EVI2 Formula.....	18
Equation 3-3: RERVI formula .....	19
Equation 3-4: RENDVI formula .....	19
Equation 3-5: RE-EVI2 formula.....	19
Equation 3-6: NDII formula.....	20
Equation 3-7: NDWI formula .....	20
Equation 3-8: AGB Allometric equation.....	21
Equation 3-9: Conversion of AGB to carbon stock .....	22
Equation 3-10: RMSE formula.....	22

# LIST OF APPENDICES

---

Appendix 1: Regression statistics summary; RE-EVI and upper canopy biomass .....	54
Appendix 2: Regression statistics summary; RERVI and upper canopy biomass.....	54
Appendix 3: Regression statistics summary; RENDVI and upper canopy biomass. ....	55
Appendix 5: Regression statistics summary; RE-EVI2 and total biomass. ....	55
Appendix 6: Regression statistics summary; RERVI and total biomass.....	56
Appendix 4: Regression statistics summary; RENDVI and total biomass.....	56
Appendix 7: Regression statistics summary; NDWI and upper canopy biomass .....	57
Appendix 8: Regression statistics summary; NDII and upper canopy biomass.....	57
Appendix 9: Regression statistics summary; NDWI and total biomass.....	58
Appendix 10: Regression statistics summary; NDII and total biomass .....	58
Appendix 11: Regression statistics summary, EVI2 and upper canopy biomass .....	59
Appendix 12: Regression statistics summary, NDVI and upper canopy biomass .....	59
Appendix 13: Regression statistics summary, EVI2 total biomass .....	60
Appendix 14: Regression statistics summary, NDVI and total biomass .....	60
Appendix 15: Downloading site of Sentinel-2 satellite image .....	61
Appendix 16: Sample plots analysed in the study area .....	62
Appendix 17: Airborne Lidar DTM and the drainage pattern .....	63

# LIST OF ACRONYMS

---

AGB	Above Ground Biomass
AHTRF	Ayer Hitam Tropical Rain Forest
ALS	Airborne Laser Scanner
ASTER	Advance Space borne Thermal Emission and Reflection Radiometer
BGB	Below Ground Biomass
CO <sub>2</sub>	Carbon dioxide
CPA	Crown Projection Area
DBH	Diameter at breast Height
ESA	European Space Agency
EVI2	Enhanced Vegetation Index 2
GHG	Green House Gases
IPCC	Intergovernmental panel on Climate change
IRECI	Inverted Red-edge Chlorophyll Index
LIDAR	Light Detection and Ranging
MRV	Measurement Reporting and Verification
ND57	Normalized Difference 57
NDII	Normalized Difference Infra-red Index
NDVI	Normalized Difference Vegetation Index
NDWI	Normalized Difference Vegetation Index
RDVI	Renormalized Difference Vegetation Index
REDD+	Reduction of Emissions from Degradation and Deforestation
RE-EVI2	Red-edge Enhanced Vegetation Index 2
RERVI	Red-edge Ratio Vegetation Index
RMSE	Root Mean Square Error
RVI	Ratio Vegetation Index
TLS	Terrestrial Laser Scanner
UNFCCC	United Nations Convention on Climate Change
UTM	Universal Transverse Agency
VHRI	Very High Resolution Image
VI <sub>s</sub>	Vegetation Indices



# 1. INTRODUCTION

## 1.1. Background

Climate change is one of the major problems that the world is facing currently. The main contributor to this phenomenon is land use changes due to an increase in anthropogenic activities such as deforestation, burning of fossil fuel and industrial expansion, among others. This results in high levels of carbon dioxide (CO<sub>2</sub>) in the atmosphere along with other Green House Gases (GHG) that trap the thermal energy and lead to global warming. This global warming phenomenon causes climate change and consequently results in natural disasters like earthquakes, floods, drought, high temperatures, wildfires and so on (NASA, 2016). In order to mitigate these effects, we need to conserve our natural resources most especially forests.

Forests play an important role in the reduction of CO<sub>2</sub> in the atmosphere (Alkama & Cescatti, 2016). In particular, tropical rainforests have a positive contribution to the global carbon cycle as they store about 40% of the world's terrestrial carbon (Mauya et al., 2015). However, despite their significance, they are being cleared at a fast rate, leading to 12-20% of the overall anthropogenic CO<sub>2</sub> emissions (Collins, 2015). Thus, an initiative was launched under the United Nations Framework Convention on Climate change (UNFCCC), where developing countries will be able to gain financially if they reduce emissions from human activities under the Reduction of Emissions from Degradation and Deforestation program (REDD+). The main objective of REDD+ Measurement Reporting and Verification (MRV), is to monitor and assess the amount of above-ground biomass/carbon stock and subsequently the carbon that has been emitted (Mermoz et al., 2015).

The greatest carbon pool of a tree is the Above-Ground Biomass (AGB), but this is mainly affected by anthropogenic activities in the forest that cause degradation by decreasing the forest areas ultimately affecting the carbon stock and the sequestration of carbon dioxide from the atmosphere. Therefore, estimation of biomass/carbon is vital in monitoring the amount of carbon fluxes (Vashum & Jayakumar, 2012). This will give more insight on the importance of forest ecosystem in reducing the impact of climate change. Hence, there is a need to use a reliable method for biomass estimation.

The methods used to estimate biomass include, a traditional approach which is a destructive way of estimating AGB since it involves cutting down of the trees. Although this method has low uncertainty, it is quite costly and time consuming since it requires a comprehensive field work. The other method is the use of a remote sensing technique which is non-destructive (Kumar et al., 2015). These methods measure and estimate forest inventory parameters such as Diameter at Breast Height (DBH), height, Crown Projection Area (CPA) which are then used in an allometric equation to estimate the forest biomass.

Remote sensing data has been one of the most commonly used methods in the past decade. Recently, the use of optical Very High Resolution Satellite (VHRS) images such as Geo-eye, to extract forest inventory parameters is becoming more common (Baral, 2011). Moreover, according to Phua et al. (2014), there is a strong positive correlation between satellite based crown area and field measured DBH. However, shadow

effects is a huge challenge with VHRS imagery since it affects the tree crown segmentation accuracy (Tsendbazar, 2011). Also, the use of active remote sensing approaches such as Light Detection and Ranging (LIDAR) is becoming prominent. LIDAR systems fixed on an aircraft are known as Airborne Laser Scanners (ALS) while ground based systems are referred to as Terrestrial Laser Scanners (TLS). ALS have high spatial resolution and high positional accuracy in obtaining information about the forest structure, its height measurement is known to be highly accurate (Maltamo et al., 2014). However, the measurement of lower canopy tree height using ALS tends to have errors when there is high tree density which causes crown edge overlapping with nearby trees (Jung et al., 2011). Even though, both VHRS and LIDAR are promising methods of biomass estimation, they are expensive and cover a small area. Thus, limiting future monitoring of the forest ecosystem (Kumar et al., 2015).

Nonetheless, the use of optical medium resolution satellite images provides a cost effective way in predicting AGB. It covers a large area, thus, it can be used for mapping at a regional scale (Kumar et al., 2015). Moreover, medium resolution images are suitable for forest monitoring due to its availability, high temporal and spectral characteristic. Images such as Landsat, ASTER, and SPOT have been used to estimate AGB by extracting Vegetation Indices (VIs) from the images and assessing its relationship with AGB using statistical techniques. Silleos et al., (2006) demonstrated that VIs are also useful in reducing atmospheric effects, soil-back ground, and sun-view angle of the optical satellite image . Furthermore, VIs have the ability to “minimize the effects of spectral noise on the relationship between reflectance and vegetation characteristics of interest compared to raw satellite images”(Das & Singh, 2016). Thus, there is a need to do more studies on the ability of VIs derived from medium-resolution optical satellite images in estimating forest biomass, especially the recently launched Sentinel-2 satellite image. Limited research has been done on the relationship between Sentinel-2 derived VIs and forest biomass in tropical forest.

## **1.2. Problem statement**

The major challenge for REDD+ is to come up with an accurate method to measure and estimate the forest biomass most specifically in tropical forests (Sousa et al., 2015). Several studies have been done using medium-resolution optical satellite images to estimate AGB (Lu et al., 2002; Gizachew et al., 2016; Muukkonen & Heiskanen, 2005; Fernández-Manso et al., 2014). These studies derived Vegetation Indices (VIs) such as Normalized Difference Vegetation Index (NDVI), Enhanced vegetation Indices (EVI) and the Simple Ratio (SR) from optical images of ASTER and Landsat-TM to estimate AGB since the indices have a correlation with AGB estimated from the field data.

Das & Singh, (2012) studied the correlation between VIs with AGB in western Ghart region of Maharashtra in India using Landsat TM image. The study findings were that Ratio Vegetation Index (RVI) and Renormalized Difference Vegetation Index (RDVI) had the highest relation with an  $r^2$  of 0.79 and 0.76 respectively. While NDVI followed closely with an  $r^2$  of 0.75. Lu et al., (2004) examined the relationship between the indices and forest stand parameters using Landsat Thematic Mapper (TM) in Brazil's Amazon forest and the findings were that not all indices have a relation with the forest stand parameters, PCA (principle component analysis first component) and KTI (brightness of the tasseled cap transformation) indices were found to have a strong relation with biomass. Moreover, Gunlu et al., (2014), estimated AGB using VIs derived from Landsat TM satellite image in a pine forest located in North west Turkey. The study developed AGB predictive model using multi-linear regression. The result showed that the model that combined Normalized Difference 57 index

(ND57) and Enhanced Vegetation Index (EVI-2) was the best predictor of AGB with an  $r^2$  of 0.606. Heiskanen, (2006) assessed the relationship between VIs and tree biomass in a birch forest. The results showed that there was a good relationship between biomass and VIs, with Simple Ratio index (SR) and NDVI having the highest correlation with an  $r^2$  of 0.90 and 0.82 respectively.

However, the saturation problems and the low spatial resolution of these images affect the accuracy of the prediction of AGB especially in complex forest structures (Lu, 2005). Recently, the launch of Sentinel-2 satellite image which has a high spatial, spectral and temporal resolution has shown to be promising in improving the accuracy of the AGB estimation, with its new red-edge spectral bands which are very useful in monitoring of vegetation parameters (Delegido et al., 2011). Frampton et al., (2013) demonstrated the potential of Sentinel-2 derived VIs in vegetation monitoring due to its high spatial resolution, the finding revealed that Inverted Red-edge Chlorophyll index (IRECI) and Normalized Difference (ND145) have a strong correlation with Leaf-area index with an  $r^2$  of 0.88 and 0.76 respectively.

In addition, due to advancements in remote sensing technology, more effective techniques are being used to estimate the forest biomass, for instance, the use of LIDAR technology. One of the strengths of this method is the ability to measure both vertical and horizontal vegetation structure at the same time giving a good accuracy with more detailed information (Wulder et al., 2012). More specifically, the use of TLS ground base LIDAR system for AGB estimation is growing in the recent years.

According to Kankare et al., (2013), TLS could be used to measure forest inventory parameters such as DBH and stem volume accurately. Based on his study, individual-tree-level biomass modelling could yield better results using TLS, especially in branch biomass since the current biomass models produced accurate outcomes with only stem and total biomass, but there was high error estimation in branch biomass. Moreover, Ghebremichael, (2016) demonstrated that there is a significant relationship between DBH and Height from TLS data and DBH and Height from the field measurement with an  $r^2$  of 0.98 and 0.70 respectively. Lawas, (2016) also showed that TLS measured DBH and the DBH from the field measurement have a high correlation with an  $r^2$  of 0.99 and a Root Mean Square Error (RMSE) of 1.03 cm. However, since the TLS is ground based, accurate capturing of the treetops becomes a challenge thus leading to errors in tree height measurements, which in the end it affects the estimation of the AGB. Thus, ALS fills the gap of the TLS since it has shown to have accurate height measurement (Sadadi, 2016).

Although several studies have been conducted on the use of remote sensing data in tropical forests in the previous years, only a few have actually combined different techniques involving field estimation to quantify the forest biomass (Næsset et al., 2016). Therefore, the aim of this study is to estimate the AGB by integrating Sentinel-2 derived VIs and TLS forest stand parameters in Ayer Hitam tropical forest in Malaysia. Even though both separate methods have some drawbacks, however, combining both techniques will improve the outcome of the results. Moreover, it will give a more detailed information on the forest structure and parameters of the upper and lower canopy, ultimately increasing the accuracy of AGB estimation since the findings would also be backed-up by field measurement data (DBH) and ALS height data for validation. Thus, moving a step forward in assisting the REDD+ initiative to achieve its goals towards sustainable forest management.

### **1.3. Research objectives**

#### **1.3.1. Main objective**

The main objective is to estimate above ground biomass/carbon stock by integrating vegetation indices (VIs) Red-edge simple Ratio vegetation Index (RERVI), Red-Edge Normalized Difference Vegetation Index (RENDVI), Red-Edge Enhanced Vegetation Index (RE-EVI2), Normalized Difference Water Index( NDWI), Normalized Difference Infrared Index (NDII), Normalized Difference Vegetation Index (NDVI) and Enhanced Vegetation Index (EVI2) derived from Sentinel-2 optical satellite images for the (upper canopy) and forest inventory parameters (DBH and Height) from TLS (lower canopy).

#### **1.3.2. Specific Objectives.**

1. To assess the relationship between VIs and upper canopy biomass estimated from ALS height and Field DBH.
2. To assess the relationship between VIs and total biomass (combination of both upper and lower canopy)
3. To combine the VIs upper canopy and lower canopy TLS AGB.
4. To compare the Linear and Exponential relationship between the VIs and AGB.

#### **1.3.3. Research Questions.**

1. Is there a significant relationship between VIs and upper canopy biomass?
2. Is there a significant relationship between VIs and total biomass?
3. Is there a significant relationship between total biomass (VIs and TLS) and total biomass (ALS and TLS)?
4. Which regression model best explains the relationship between the VIs and AGB?

#### **1.3.4. Hypothesis or anticipated results.**

1.  $H_0$  = There is no significant relationship between VIs and upper canopy biomass.  
 $H_1$  = There is a significant relationship between VIs and upper canopy biomass.
2.  $H_0$  = There no significant relationship between VIs and total biomass.  
 $H_1$  = There is a significant relationship between VIs and total biomass.
3.  $H_0$  = There is no significant relationship total biomass (VIs and TLS) and total biomass (ALS and TLS).  
 $H_1$  = There is a significant relationship total biomass (VIs and TLS) and total biomass (ALS and TLS).

## 2. LITERATURE REVIEW

### 2.1. Tropical Rainforest

Tropical rainforests are located around the equator in humid areas between 10° N and 10° S latitude at an elevation below 3000 feet, they are grouped into three main types; Neotropical, African and the indo-Malaysian (CLOUDBRIGE nature reserve, 2016). The forest covers 6% of the world's land and provides habitat for plant species. A quarter of the world's medicine comes from the tropical forest. These forest ecosystem have a complex structure which is divided in to four layers (Figure 2.1: Tropical Rainforest Structure): the emergent top layer is the composed of trees that range from 100 to 240 feet (30-70 meters) tall. These trees are usually very large and they are not closely packed. They are characterized by smooth trunks with few branches and they also lose their leaves during dry monsoon wind. The upper canopy trees are composed of trees with height ranging from 60 to 130 feet (20-40 meters) tall. They reduce penetration of light into the lower canopy and it also provides habitat for many animal species, since food is abundant at this layer. The lower canopy layer comprises of trees which are 60 feet (20 meters) height or lower and it's characterized by shrub, plants, and small trees. Lastly, the forest floor is the lowest layer in a tropical forest, most of the parts in this layer receive little light and its top soil is also very thin with poor soil (Michael, 2001).

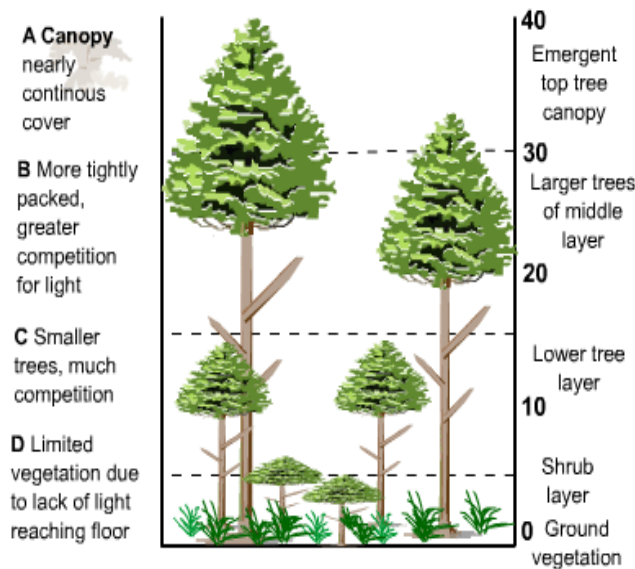


Figure 2.1: Tropical Rainforest Structure  
Source: (S-cool, 2016)

### 2.2. Biomass and Carbon

(IPCC, 1996) defines biomass as all living or dead organic matter. The vegetation biomass changes with time per unit area. The biomass of a terrestrial ecosystem is an important climate variable since it absorbs and releases carbon into the atmosphere. According to IPCC, (1996) biomass in a terrestrial ecosystem is divided into Above Ground Biomass (AGB) which defined as all living biomass above the soil including, stem, stump, branches, bark, seed and foliage and Below Ground Biomass (BGB) which are all living biomass of live roots.

### 2.3. Overview of Terrestrial Laser Scanner

Terrestrial Laser Scanner (TLS) is an active remote sensing system which does not depend on sun energy, it's a type of Light Detection and Ranging system (LIDAR) which is ground based (Hudak et al., 2009). It works by sending laser pulse as seen in Figure 2.3 of light which is returned back to the receiver. It will then record the time taken by the pulse to bounce back to the receiver, divides it by two and lastly multiplies it by the speed of light to get the distance (Lefsky et al., 2002). The laser pulse is then stored as a 3D point cloud. There are two types of scans that can be used to acquire data Multiple Scans and Single Scans. Multiple scans provide detail information since it has a wide coverage compared to single scans, while multiple scan functions by taking one scan at the center of the plot and three other scans will be taken outside the sample plot (Weiß, 2009). The scanner comes with its retro reflective targets (tie points) which should be set on the sample plot. One should ensure that at least three reflectors are visible. The reflectors enable the scanner to record the geographic position of each scan (Bienert et al., 2006). In forestry, the TLS is used to extract forest inventory parameters such as Diameter at Breast Height (DBH), height, and crown diameter (Srinivasan et al., 2015). The forest stand parameters can either be extracted manually or automatically. Although the manual extraction is time consuming, it yields more accurate results when compared to the automatic method (Maas et al., 2008). Based on several studies that have been done using TLS such as (Liang et al., 2016; Kankare et al., 2013). It has shown to be a promising technique that will reduce uncertainties in forest biomass estimation since it yielded accurate results. Calders et al., (2015) demonstrated that TLS can be used for developing and testing new allometric equation and at the same time testing existing allometric equation. However, since TLS is ground based it cannot measure the tree top, especially in complex forest structure with different levels of canopy because of occlusion, thus, causing errors in the estimation of tree height (Jung et al., 2011).

Furthermore, TLS is a heavy equipment which makes it difficult to carry around during field work, it is also not suitable for all weather conditions, since it is affected by wind conditions, precipitation, and some instruments need direct sunlight (Petrie & Toth, 2008). There are several TLS instruments that are being used. They vary in price and its specification, the instruments record point clouds ranging from 1000 to 50,000. For this study the RIEGL V2 – 400 TLS scanner will be used (Figure 2.2).



Figure 2.2: RIEGL V2- 400 TLS with its main feature

Source: (RIEGL, 2016)

**Terrestrial laser scanning**

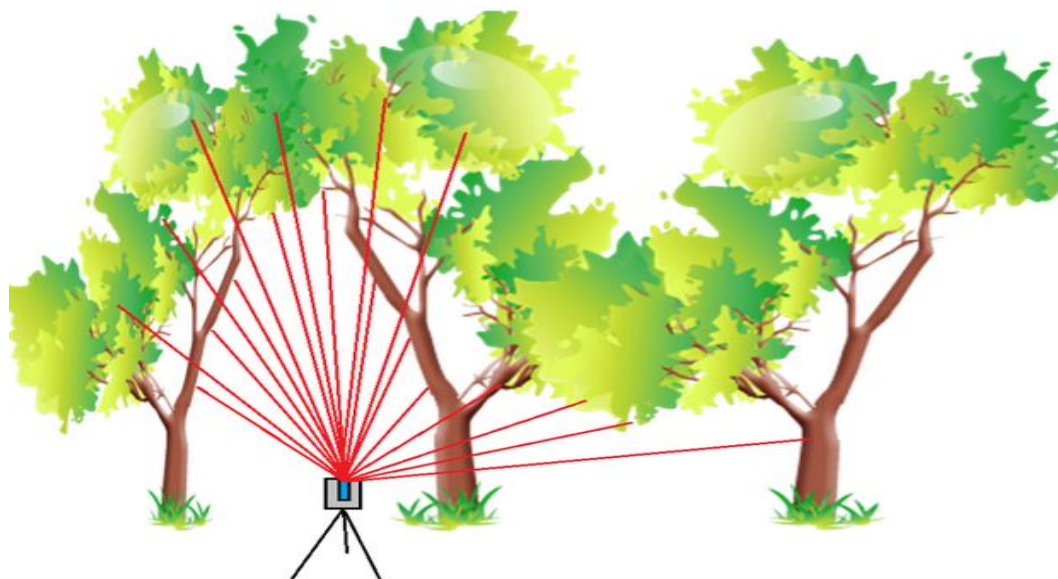


Figure 2.3: An example of how TLS sends and receives laser pulse

Source: (AWF-WIKI, 2016)

**2.4. Sentinel-2 Optical Satellite image.**

Sentinel-2 is a multi-spectral sensor that was launched in June 2015, through the Global Monitoring for Environmental and Security program (GMES) in partnership with European Space Agency (ESA) (EO, 2016). The image has a spatial resolution 10m, 20m, and 60m with a swath width of 290 kilometers. It has a 10 day revisit time for one sensor and it also has 13 spectral bands (Table 2.1) (SIC, 2016). The bands shares similarities with Landsat 8 bands with an exemption of the thermal bands (Figure 2.4). The images can freely be acquired and accessed online through the ESA scientific hub website (Appendix 15). The Sentinel-2 images can be used in various applications for monitoring of spatial planning, Agro-environmental, water, forest and vegetation, natural resources and Global crop monitoring (ESA, 2015).

Table 2.1: Sentinel-2 spectral bands with its resolution

Sentinel-2 Bands	Central Wavelength ( $\mu\text{m}$ )	Resolution (m)
Band 1 - Coastal aerosol	0.443	60
Band 2 - Blue	0.490	10
Band 3 - Green	0.560	10
Band 4 - Red	0.665	10
Band 5 - Vegetation Red-edge	0.705	20
Band 6 - Vegetation Red-edge	0.740	20
Band 7 - Vegetation Red-edge	0.783	20
Band 8 - NIR	0.842	10
Band 9 - Water Vapour	0.945	60
Band 10 - SWIR - Cirrus	1.375	60
Band 11 - SWIR	1.610	20
Band 12 - SWIR	2.190	20

Source :( SIC, 2016)

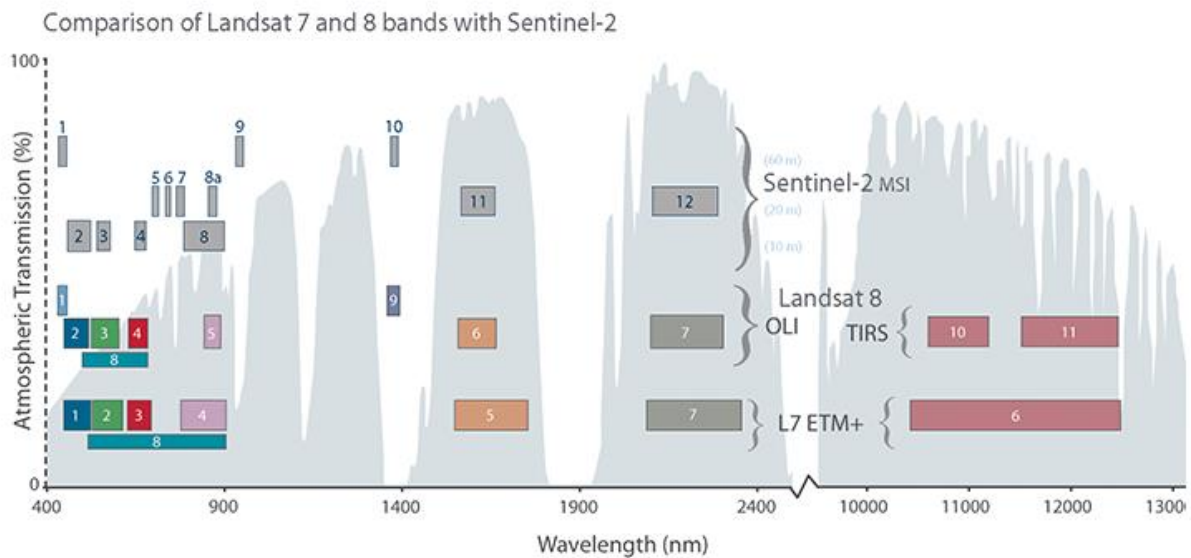


Figure 2.4: Comparison of Landsat 7 and 8 bands with Sentinel-2 sensors

Source: (EROS, 2016)

## 2.5. Vegetation Indices for biomass estimation

Vegetation Indices (VIs) are a mathematical combination of spectral bands that highlight the spectral properties of green plants so they can be distinguished from other features, it is calculated by combining the red spectral band (Chlorophyll absorbent) with the Near-infrared band (non-absorbent) some indices also include short-wave infrared band (Njoku, 2013). “The computation is done by rationing, differencing, rationing differences and sums by forming a linear combination of band” (X Zhang & Ni-meister, 2014).

Throughout the year's VIs have been used in applications such as agriculture and forestry. In agricultural application studies such as (Wiegand et al., 1991; Zhang et al., 2003), used VIs most commonly Normalized Difference Vegetation index (NDVI) and Enhanced Vegetation Index (EVI) to study the health of the crop. The higher the NDVI value the healthier the vegetation. Also, studies such as (Dong et al., 2016; Sibanda et al., 2017) have used VIs in estimating crop biomass. In forestry application, research such as (Gunlu et al., 2014; Anderson et al., 1993), used the indices to estimate forest biomass either by using statistical techniques such as simple, multi-linear regression, neural network and k-nearest neighbour algorithm models to come up with a predicted biomass. The accuracy of the prediction varied depending on how strong the correlation was between the AGB estimated from the field data with the indices. However, the major challenge of using the VIs is the saturation problems which affect the accuracy of the estimation leading to uncertainties (Lu et al., 2014).

Zhao et al., (2016) demonstrated how the use of stratification based on vegetation types and topography improves AGB estimation by reducing the saturation effect on Landsat Thematic Mapper (TM). The study compared the AGB estimation of the study area with stratification against the one with no stratification. The findings revealed that the Root Mean Square Error (RMSE) reduced from 29.3 to 24.5 Mg/ha by using stratification. Moreover, studies as (Fernández-Manso et al., 2016; Guo et al., 2017; Padilla et al., 2017) have also shown that the red-edge VIs reduces saturation especially in complex structure Vegetation.

## 2.6. Integration of Remote Sensing Methods for biomass Estimation.

Sium, (2015) estimated carbon stock in Royal Belum tropical forest Malaysia, by combining TLS height and Crown Projection Area (CPA) from Worldview-2 Very High Resolution Satellite image (VHRS). The study combined TLS height and CPA using multiple linear regression models. The estimated carbon stock had an average of 185Mg per hectare with a model accuracy of 84% and RMSE of 29.3%.

Karna et al., (2015) estimated the Carbon stock of the tree species in Kayar Khola watershed, Nepal by combining airborne LIDAR Canopy Height Model (CHM) and WorldView-2 VHRS images. The study extracted individual tree height and CPA from the integrated dataset. These variables were then used as input in multiple linear regression models as independent variables and AGB/carbon estimated from the field data as dependent variables. The model resulted in a carbon stock estimation of the tree species *S.robusta*, *L.parviflora*, *T.tomentosa*, *S.wallichii* and others with an accuracy of 94%, 78%, 76% and 84% respectively.

Badreldin et al., (2015) developed an approach of integrating airborne LIDAR, TLS and Multi-temporal Landsat Satellite image, so as to find out the relationship between forest stand parameters and VIs derived from Landsat optical satellite image. It was then used to directly estimate biomass of coniferous forest in Coral Valley Canada. The study developed a best fit model for biomass estimation by using Stepwise multiple regression analysis, using canopy height and the VIs (NDVI, EVI2, and TCA). The best model had an  $r^2$  of 0.78 and an RMSE of 44Mg per hectare.

Sinha et al., (2016) integrated ALOS POLSAR and Landsat TM in order to estimate tropical forest biomass. The NDVI computed from the optical image spectral bands, had a poor relationship with biomass obtaining an  $r^2$  of 0.29. However, when the VIs was combined with L-band extracted from the Synthetic Aperture Radar (SAR). The accuracy of the model improved obtaining an  $r^2$  of 0.89.

## 2.7. Allometric Equation

The allometric equation is a statistical regression model developed to estimate biomass using forest inventory parameters such as tree height, Crown CPA, and DBH, some allometric models are species specific (Basuki et al., 2009). These models were developed to replace the destructive method of estimating biomass. Which was cumbersome and time consuming. The accuracy of the biomass estimation using the equation depends on field measurement of the forest parameters, if there is an error in measurement it will be propagated to the equation (Breu et al., 2012).



### 3. MATERIALS AND METHODS

#### 3.1. Study Area

Ayer Hitam Forest Reserve (AHFR) was considered as a suitable study area for this research since it is a tropical forest with a multi-layered complex structure. Also, the forest was leased to the University Putra Malaysia (UPM) for research purposes by the state government of Selangor. Hence, it is mostly used for research and educational purposes (Mohd et al., 1999).

##### 3.1.1. Geographic Location.

AHFR is located in Puchong (Latitude  $2^{\circ} 56' N - 3^{\circ} 16' N$  and Longitude  $101^{\circ} 30' E - 101^{\circ} 4' E$ ), Selangor Malaysia (Figure 3.1). It is situated 45km from the Centre of Kuala Lumpur and 25km from the UPM. The forest covers an area of 1,217.90 hectares (Hasmadi et al., 2010).

##### 3.1.2. Climate and Topography

The area is part of a tropical rain forest which is mostly humid at  $83^{\circ}$  with an average rainfall of 2178mm. The temperature vary from a minimum of  $22.7^{\circ}$  and a maximum of  $32.1^{\circ}$ . The Elevation ranges from 15m to 233m with most of the topographic features including ridge, hill shade and valley (Saari et al., 2014).

##### 3.1.3. Vegetation and Structure

The forest is dominated by a lowland dipterocarp, the two dominant species *Eugena* and *Cahhnarium*, the forest has more than 430 tree species with 203 genus and 72 families. The species are classified into categories dipterocarp (*Shorea*, *Dipterocarpus* and *Ansoptera*) and non-dipterocarp (*Xanthophyllum*, *Knema* and *Callophyllum*)(Adnan et al., 2005).

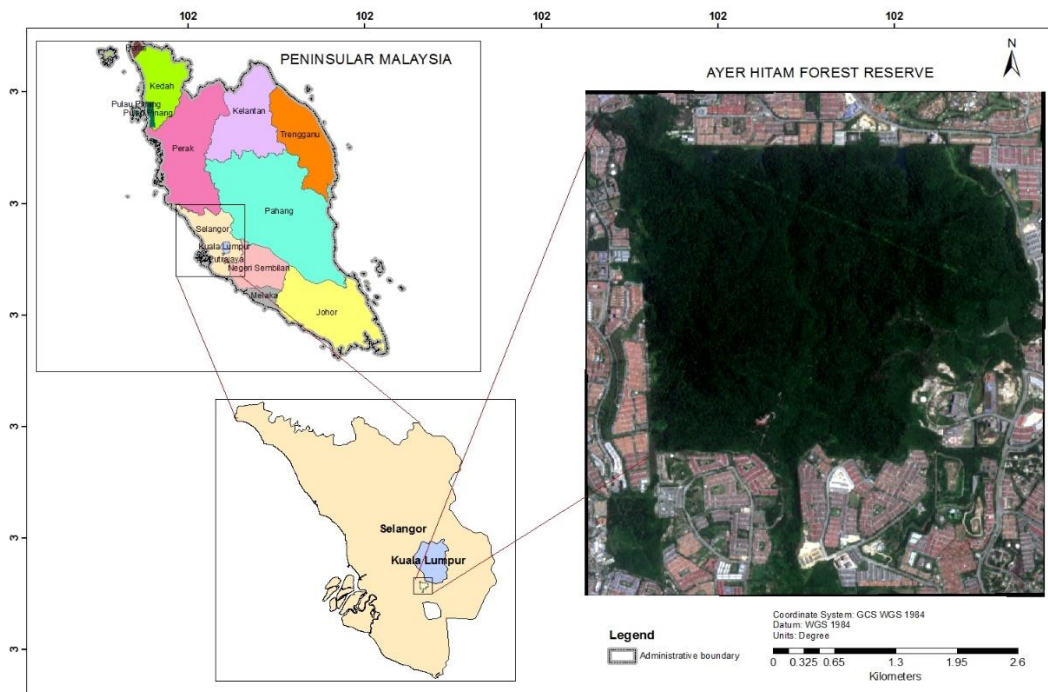


Figure 3.1: Location of the study area

### 3.2. Materials

#### 3.2.1. Field instruments/images/Airborne laser scanner (ALS) height data.

A number of field measuring equipment were used for data collection (Table 3.1), including Sentinel-2 optical satellite image.

Table 3.1: the list of the field equipment and image with their purpose.

Field Martials	Purpose
Diameter tape (5m)	DBH measurement
Disto Laser	Tree Height measurement
Measuring tape (30m)	To outline the plot
Garmin GPS	Navigation
Sentinal-2 image	Deriving vegetation indices
Riegl-VZ 400	Terrestrial Lesser scanning
ALS height data	For validation/ accuracy assessment

#### 3.2.2. Software and tools

The software and tools which were used for processing and analysis of the data are listed in Table 3.2.

Table 3.2: Software and tools for processing and analysis

Software	Purpose
ENVI	Image processing
QGIS	Vegetation indices calculation
Arc GIS	Extracting Vegetation indices pixel value.
RISCAN	TLS point cloud processing and analysis
SNAP Tool box	Resampling sentinel image
SPSS	Statistical analysis
Microsoft office word	Project report writing
Microsoft office excel	Statistical analysis

### 3.3. Methods

The methodology of this study breaks down into 4 main steps (Figure 3.2) based on the objectives of the study:

**Step 1;** This step involved the use of ALS to estimate biomass of the upper canopy, through an allometric equation that used the field Diameter at Breast height (DBH) and ALS height.

**Step 2:** The TLS point cloud data was registered of which individual trees were extracted. This was followed by measurement of the DBH and height of each individual trees. These parameters were then used to estimate the Above Ground Biomass (AGB) of the lower canopy trees using an allometric equation. The lower canopy biomass was then combined with the upper canopy biomass (step1) from ALS to obtain a total biomass.

**Step 3:** In this step, the Sentinel-2 satellite image was processed by applying radiometric correction. The rectified image was then used as an input for computation of Vegetation Indices (VIs) which included; NDII, EVI-2, RE-EVI2, NDVI, RENDVI, RERVI, and NDWI. These VIs were then analysed by assessing its relationship with AGB of both the upper canopy and the total biomass (combined upper and lower canopy biomass) by using both linear and exponential regression models.

**Step 4:** Involved combining the upper canopy biomass estimated from the best VI regression model equation obtained in step 3, with the lower canopy biomass estimated from the TLS data to obtain total biomass. The result was then validated using the total biomass obtained by combining the upper canopy biomass (Step1) and the lower canopy biomass (Step 2).

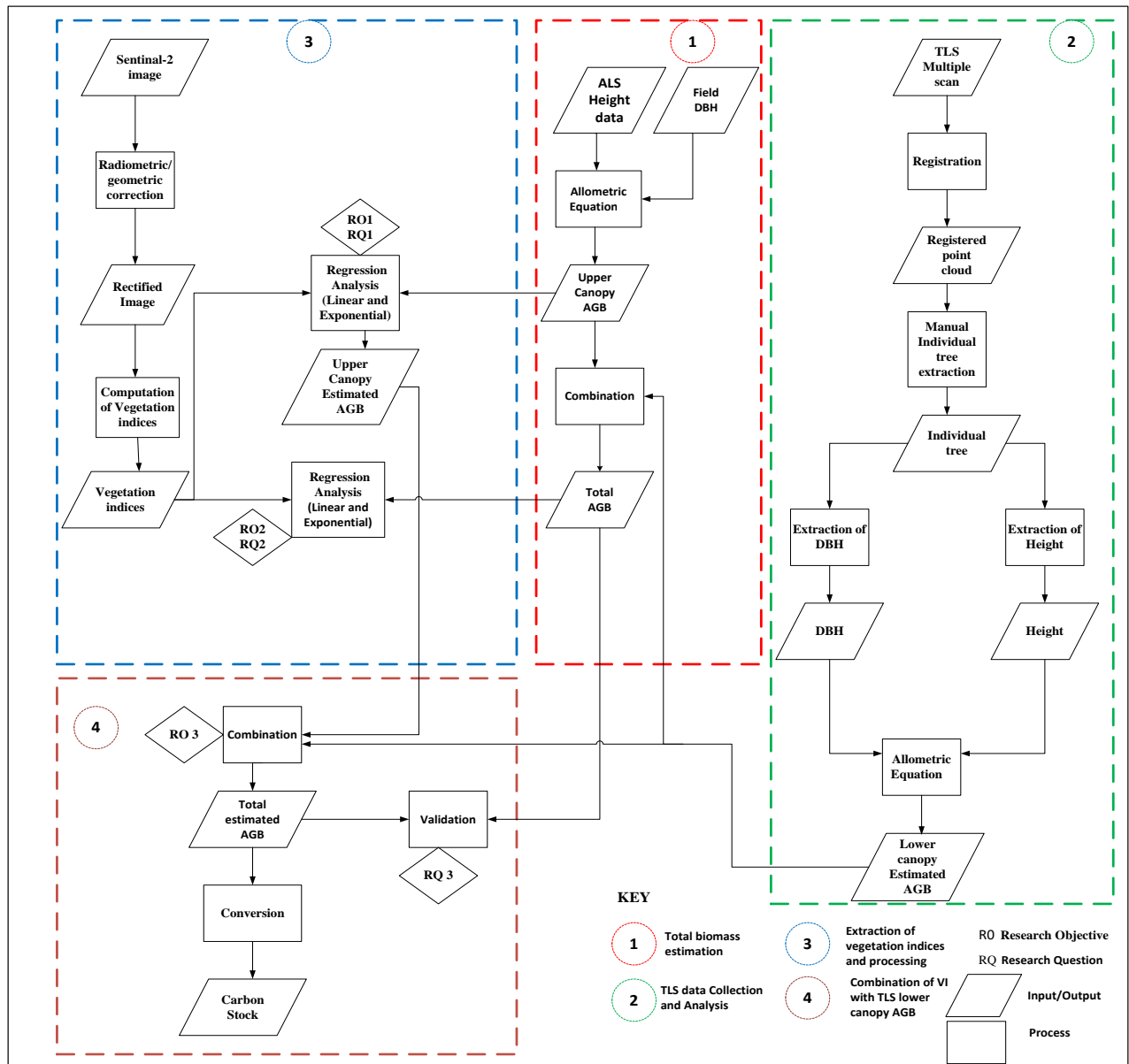


Figure 3.2: Flow chart of the research method

### 3.3.1. Pre-field work

This process involved training and familiarizing with field equipment which were used for measurement in the field and also preparing field materials. The activities included:

- Training on how to operate TLS,
- Navigation using the LOCUST GPS and data collection skills,
- Loading google earth image on LOCUST that was used for navigation in the field,
- Participating in an experiment that tested the accuracy of hand held field equipment in measuring the height of an object encompassing solitary trees, complex trees, and buildings, and
- Preparation of field data sheets for collecting biometric data.

### 3.3.2. Plot size

A circular plot of 500m<sup>2</sup> (0.05 ha) with 12.6m radius was used (Figure 3.3) .This is because it was more easy to set up than square plot and it reduces the amount of trees at the edge of the plot. Moreover, a circular plot is suitable for the TLS(Van Laar & Akca, 2007) . A measuring tape (30m) was used to measure the sample plot radius.

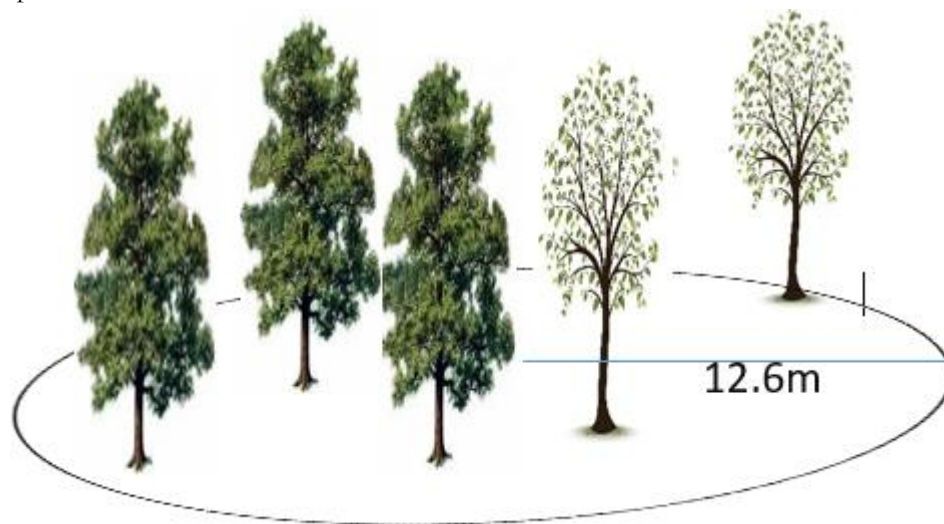


Figure 3.3: Circular plot of 500m<sup>2</sup>

### 3.3.3. Sampling-design

Purposive sampling design which is a non-probability sample that is based on the judgement of the researcher was used in the fieldwork. A total of 27 plots were sampled. The sample plots were selected based on the following criteria:

**Slope:** areas that were less sloppy were mostly preferred due to the heaviness of the TLS equipment. It was difficult to carry it on a steep slope, of which some areas in the forest had such terrain. Furthermore, samples areas that had a flat terrain were easily accessible which eventually saved time when navigating to another the sample area.

**Accessibly:** areas that were easy to access were taken into consideration. Thus, we were able to save more time in terms of navigating to the sample area. Hence, covering more samples per day as compared to wasting time just to be able to access one sample plot.

Moreover, areas with less undergrowth were favoured because it took time to clear the plot, since it involved cutting down of the twigs and undergrowth, which was deemed necessary in order to reduce occlusion for the TLS point cloud data.

### 3.4. Data collection

The fieldwork exercise was conducted from September 30<sup>th</sup> to October 15<sup>th</sup>. A circular plot of radius 12.6m was demarcated in each plot. A total of 27 plots were sampled (Appendix 16), having 762 trees and 163 tree species. The data collection process was carried out through the following steps:

#### 3.4.1. Demarcation of the circular plot

After identifying the plot, a suitable centre position with less undergrowth was first established. A circular plot was then demarcated by measuring 12.6 meter radius from the centre position. Trees at the boundary of the plot were then marked with chalk to clearly delineate the circular plot, which was prepared by cutting down undergrowth to reduce occlusion that might hinder the scanning of the point cloud data by TLS. Furthermore, the trees were then tagged by laminated numbers as seen in Figure 3.4 so that they can be identified on the TLS point cloud data and matched with biometric data.



Figure 3.4: Tagged sample trees

#### 3.4.2. Biometric Data collection.

The coordinates of each tree were recorded using the Garmin GPS so that each tree location can be identified during data analysis and matching the trees with other sensors. The forest stands parameters DBH and Height were then measured. The Disto Laser instrument was used to measure the height of trees. This instrument was chosen for the field survey based on the experiment that was conducted before the field work. The result of the experiment showed that Disto instrument was the most accurate compared to the forest range finder and true pulse in height measurement. A diameter tape was used to measure the DBH at 1.3 meters above the ground (Maas et.al., 2008). The measurements were carried out for every tree that was inside the sample plot except for the trees which had a DBH which was less than 10cm. This process was done for each sample plot in the study area. The measurements and tree species names were then recorded on the field datasheet, which was then transferred to Microsoft Office Excel data sheet for further analysis of the data.

### 3.4.3. TLS data Collection

#### Positioning the reflectors

The tie points also known as retroreflectors were placed around the circular plot (Figure 3.5), both cylindrical and circular tie points were used. They were placed in areas that were clearly visible by the TLS scan. The cylindrical retroreflectors were useful for registration of multiple scanning positions while the purpose of the circular reflectors were for geo-referencing the plots (Prasad et al., 2016).



Figure 3.5: circular retroreflectors (1) and cylindrical retroreflectors (2)

#### TLS Data Acquisition

Multiple-scans were carried out around the circular plot with 4 scans in each plot one in the centre of the plot and the others three around the plot boundary (Figure 3.6). Multiple scans was preferred because it yields more accurate results as compared to single scan (Maas et al., 2008). It also captures more trees, since it reduces the error that might be caused by occlusion of twigs.

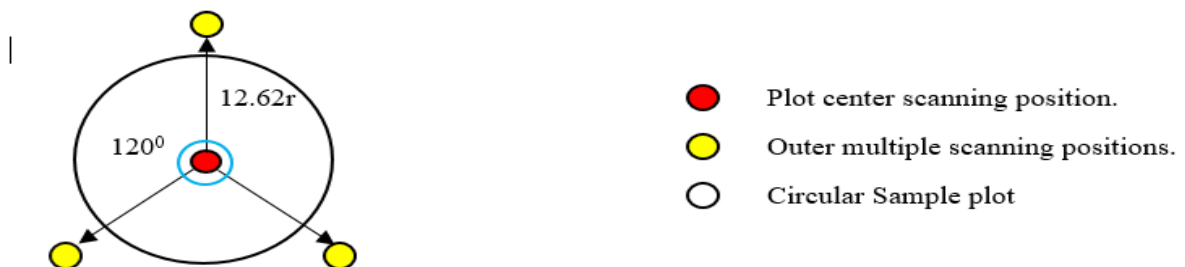


Figure 3.6: Multiple Scanning Positions

#### 3.4.4. Sentinel-2 Image acquisition

The Sentinel-2 level 1C satellite image which is composed of 100\*100 km<sup>2</sup> tile (Orhto-images with UTM/WGS84 projection), was downloaded from the Sentinel-2 scientific hub through the ESA website (Appendix 15). The acquisition date of the image was on 1<sup>st</sup> April 2016. This is because at that particular time, the image was less or not covered with clouds in the study area (Figure 3.7). The image was already pre-processed into Top of the Atmosphere reflectance (TOA). Thus, it required minimal pre-processing as compared to other satellite images. The image was considered to be suitable for this research since it has a high spatial resolution of 10m. It also comes with three red-edge spectral bands that are useful for vegetation monitoring.

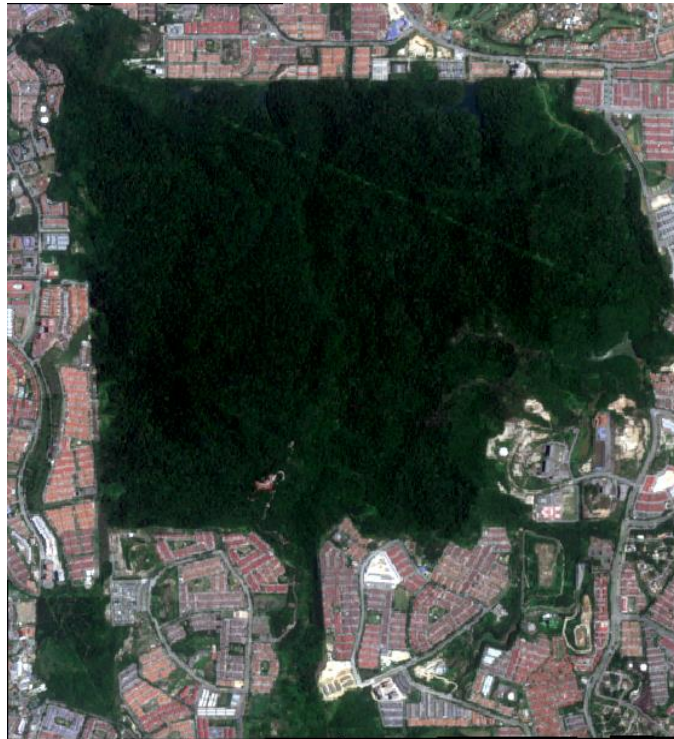


Figure 3.7: Sentinel-2 Multispectral image

### 3.5. Data Processing

The data analysis process was carried out in different phases, depending on the type of data which included TLS and Sentinel-2 Image. The processing was done using various softwares such as RiSCAN pro, ArcGIS, Qgis and ENVI.

#### 3.5.1. TLS data processing

##### Registration of point cloud

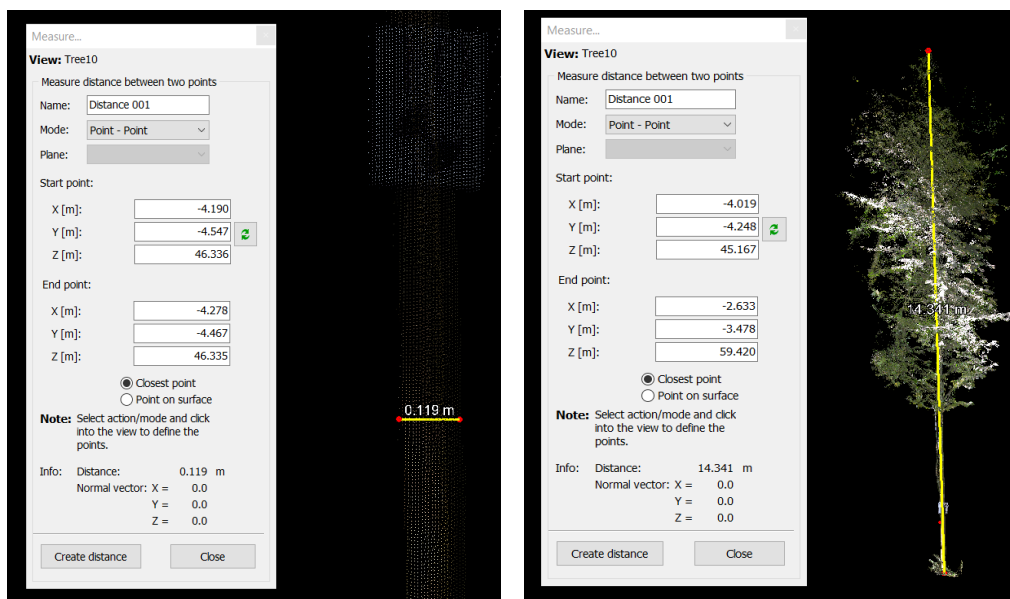
Registration of the TLS point clouds, was done to ensure that all the point cloud data were georeferenced. This was carried out using automatic marker based registration method. In which target points (tie points) are used to precisely merge the multiple scans point clouds together, in order to have a common reference (Kociuba et al., 2014). In this method the second, third, and fourth scanning positions were matched with the first scanning positions. This method was preferred to the coarse manual method, since it is less time consuming. The multi-station adjustment was then applied to reduce the standard deviation error. This step was followed by plot extraction to filter out point clouds data that was not within sample plot boundary.

## Plot Extraction

The registered point cloud data also captured trees that were outside the plot, which was not needed for the analysis. Therefore, the point cloud data had to be filtered by extracting only the trees that fell within the circular plot using the range function on the RiSCAN pro software.

## Extraction of Individual Tree and measurement of the forest stand parameters

The individual trees were extracted manually using the RiSCANPRO software. This was done by using the selection mode tool (polyline), of which it was later saved as polydata through create polydata tool. The naming of the polydata was based on the tree tag number. This step was then followed by measurement of the DBH and Height which was done using the measure distance between two points tool. The DBH was measured at 1.3 meters (Figure 3.8a), while the height was measured by selecting lowest point cloud and the highest point (Figure 3.8b). The measurements were then recorded on Microsoft Excel data sheet for further analysis.



a) b)  
Figure 3.8:a) DBH Measurement and b) Height Measurement using RiSCANPRO software

### 3.5.2. Processing/ radiometric correction of Sentinel-2 image

Radiometric correction of Sentinel-2 optical image was done to improve the quality of the image by using ENVI software. The main purpose of radiometric correction was to reduce atmospheric and sun angle effects (Baillarin et al., 2012). The image was transformed from radiance to surface reflectance, by applying the Dark Object Subtraction (DOS) method using the semi-automatic classification plugin (SCP) in Qgis software. The DOS method works by removing the darkest pixel in each band that might be affected by atmospheric scattering (Chavez, 1988). The advantage of this method is that it is easy to apply. Furthermore, it is image based, thus, it does not require ground truth data (Chavez, 1996). Moreover, the red-edge bands and the shortwave infrared bands, which were of 20m resolution were resampled into a 10m resolution using the SNAP toolbox. This was done because some of the indices that were used for the study were computed by combining spectral bands with a spatial resolution 10 m and 20m (Table 2.1). Moreover, with the 10m resolution data, the variation was increased in terms of pixels values per plot, as compared to 15m and 20m resolution since the plot size was only 500m<sup>2</sup> (Figure 3.9 a, b).

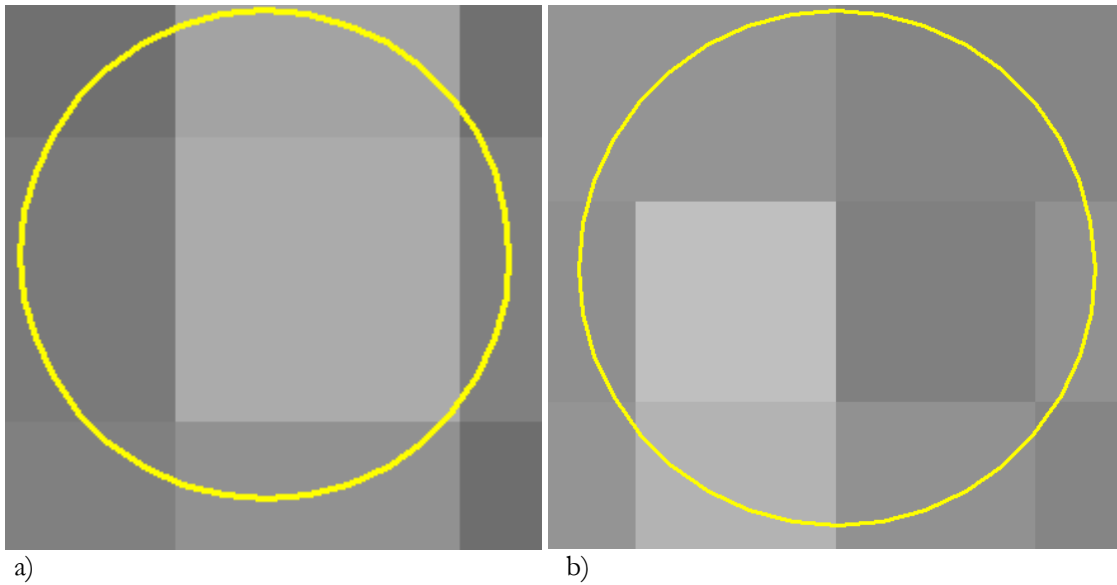


Figure 3.9: Comparison between the 15m (a) and the 10m (b) spatial resolution within the circular plot.

### 3.5.3. Deriving Vegetation Indices (VIs) from Sentinel-2 optical satellite image

The indices were computed using Sentinel-2 image spectral bands through the semi-automatic classification plugin in Qgis software. The selection of the indices was based on its performance in biomass estimation in previous studies. There are over 150 vegetation indices but for this study, only 7 indices were selected. Three categories were considered in the selection of the VIs, which include:

#### Broadband VIs

This category of the VIs is sensitive to the canopy leaf area. The indices are used for monitoring of the vegetation, since they use the near-infrared (NIR) spectral band which has a high reflectance of vegetation and the red spectral band which has high absorption by vegetation. For this study the following broadband indices were used:

#### Normalized Difference vegetation index (NDVI)

NDVI is one of the most commonly used VI for biomass estimation (Rouse et.al., 1974). Based on previous studies it has shown to have a reasonable correlation with biomass depending on the type of vegetation cover.

Equation 3-1: NDVI formula;

$$NDVI = \frac{\rho_{NIR} - \rho_{red}}{\rho_{NIR} + \rho_{red}}$$

Where: NIR is of 842nm wavelength which is spectral band 8, while the red is spectral band 4 of 665nm wavelength of Sentinel-2 satellite image.

#### Enhanced vegetation index (EVI-2)

This index is an improvement version of NDVI. It also reduces atmospheric effects (Jiang et al., 2008).

Equation 3-2: EVI2 Formula;

$$EVI2 = 2.5 \times \frac{\rho_{NIR} - \rho_{red}}{\rho_{NIR} + 2.4\rho_{red} + 1}$$

Where: NIR is of 842nm wavelength which is spectral band 8, while the red is spectral band 4 of 665nm wavelength of Sentinel-2 satellite image. The 2.5 value is the gains factor. The 2.4 is the coefficient is used to reduce aerosol effects and the value 1 is the soil adjustment factor, used to reduce soil background effects.

### **Narrow red edge band VIs**

This includes the VIs that use the red-edge spectral band. This category of indices also use the NIR band, but instead of using red spectral band they use the red-edge spectral band, which range from 690-740 nm. It is located between the highest absorption band (red) and the highest reflectance band (NIR) of vegetation. They are mainly used to study the biophysical characters of vegetation (Mutanga & Skidmore, 2004). The indices that were selected under this category include:

### **Red-edge Ratio Vegetation index (RERVI)**

RERVI is a ratio between the NIR band and Red-edge spectral band (Cao et al., 2016). Limited research has been done on the potential of this index in estimating forest biomass.

Equation 3-3: RERVI formula;

$$RERVI = \frac{\rho NIR}{\rho RE}$$

Where: NIR is of 842nm wavelength which is spectral band 8, while the red-edge is spectral band 6 of 740nm wavelength of Sentinel-2 satellite image.

### **Red-edge Normalized Difference Vegetation Index (RENDVI)**

The index is a modification of NDVI (Chen et al., 2007). Thus, the index uses the NDVI formula but instead of using the red spectral band it uses the red-edge spectral band 6 of 740nm wavelength.

Equation 3-4: RENDVI formula;

$$NDVI = \frac{\rho NIR - \rho red}{\rho NIR + \rho red}$$

Where: NIR is of 842nm wavelength which is spectral band 8, while the red-edge spectral band 6 of 740nm wavelength of Sentinel-2 satellite image.

### **Re-edge Enhanced vegetation index (RE-EVI2)**

This index is a modification of EVI-2 (Abdel-rahman et al., 2017). However, Red-edge spectral band is used instead of the red spectral band.

Equation 3-5: RE-EVI2 formula;

$$RE_{EVI2} = 2.5 \times \frac{\rho NIR - \rho RE}{\rho NIR + 2.4 \rho RE + 1}$$

Where: NIR is of 842nm wavelength which is spectral band 8, while the red-edge is spectral band 6 of 740nm wavelength of Sentinel-2 satellite image.

### **Canopy Water content indices**

The VIs in this category are computed by using the shortwave infrared (i.e. middle infrared) spectral band and the near-infrared spectral band. It is used for studying the water content in the vegetation. In this category two indices were selected:

#### **Normalized Difference Infrared Index (NDII)**

This index is sensitive to the canopy water content. Its value increase with increase in the canopy water content (Hunt & Qu, 2013)

Equation 3-6: NDII formula;

$$NDII = \frac{\rho_{NIR} - \rho_{SWIR}}{\rho_{NIR} + \rho_{SWIR}}$$

Where: NIR is of 842nm wavelength which is spectral band 8, while the shortwave infrared (SWIR) is of 2190 nm wavelength which is spectral band 13 of the Sentinel-2 satellite image.

#### **Normalized Difference Water Index (NDWI)**

NDWI (Gao, 1996) is one of the most commonly used VIs in monitoring the water content since it is sensitive changes in spongy mesophyll of vegetation canopies (Ceccato et al., 2001).

Equation 3-7: NDWI formula;

$$NDWI = \frac{\rho_{NIR} - \rho_{SWIR}}{\rho_{NIR} + \rho_{SWIR}}$$

Where: NIR is of 842nm wavelength which is spectral band 8, while the shortwave infrared (SWIR) is of 1610 nm wavelength which is spectral band 12 of the Sentinel-2 satellite image.

#### **3.5.4. Canopy separation.**

It was considered necessary for this research to separate the canopy layers into upper and lower canopy. In order to detect more trees and to minimize the error of height measurement in each plot, by using ALS and TLS for the upper and lower canopy trees respectively. In order to improve the accuracy of the AGB estimation. The separation was done using ALS Canopy Height Model (CHM). Trees that could not be matched with the ALS CHM, due to the fact that the crown was not or only partially visible in ALS-CHM, were considered to be lower canopy trees which on average turned out to be trees with height less than 12m. On the other hand, trees with height >12m were categorized as upper canopy. However, this value varied depending on the type of the forest layer found on a sample plot, since the forest layers varied in the study area. Although majority of the sample plots had a multiple upper canopy layer, some plots such as plot 1, 26 and 27 have a single upper canopy layer. Hence, they had less trees that were lower canopy as compared to other plots.

#### **3.5.5. Removal of outliers**

The individual trees did not have a one to one relationship with the VIs pixel value. This is due to the data spatial resolution of the Sentinel-2 satellite image which was 10m. Therefore, the biomass had to be estimated at a pixel level, in which the total biomass of a pixel was obtained by summing up the AGB of all the trees that fell within a particular pixel in each plot. The pixel values, were extracted using Arc GIS software spatial analysis tool (extract values by points). However, there were some pixels which are considered to be outliers because they were not fully covered within the plot (Figure 3.10). This means that

some trees were left out since they were not part of the sample. Hence, the reflectance value of the pixel did not coincide with the number of trees found within the pixel. Therefore, such pixels were filtered out from the data.

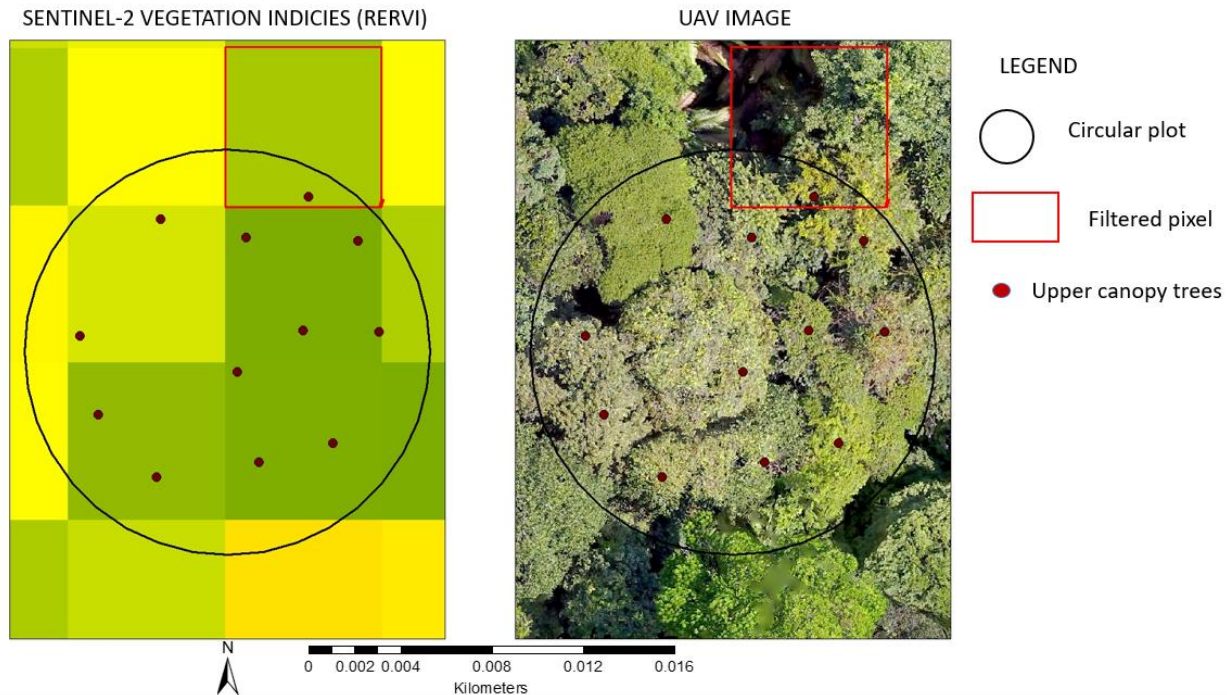


Figure 3.10: Pixels that were considered to be outliers

### 3.6. Calculation of AGB and Carbon stock estimation

The AGB and carbon stock was computed based on two categories, upper and lower canopy. An allometric equation was used to calculate the AGB by using the forest stand parameters: DBH and Height. The TLS DBH and Height were used to calculate lower canopy biomass while ALS height and Field DBH were used to calculate upper canopy biomass. The ALS height was used for the upper canopy instead of the field height. This was based on the findings of the experiment conducted before we embarked for fieldwork. Which showed that manual measurement of the tree height using hand held instruments, results to inaccuracy of the height. The lower canopy was combined with the upper canopy to obtain total biomass. The upper canopy and total biomass were then used to test the accuracy of the VIs in predicting AGB. The lower canopy biomass could not be used on its own, since the Setinel-2 optical Satellite image views the forest from the top. Thus, it cannot capture the lower canopy trees.

The allometric equation which was used in this research was formulated by Chave et al., (2014). It was found to be the best fit pan-tropic model for biomass estimation. It is also suitable for all forest types and bioclimatic conditions. The wood density values used was species specific (Gisel Reyes et al., 1992).

Equation 3-8: AGB Allometric equation used in this study.

$$AGB = 0.0673 \times (\rho D^2 H)^{0.976}$$

Where AGB= Above-ground biomass

$\rho$  = Specific wood density ( $g/cm^3$ )

$D^2$ = Diameter at breast height (DBH) (cm)

H= Height of tree (m)

The above-ground biomass was then be converted into carbon using the (CF) factor 0.47 formulated by IPCC, (2006).

Equation 3-9: Conversion of AGB to carbon stock

$$C = AGB \times CF$$

Where,

C: carbon stock (Mg C)

AGB: Above ground biomass

CF: fraction of above ground biomass (0.47)

### 3.7. Statistical Analysis

Statistical analysis was carried out using SPSS software and Microsoft Excel. Linear and exponential regression models were used to assess the relationship between each VIs and AGB. A total of 112 pixel samples were used, having an average of four pixels for each of the 27 plots. The statistical analysis was carried out to assess the following relationships:

- a) Linear and exponential relationship between VIs and upper canopy biomass.
- b) Linear and exponential relationship between VIs and total biomass (combined ALS and TLS biomass)

The goodness of fit of the model was evaluated based on the Root Mean Square Error (RMSE) and coefficient of determination ( $r^2$ ). In which the best model was determined by the highest  $r^2$  and a Low RMSE. The  $r^2$  was preferred since it has a standard measure with values ranging from 0 to 1. The  $r^2$  also shows the percentage of the variability explained by the model. Thus, making it easy to understand the relationship between the independent and dependent variable (Peters, 2007). The significance of the model was assessed using the P-Value, if it is less than 0.05 the model is considered significant. The equation obtained from the regression model was then used to estimate AGB. The estimated VIs upper canopy biomass using the best regression model, was combined with TLS lower canopy biomass to obtain total biomass. It was then validated using the combined TLS and ALS total biomass.

Equation 3-10: RMSE formula

$$RMSE = \sqrt{\frac{\sum_{i=1}^n (y_i - \hat{y})^2}{n}}$$

Where:  $Y_i$  = Measured Value of the Dependent Variable  
 $\hat{Y}_i$  = Measured Value of the Dependent Variable  
 $n$  = Number of samples



## 4. RESULTS

### 4.1. Calculation of Vegetation Indices (VIs)

The calculation of the VIs was done using Semi automatic classification plugin (band calc tool) in Qgis software. All seven indices were computed using the formulas stated in the methodology. The seven VIs resulted images which can be as seen in Figure 4.1. The indices are, Red-edge simple Ratio vegetation Index (RERVI), Red-Edge Normalized Difference Vegetation Index (RENDVI), Red-Edge Enhanced Vegetation Index (RE-EVI2), Normalized Difference Water Index (NDWI), Normalized Difference Infrared Index (NDII), Normalized Difference Vegetation Index (NDVI) and Enhanced Vegetation Index (EVI2). The images show that the narrow spectral bands red-edge indices are the least saturated when compared to broad band and canopy water content VIs. Also, the broadband VIs are sensitive to Ecological effects such as drainage pattern and topography (Appendix 17) of which the other two categories of VIs do not have. Areas along river had a high VI value.

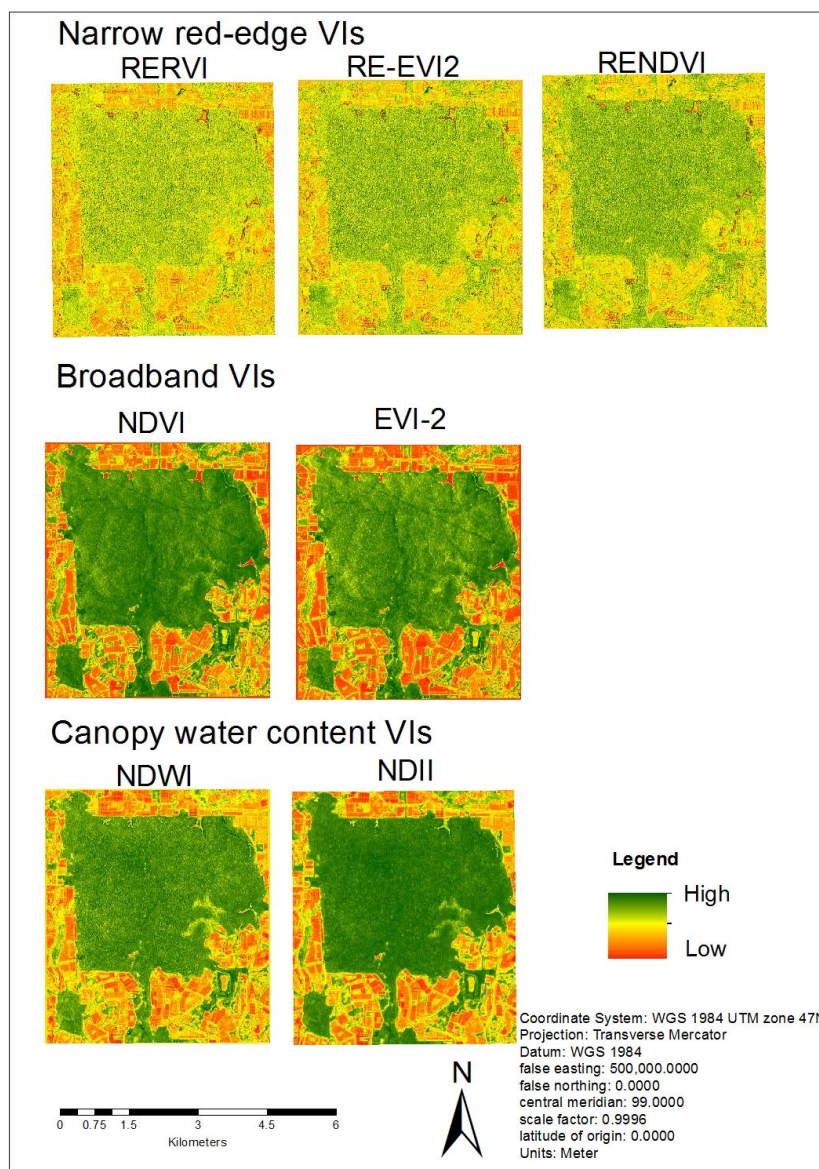


Figure 4.1: Three categories of VIs; Narrow red-edge, canopy water content and broad band VIs

## 4.2. Above ground biomass estimation (AGB)

The first step taken was to separate the upper and lower canopy trees using the criteria described in methodology. The biomass was then calculated using the allometric (Equation 3-8), which uses the tree height, DBH and wood density, for the AGB estimation. The wood density was assigned per tree species, based on the Asian tropical rain forest standardized values (Reyes et al., 1992).

### 4.2.1. Upper canopy Biomass

The ALS height and the field DBH was used to calculate the upper canopy biomass using the allometric model (Equation 3-8). The number of upper canopy trees varied among the plots as shown in (Table 4.1). Plot 27, 26 and 1 had the highest number of trees in the upper copies because they were single upper canopy layered plots. Thus almost all the trees could be captured clearly with ALS point cloud data.

Table 4.1: Descriptive statistics of upper canopy biomass

Upper canopy biomass								
Plot no	Mean Mg/plot	Std.dev	Min	Max	Sum	Number of trees	Mean height(m)	Mean DBH(cm)
1	0.19	0.19	0.03	0.77	3.59	19	12.46	17.82
2	0.53	0.83	0.05	3.14	6.92	13	17.56	27.02
3	0.48	0.57	0.04	1.74	6.20	13	18.21	25.11
4	0.85	0.83	0.09	2.18	5.97	7	21.72	34.63
5	0.42	0.27	0.12	1.01	4.64	11	21.29	29.35
6	0.60	0.65	0.06	2.11	6.61	11	18.95	27.28
7	1.08	0.92	0.18	2.93	16.17	15	23.95	34.85
8	0.32	0.29	0.09	1.09	5.43	17	16.66	23.56
9	0.69	1.35	0.06	3.75	4.85	7	18.35	28.36
10	0.25	0.16	0.07	0.64	2.52	10	19.22	22.08
11	0.29	0.29	0.05	0.96	2.60	9	15.31	22.23
12	0.84	1.04	0.16	3.29	6.70	8	20.44	30.30
13	0.27	0.30	0.06	1.02	4.55	17	15.75	22.79
14	0.43	0.48	0.12	1.63	6.08	14	16.73	25.46
15	0.62	0.40	0.10	1.33	9.88	16	19.06	31.26
16	0.26	0.18	0.07	0.61	3.44	13	17.59	20.65
17	0.61	0.79	0.05	2.88	10.36	17	17.85	27.22
18	0.62	1.01	0.06	3.38	6.24	10	19.86	25.77
19	0.28	0.20	0.11	0.90	5.37	18	18.76	21.29
20	0.47	0.53	0.10	1.66	5.61	12	23.54	25.63
21	0.31	0.21	0.07	0.99	6.14	19	19.80	22.03
22	0.47	0.63	0.04	2.68	8.03	17	20.94	24.52
23	0.83	1.50	0.13	5.70	10.82	13	23.87	28.38
24	0.52	0.45	0.10	1.81	6.20	12	20.55	29.23
25	0.57	0.41	0.12	1.27	4.56	8	22.52	29.30
26	0.23	0.40	0.04	1.72	4.40	19	12.96	20.11
27	0.09	0.08	0.02	0.41	1.92	22	12.93	14.31

#### 4.2.2. Lower canopy biomass

The lower canopy biomass was computed using DBH and height extracted from TLS point cloud data. The number of trees group in this category also varied per plot (Table 4.2). In multiple upper canopy layered plots, the TLS point cloud could not capture the tree top accurately compared to ALS. Thus, it resulted in more trees being grouped as lower canopy.

Table 4.2: Descriptive statistics of lower canopy biomass

Lower canopy biomass								
Plot No	Mean Mg/plot	Std.dev	Min	Max	Total	Number of trees	Mean Height(m)	Mean DBH(cm)
1	0.03	0.01	0.03	0.04	0.09	3	6.46	12.0
2	0.06	0.03	0.02	0.10	0.53	9	9.69	14.2
3	0.05	0.03	0.01	0.08	0.55	12	9.34	11.7
4	0.05	0.03	0.01	0.10	0.56	12	9.86	13.0
5	0.05	0.03	0.02	0.13	0.63	13	9.99	12.9
6	0.06	0.02	0.04	0.08	0.28	5	10.51	13.1
7	0.05	0.02	0.03	0.09	0.26	5	8.14	13.4
8	0.07	0.05	0.02	0.14	0.54	8	9.47	14.5
9	0.05	0.03	0.01	0.11	0.62	12	9.60	13.0
10	0.06	0.04	0.02	0.12	0.66	12	8.93	13.6
11	0.06	0.07	0.02	0.24	0.54	9	9.28	13.4
13	0.06	0.02	0.03	0.08	0.33	6	10.60	12.2
14	0.07	0.03	0.04	0.13	0.78	11	10.56	14.1
15	0.07	0.01	0.07	0.08	0.22	3	11.50	13.4
16	0.06	0.03	0.03	0.13	0.71	11	11.04	13.1
17	0.05	0.02	0.02	0.08	0.27	6	10.40	11.9
18	0.08	0.06	0.02	0.18	0.75	10	12.00	13.1
19	0.08	0.08	0.03	0.22	0.39	5	9.54	15.7
20	0.06	0.03	0.03	0.13	0.78	12	11.90	13.2
21	0.04	0.02	0.02	0.10	0.45	10	10.47	12.0
22	0.06	0.02	0.03	0.09	0.58	10	11.70	12.2
23	0.09	0.05	0.03	0.19	1.12	13	10.62	14.3
25	0.07	0.06	0.03	0.20	0.85	12	11.50	12.6
26	0.05	0.03	0.02	0.12	0.42	9	9.22	12.8
27	0.05	0.02	0.03	0.09	0.64	13	10.49	12.4

#### 4.2.3. Summary of the lower and upper canopy biomass

A total of 610 trees were used for the analysis of which 62% belonged to the upper canopy while 38% for the lower canopy (Table 4.3). The total biomass obtained was 182 Mg per plot of which 168Mg was of the upper and 14Mg for the lower canopy. The lower canopy biomass was less compared to the upper canopy biomass, since the upper canopy trees had higher height and DBH than the lower canopy trees (Table 4.1 and Table 4.2).

Table 4.3: Descriptive statistic of lower and upper canopy Biomass.

Statistics	Upper Canopy Biomass	Lower Canopy Biomass
Mean Biomass Mg/plot	0.443	0.058
Standard Deviation	0.621	0.036
Minimum	0.022	0.008
Maximum	5.704	0.241
Total biomass Mg/plot	167.91	13.57
No of trees	379	231

#### 4.2.4. Carbon stock estimation

The AGB was converted to carbon stock using (Equation 3-9). A combined upper and lower canopy carbon stock resulted to a total of 85 Mg per plot for 610 trees (Table 4.4). The carbon stock of the upper canopy was higher compared to the lower canopy.

Table 4.4: Descriptive statistics of lower and upper canopy carbon stock.

Statistics	Upper canopy carbon	Lower canopy carbon
Mean Carbon stock Mg/plot	0.208	0.027
Standard Deviation	0.292	0.017
Minimum	0.010	0.003
Maximum	2.680	0.113
Total Carbon stock Mg/plot	78.92	6.37
No of trees	379	231

### 4.3. Statistical Analysis

The following results are based on the statistics analysis done to assess the relationship between VIs and AGB. Linear and exponential regression were used to assess the relationship between VIs and upper Canopy biomass estimated from the ALS height and field DBH. The regression models were also used to assess the relationship between the VIs and the total biomass, which is a combination of upper canopy biomass and lower canopy biomass estimated from TLS height and DBH. A total of 112 pixels were used for the analysis. An average of four pixel values were obtained in each of the 27 plots used for this study.

#### 4.3.1. Linear relationship between upper canopy biomass and vegetation Indices.

##### Narrow red-edge band VIs

In this category, the VIs were computed using the red-edge spectral bands, which has proven to reduce saturation of the VIs (Figure 4.1). Three VIs were studied under this category, Red-edge Ratio Vegetation index (RERVI), Red-edge Normalized Difference Vegetation Index (RENDVI) and Red-edge Enhanced vegetation index (RE-EVI2). The results obtained are shown in the following sections.

##### Relationship between narrow red-edge indices and upper canopy biomass

The result (Figure 4.2a, b and c) show that there is a good linear relationship between upper canopy biomass and VIs. The coefficient of determination ( $r^2$ ) ranged from 0.59 to 0.63. RERVI explains most of the relationship with upper canopy biomass with 63 % meaning that 34% of the variation in the upper canopy biomass is not explained by the indices. Also, there is a minimal difference in the prediction level of the

three indices. The summary of the simple linear regression model (Table 4.5 and Appendix 1-3) showed that all the relationships were significant since the P-Value < 0.05.

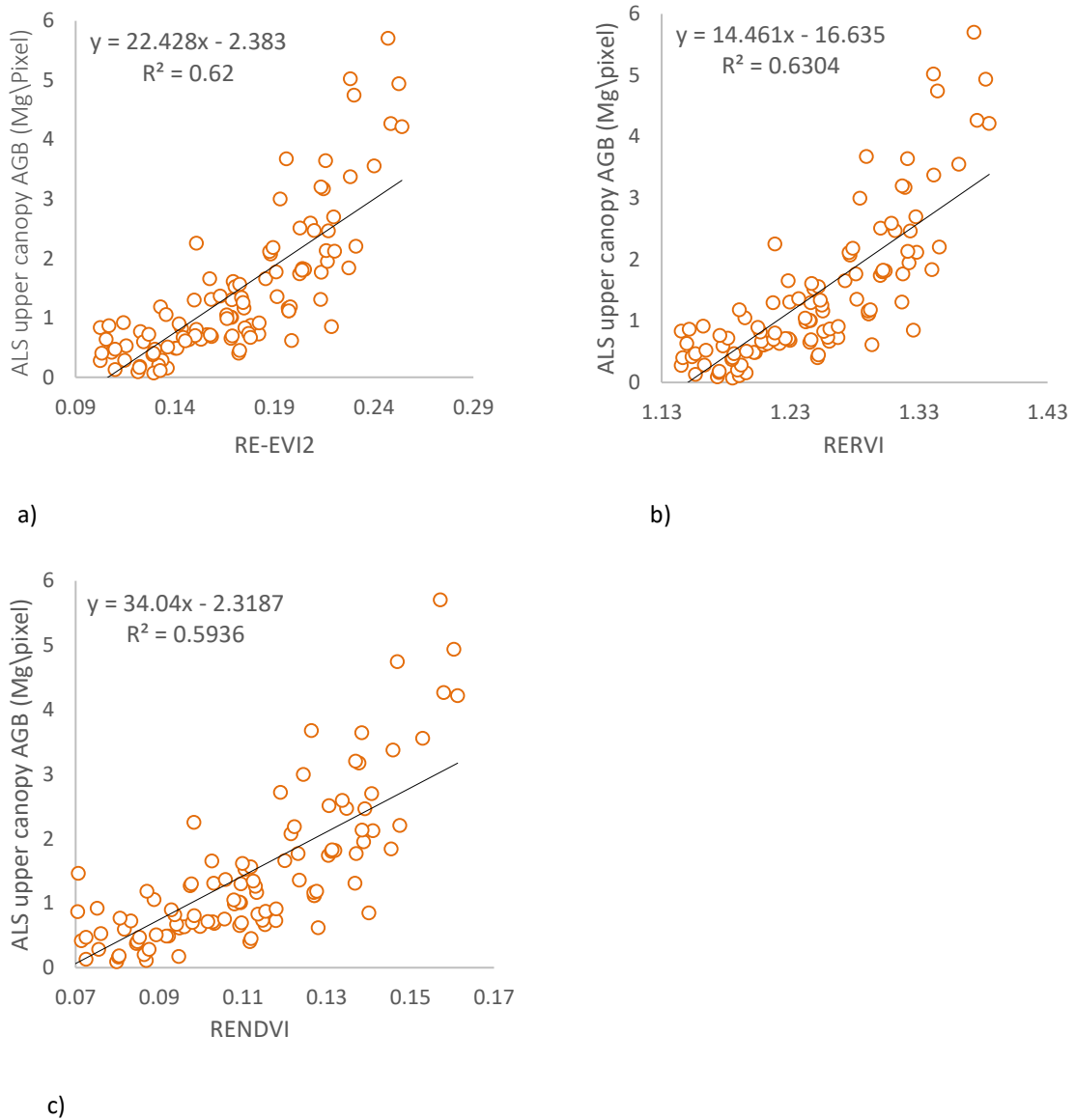


Figure 4.2: Scatter plot a b and c for the relationship between Narrow Red-edge vegetation indices and upper canopy biomass.

Table 4.5 : Regression statistics summary; Narrow Red-edge VIs and upper canopy biomass.

Spectral Index	R <sup>2</sup>	P-Value	Standard Error (Mg)
RE-EVI2	0.62	7.45E-25	0.736
RERVI	0.63	1.59E-25	0.725
RENDVI	0.59	3.40811E-23	0.723

P-Value <0.05 at 95 % confidence interval. Decision: There is a significant relationship between VIs and Upper Canopy biomass.

**Relationship between narrow red-edge indices and total biomass**

The results of the scatter plot (Figure 4.3 a b and c) show a good linear relationship between the VIs and total biomass. The  $r^2$  ranged from 0.60 to 0.64, RERVI had the highest relation with total biomass, explaining 64% of the total biomass, thus leaving 36% unexplained. The summary of the regression model (Table 4.6 and Appendix 4-6) also shows that the model is significant since the P-Value < 0.05.

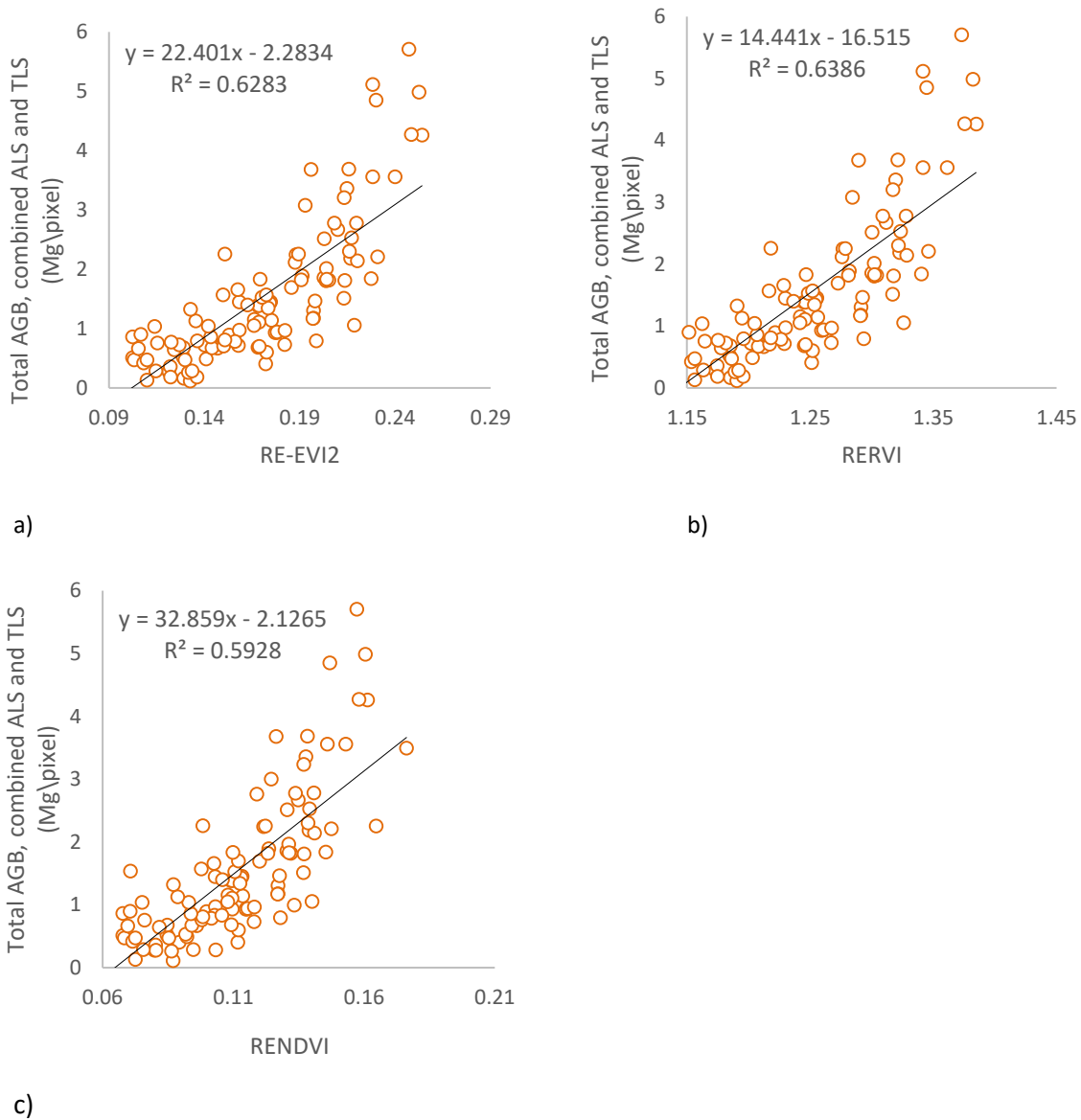


Figure 4.3: Scatter plot a b and c for the relationship between Narrow Red-edge vegetation indices and total biomass.

Table 4.6: Regression statistics summary; Narrow Red-edge VIs and total biomass.

Spectral Index	R <sup>2</sup>	P-Value	Standard Error (Mg)
RE-EVI2	0.63	2.18559E-25	0.722
RERVI	0.64	4.6003E-26	0.712
RENDVI	0.60	3.06071E-23	0.731

P-Value <0.05 at 95 % confidence interval. Decision: There is a significant relationship between VIs and total biomass

**Canopy water content VIs**

The indices in this category were computed by using the shortwave infrared (SWIR) and (NIR) spectral bands. In this category Normalized Difference Water Index (NDWI) and Normalized Difference Infrared Index (NDII) were analysed.

**Relationship between canopy water content indices and upper canopy biomass**

The results from the scatter plot (Figure 4.4 a, b), show that the indices NDWI and NDII have a weak linear relationship with upper canopy biomass. They only explain 23% to 31% of the variation, leaving an average of 73% of the upper canopy biomass unexplained. However, the linear regression summary (Table 4.7 and Appendix 7- 8) shows that both indices model are significant since the P-value < 0.05.

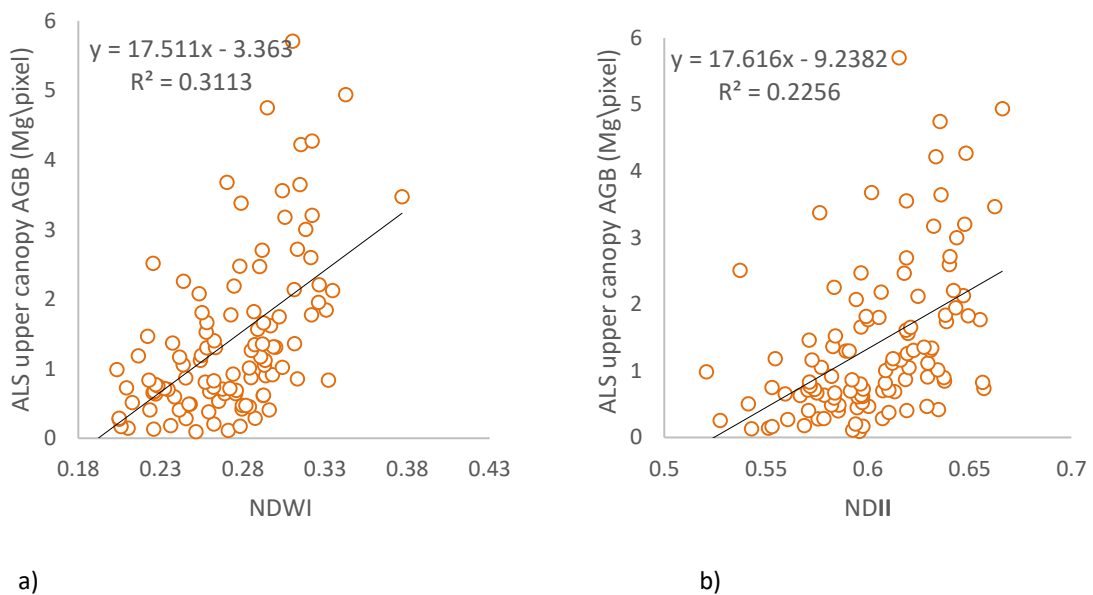


Figure 4.4: Scatter plot a, b showing the relationship between canopy water content VIs and upper canopy biomass.

Table 4.7: Regression statistics summary; canopy water content VIs and upper canopy biomass.

Spectral Index	R <sup>2</sup>	P-Value	Standard Error (Mg)
NDWI	0.31	1.43082E-10	0.959
NDII	0.23	1.2111E-07	1.019

P-Value <0.05 at 95 % confidence interval. Decision: There is a significant relationship between VIs and upper canopy biomass.

**Relationship between canopy water content indices and Total biomass**

The scatter plot results (Figure 4.5 a, b) shows a weak linear relationship between the canopy water content indices (NDWI and NDII) with total biomass. NDWI had a better relationship compared to NDII explaining 31 % of the variation while NDII follows with 23 percent. The model is also statistically significant based on the of the summary simple linear regression model (Table 4.8 and Appendix 9-10).

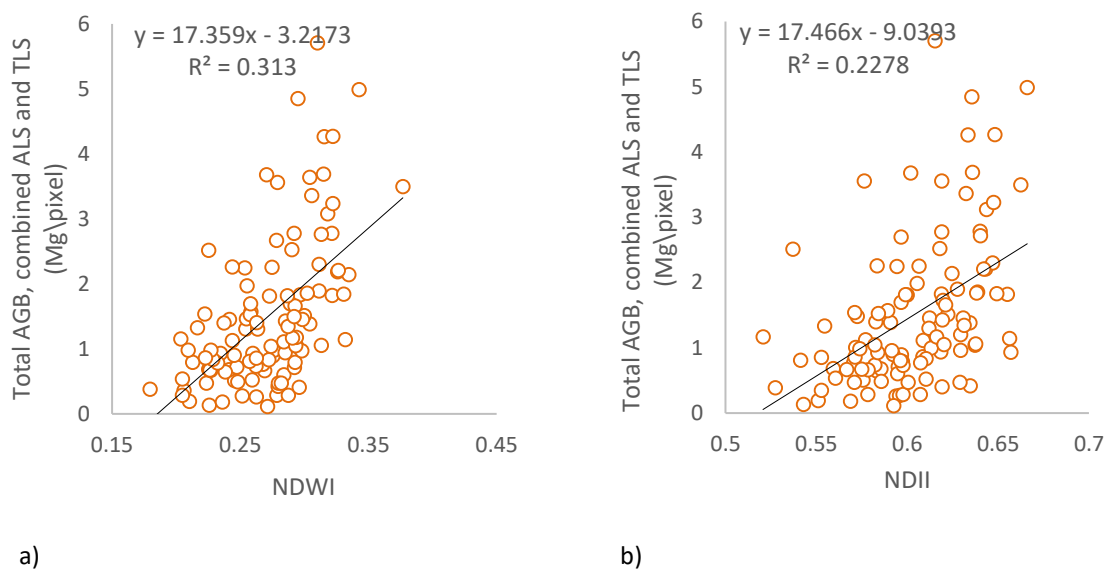


Figure 4.5: Scatter plot showing the relationship between canopy water content indices and total biomass

Table 4.8: Regression statistics summary; canopy water content VIs and total biomass

Spectral Index	R <sup>2</sup>	P-Value	Standard Error (Mg)
NDWI	0.31	1.43082E-10	0.477
NDII	0.23	1.03704E-07	1.004

P-Value <0.05 at 95 % confidence interval. Decision: There is a significant relationship between VIs and Total biomass

**Broadband VIs**

In this category the VIs were computed by using the red and NIR spectral bands. In this category, two vegetation indices were studied; Normalized Difference Vegetation Index (NDVI) and Enhanced Vegetation Index (EVI2).

**Relationship between broad band indices and upper canopy biomass**

The results of the scatter plot (Figure 4.6) shows that the VIs have a poor relationship with upper canopy biomass. There was also a minimal difference of 0.05 between the coefficient determination of both EVI2 and NDVI. Even though both relationships were poor, EVI2 performed better compared to NDVI. Moreover, the linear model of both indices was statistically significant based on the model summary results (Table 4.9 and Appendix 11-12).

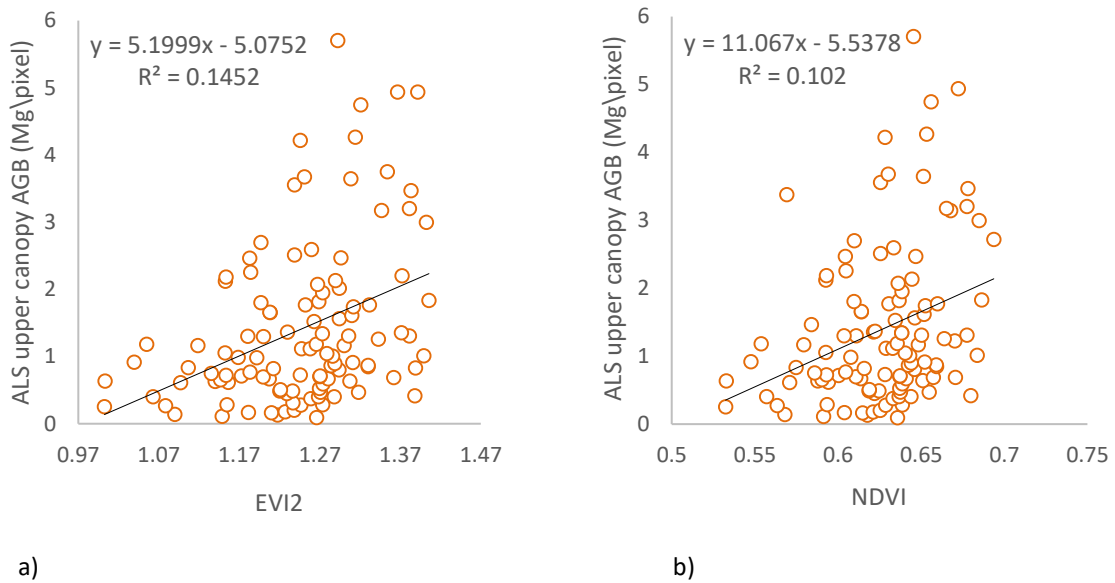


Figure 4.6: Scatter plot (a, b) showing the relationship between broad band indices and total biomass.

Table 4.9: Regression statistics summary; Broad band VIs and upper canopy biomass

Spectral Index	R <sup>2</sup>	P-Value	Standard Error (Mg)
EVI2	0.15	3.40229E-05	1.119
NDVI	0.10	0.000597362	1.104

P-Value <0.05 at 95 % confidence interval. Decision: There is a significant relationship between VIs and Upper canopy biomass

**Relationship between broadband indices and total biomass**

The result of the scatter plot (Figure 4.6a, b) show a weak relationship between the broadband indices and total biomass, EVI2 explains 15% of the relationship which is followed closely by NDVI with only 10% hence an average of 87% of the total biomass is not explained by the broadband indices models. The results of the regression models (Table 4.10 and Appendix 13-14) show that it's significant with all the VIs having a P-value < 0.05.

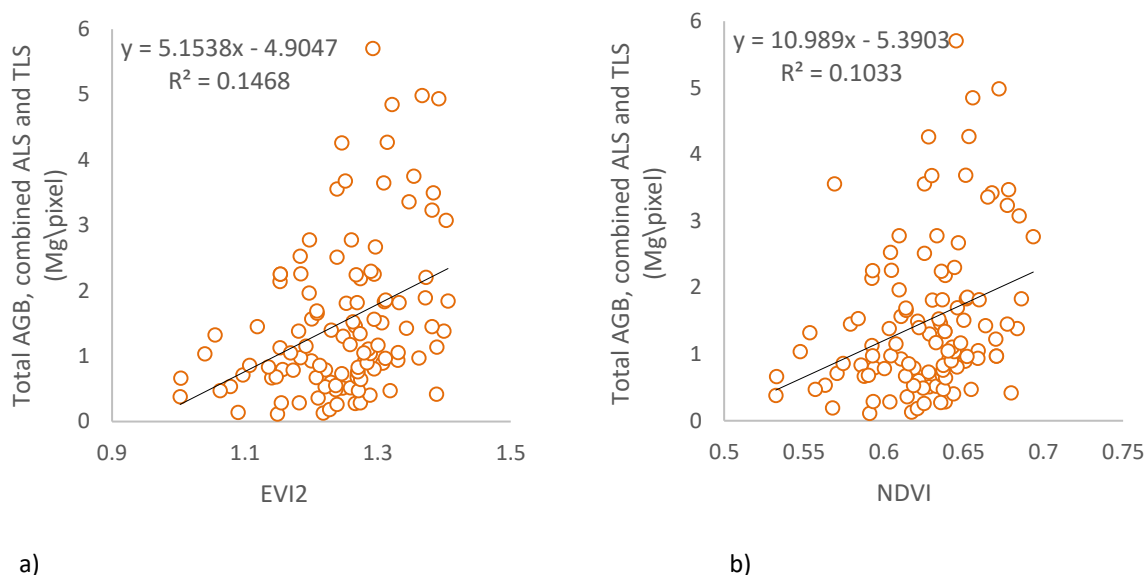


Figure 4.6: Scatter plot (a, b) showing the relationship between broad band indices and total biomass.

Table 4.10: Regression statistics summary; Broad band VIs and total biomass

Spectral Index	R <sup>2</sup>	P-Value	Standard Error (Mg)
EVI2	0.15	3.05E-05	1.101
NDVI	0.10	0.000549	1.093

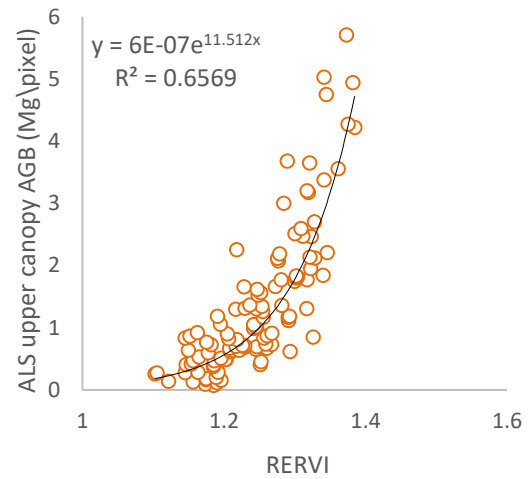
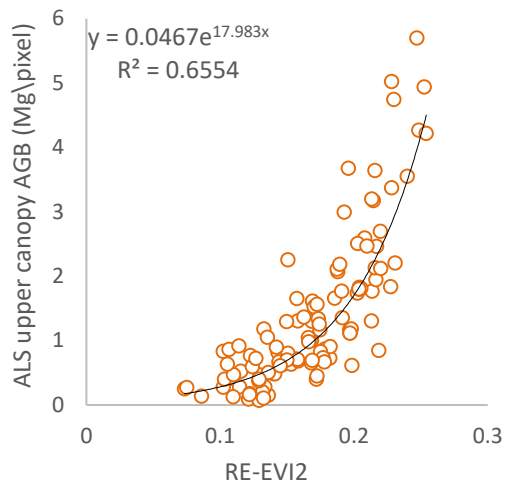
P-Value <0.05 at 95 % confidence interval. Decision: There is a significant relationship between VIs and Total biomass.

#### 4.3.2. Exponential relationship between VIs and upper canopy biomass

The exponential model shows the non-linear relationship between VIs and AGB. This means the VI does not increase with the increase in AGB since it reaches some point in which the VI becomes saturated.

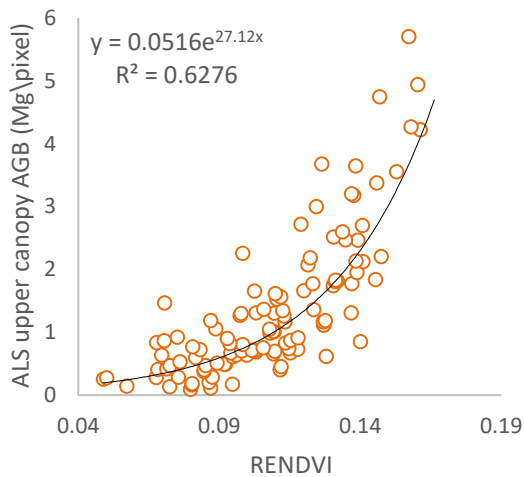
##### Narrow red-edge VIs

For this category the indices had a good non-linear relationship with the upper canopy biomass (Figure 4.7a, b and c). The RE-EVI2 and RERVI had the highest relationship explaining 66% of the upper canopy biomass, which is then followed closely with RENDVI explaining 63% of the relations. The  $r^2$  is slightly higher compared to the results of the linear regression model.



a)

b)



c)

Figure 4.7: Scatter plot a b and c showing the exponential relationship between Narrow Red-edge vegetation indices and upper canopy biomass.

#### Canopy water Content VIs

The results show a weak relationship between canopy water content indices with upper canopy biomass (Figure 4.8a, b). 32% of the relationship is explained by NDWI while 26% is explained by NDII. Thus, an average of 71 % of the variation in the upper canopy biomass is unexplained. This percentage is slightly lower compared to linear relationship model which had 73% of the relationship unexplained.

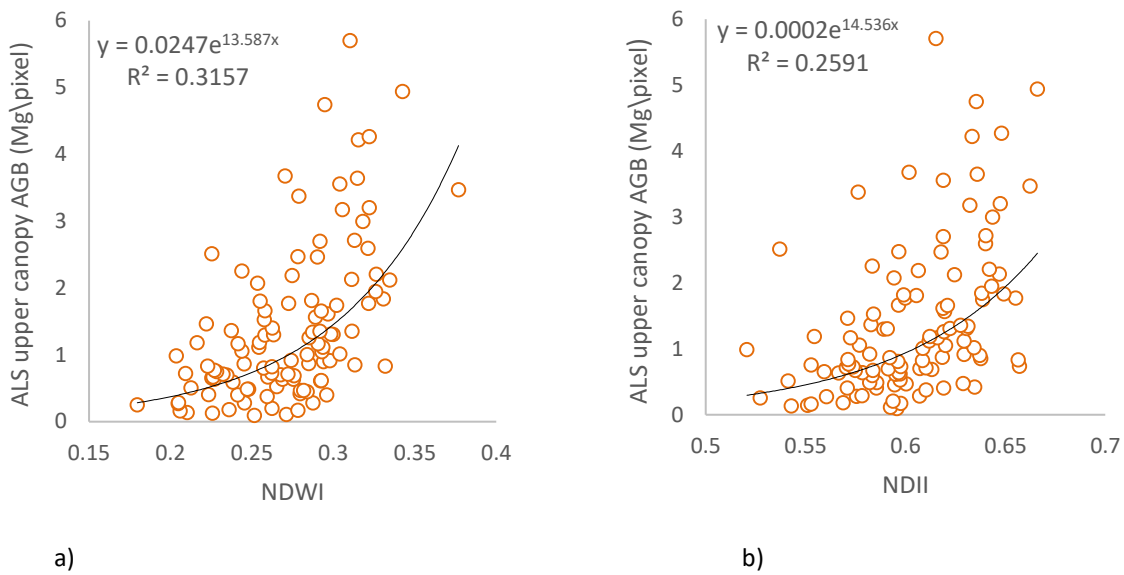


Figure 4.8: Scatter plot a, b showing exponential relationship between canopy water content vegetation indices and upper canopy biomass.

#### Broadband VIs

The results of the exponential relationship between broad band indices and upper canopy biomass showed to have a poor relationship with upper canopy biomass (Figure 4.9a, b). EVI2 explained only 15% of the variation of upper canopy biomass leaving 85% unexplained. Even though it is slightly higher than the linear relationship model. However, there was no significant improvement since it improved by only 0.003 for EVI2 and NDVI by 0.008 for the NDVI.

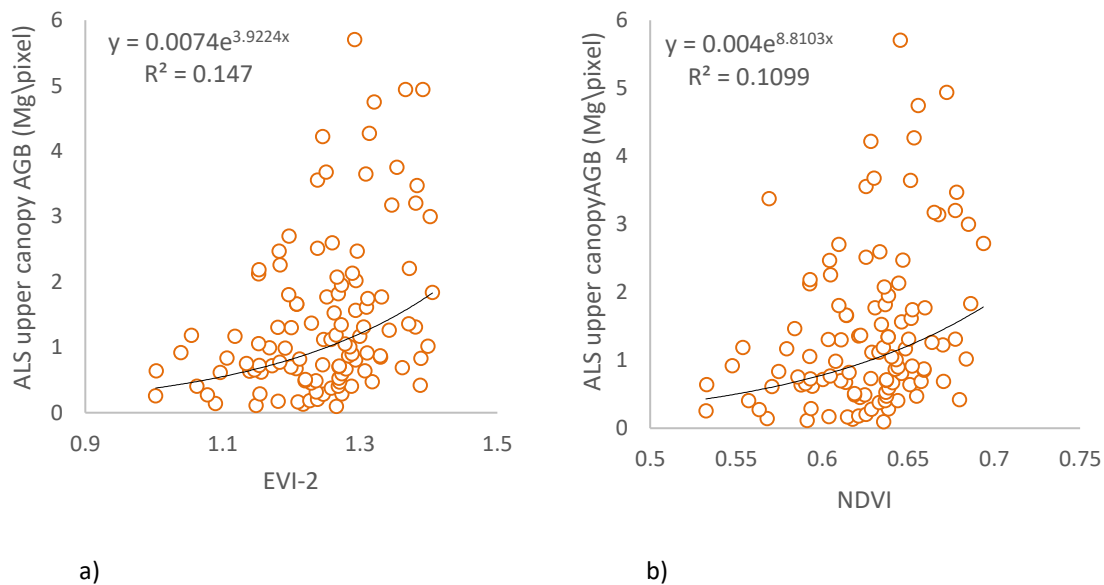
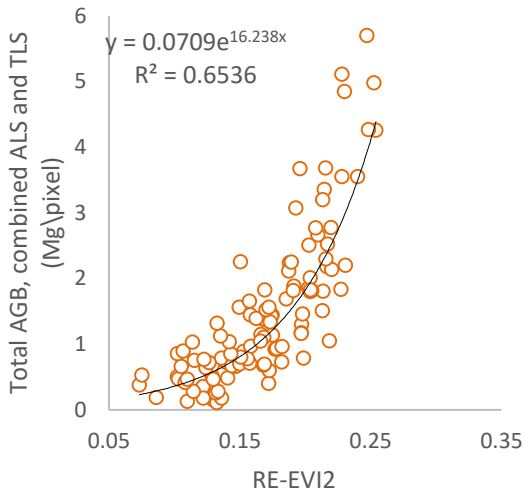


Figure 4.9: Scatter plot a, b showing exponential relationship between broadband vegetation indices and upper canopy biomass.

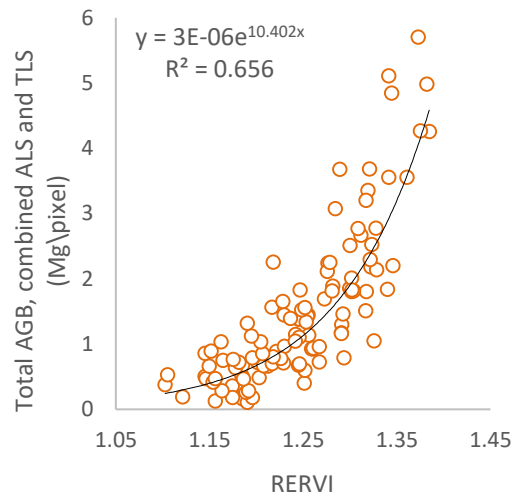
### 4.3.3. Exponential relationship between VIs and total biomass

#### Narrow edge band VIs

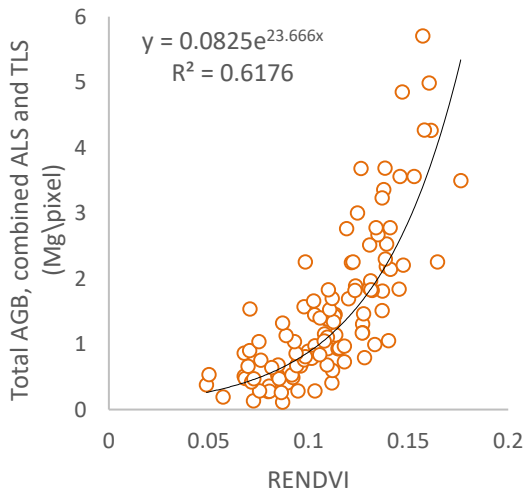
The results show a good exponential relationship between VIs and total biomass (Figure 4.10a b and c). The  $r^2$  ranged from 0.62 to 0.66 with RERVI having the highest relation with total biomass explaining 66% of the variation. This performance was better compared to the linear model which only explained 64% of the variations in the total biomass.



a)



b)



c)

Figure 4.10: Scatter plot a, b showing the exponential relationship between Narrow-edge vegetation indices and total biomass.

### Canopy water content VIs

The scatter plot (Figure 4.11a, b) results shows a weak non-linear relationship between the canopy water content indices with total biomass. NDWI had a slightly better relationship compared to NDII explaining 30% of the variation in the total biomass.

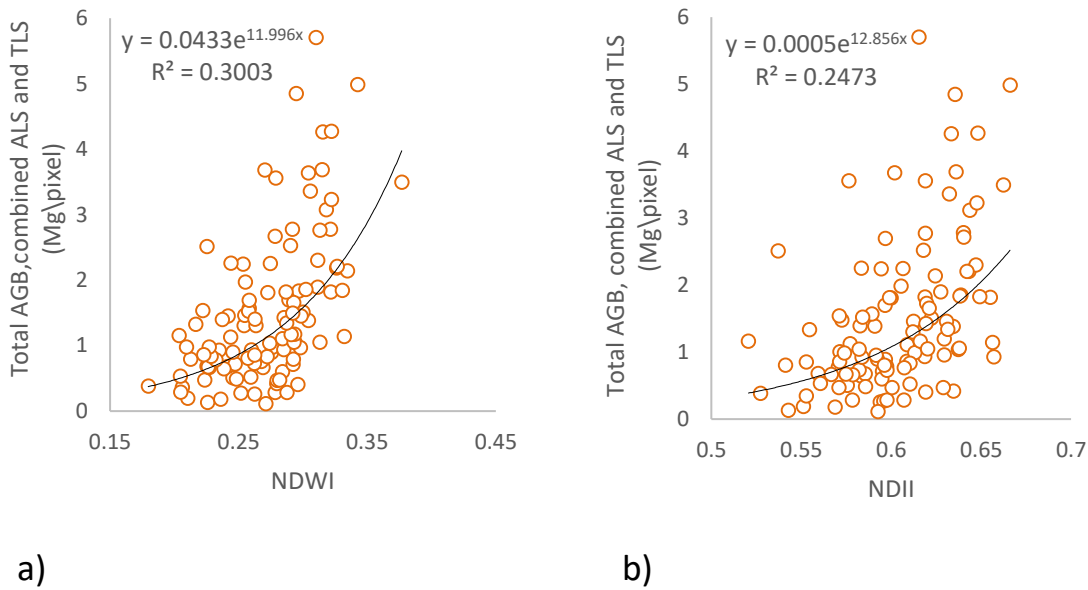


Figure 4.11: Scatter plots a, b showing the exponential relationship between canopy water content indices and total biomass.

### Broadband VIs

The result of the scatter plot (Figure 4.12a, b) show a weak relationship between the broadband indices and total biomass, having EVI2 explaining 15% of the relationship which is followed closely by NDVI with only 11%. Hence, an average of 87% of the total biomass which was not explained by the broad band indices.

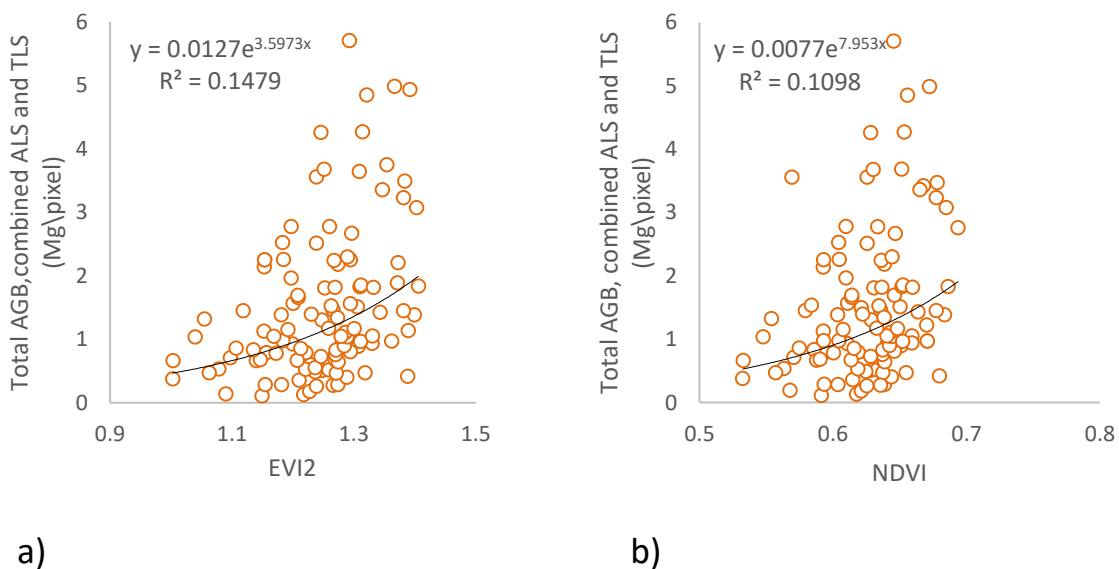


Figure 4.12: Scatter plots a, b showing exponential relationship between broadband indices and total biomass.

#### 4.3.4. Summary of the linear relationship and Exponential relationship with upper canopy biomass.

The results show that most of the indices performance was improved when using the exponential relationship when compared to the linear regression model. The  $r^2$  ranged from 0.63 to 0.1 for the linear relationship and 0.66 to 0.11 for the exponential model. Also, the RMSE reduced when using the exponential model (Table 4.11). Moreover, narrow red edge indices had the highest correlation, followed by the canopy water content indices and lastly the broadband VIs having the lowest relationship with upper canopy biomass for both exponential and the linear relationship models.

Table 4.11: Comparison between linear and exponential relationship; VIs and upper canopy biomass.

UPPER CANOPY BIOMASS					
Linear Relationship			Exponential Relationship		
Spectral Indices	R <sup>2</sup>	RMSE(Mg)	Spectral Indices	R <sup>2</sup>	RMSE(Mg)
RERVI	0.63	0.689	RERVI	0.66	0.599
RE-EVI2	0.62	0.729	RE-EVI2	0.66	0.618
RENDVI	0.59	0.721	RENDVI	0.63	0.618
NDWI	0.31	0.951	NDWI	0.32	0.980
NDII	0.23	0.990	NDII	0.26	0.991
EVI-2	0.15	1.109	EVI-2	0.15	1.170
NDVI	0.1	1.095	NDVI	0.11	1.150

#### 4.3.5. Summary of the linear relationship and Exponential relationship and total biomass

The results show that most of VIs relationship with the total biomass increased with the exponential model compared to the linear model (Table 4.12). The linear relationship model  $r^2$  ranged from 0.64 to 0.10, while for the exponential relationship it ranged from 0.66 to 0.11. Moreover, the RMSE also reduced for the exponential relationship. However, when the RMSE of the upper canopy biomass results is compared to the total biomass, the first was slightly higher.

Table 4.12: Comparison between linear and exponential relationship; VIs and total biomass

TOTAL BIOMASS					
Linear Relationship			Exponential relationship		
Spectral Indices	R <sup>2</sup>	RMSE(Mg)	Spectral Indices	R <sup>2</sup>	RMSE(Mg)
RERVI	0.64	0.706	RERVI	0.66	0.611
RE-EVI2	0.63	0.716	RE-EVI2	0.66	0.615
RENDVI	0.59	0.725	RENDVI	0.63	0.691
NDWI	0.31	0.939	NDWI	0.32	0.962
NDII	0.23	0.995	NDII	0.26	1.009
EVI-2	0.15	1.092	EVI-2	0.15	1.143
NDVI	0.103	1.084	NDVI	0.11	1.133

**4.3.6. Combination of VIs with TLS**

The estimated upper canopy biomass computed from the best VI model, which was the exponential equation for RERVI, was combined with estimated lower canopy biomass based on TLS data to obtain total biomass. The accuracy was assessed using total biomass obtained from combining ALS and TLS data. The results show a good linear relationship (Figure 4.13). The combined total biomass (VIs and TLS) explained 74% of the total biomass (measurements from ALS and TLS). Furthermore, the linear model is also significant (Table 4.13) since the P-value<0.05. Also, it has the lowest RMSE of 0.161 Mg.

Table 4.13: Regression statistics summary; Total biomass (VIs and TLS) and total biomass (ALS and TLS)

<i>Regression Statistics</i>	
Multiple R	0.859
R Square	0.739
Adjusted R Square	0.737
Standard Error	0.484
Observations	112

ANOVA					
	<i>df</i>	<i>SS</i>	<i>MS</i>	<i>F</i>	<i>Significance F</i>
Regression	1	73.155	73.155	312.272	6.50844E - 34
Residual	110	25.769	0.234		
Total	111	98.924			

	<i>Coefficients</i>	<i>Std.Error</i>	<i>t Stat</i>	<i>P-value</i>
Intercept	0.330	0.074	4.471	1.89981E-05
X Variable 1	0.689	0.039	17.671	6.50844E-34

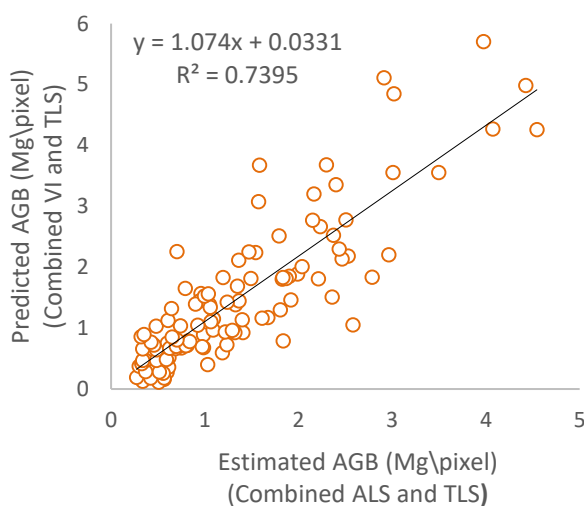


Figure 4.13: Scatter plot showing the relationship between Predicted AGB combined VIs (upper canopy) and TLS (lower canopy) and Estimated AGB combined ALS (upper canopy) and TLS (lower canopy) in Mg per 10m pixel size.

## 5. DISCUSSION

### 5.1. Above Ground Biomass Estimation

Ayer Hitam tropical rain forest is a multilayer forest with a complex structure which makes extracting accurate forest stand parameters such as height difficult. This is due to the high density of the forest. Therefore, it was considered necessary for this study to separate the forest layers into upper and lower canopy in order to minimize the errors in terms of extracting height (Lawas, 2016). Thus, the study used both LIDAR systems TLS and ALS which have their strength and weakness but by combining both systems it reduces the error when it comes to extracting forest stand parameters (Jung et al., 2011). Airborne LIDAR or Airborne Laser Scanner (ALS) has the strength to measure accurate height measurement. However, in a very dense forest structure the laser beam cannot penetrate into the lower canopy trees (Sadadi, 2016). On the other hand, with TLS there is a challenge in capturing the tree top of the upper canopy trees due to occlusion caused by the lower canopy trees (Figure 5.1), as a result, it leads to inaccurate height measurement (Dassot et al., 2011).

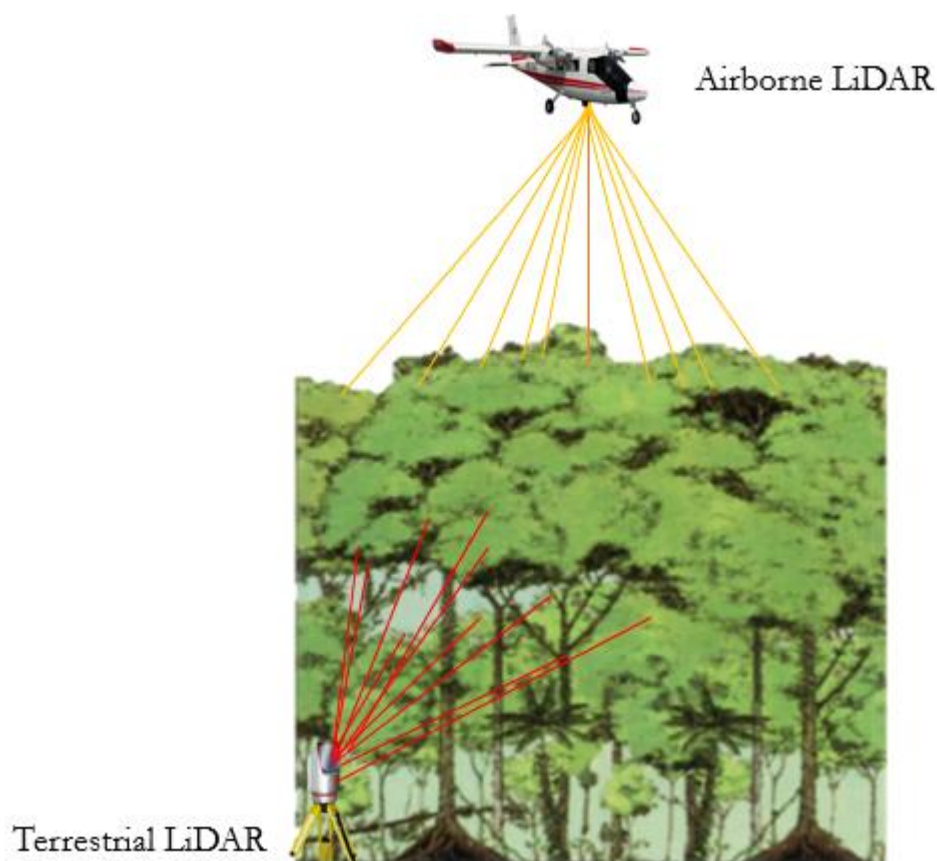


Figure 5.1: Airborne Lidar and Terrestrial laser scanner data acquisition.

Thus, forest biomass was calculated in two categories; upper and lower canopies biomass using an allometric equation (Chave et al., 2014), which used Height and DBH with the tree specific wood density. The upper canopy biomass was computed by using the field DBH and ALS height, while the lower canopy biomass

was computed using Height and DBH extracted from TLS point clouds data. A total biomass of 167.91 Mg and 13.71Mg per plot was obtained for the upper and lower canopy trees respectively. The biomass was combined to obtain a total biomass AGB of 181.49 Mg per plot. The AGB was then converted to carbon stock using Equation 3-9. A total of 85 Mg for the carbon stock was obtained having 78.92 Mg for the upper canopy trees and 6.38 Mg per plot for the lower canopy trees.

Finally, the AGB obtained was used to assess the relationship between VIs and AGB (upper canopy and total biomass) using linear and non-linear regression models. However, when it came to compare the upper canopy and total biomass performance with the VIs (Table 4.11 and Table 4.12), it was noted that there was a very minimal improvement in the  $r^2$  (0.0025). This was caused by the fact that there was a large number of trees in the upper canopy with 62% and 38% for the lower canopy trees. Moreover, the upper canopy has a high AGB of 168Mg, while the lower canopy only has 14Mg per plot. This means that the lower canopy trees contribute 8% to the total biomass, which was 185Mg while the upper canopy trees 92% (Table 4.3). In the study area most of the lower canopy trees also had a small DBH and height compared to the upper canopy trees (Table 4.1and Table 4.2), since the trees were younger. Thus, as seen in Figure 5.4 the upper canopy biomass is larger than the lower canopy biomass. Hence, a higher DBH and height resulted a high biomass and vice versa (Figure 5.2 and Figure 5.3). As can be seen in Figure 5.4 plot 12 and 24 did not have a lower canopy biomass. This is because the trees fell on the pixels that were considered as outliers since the pixels were not fully captured within the plot area.

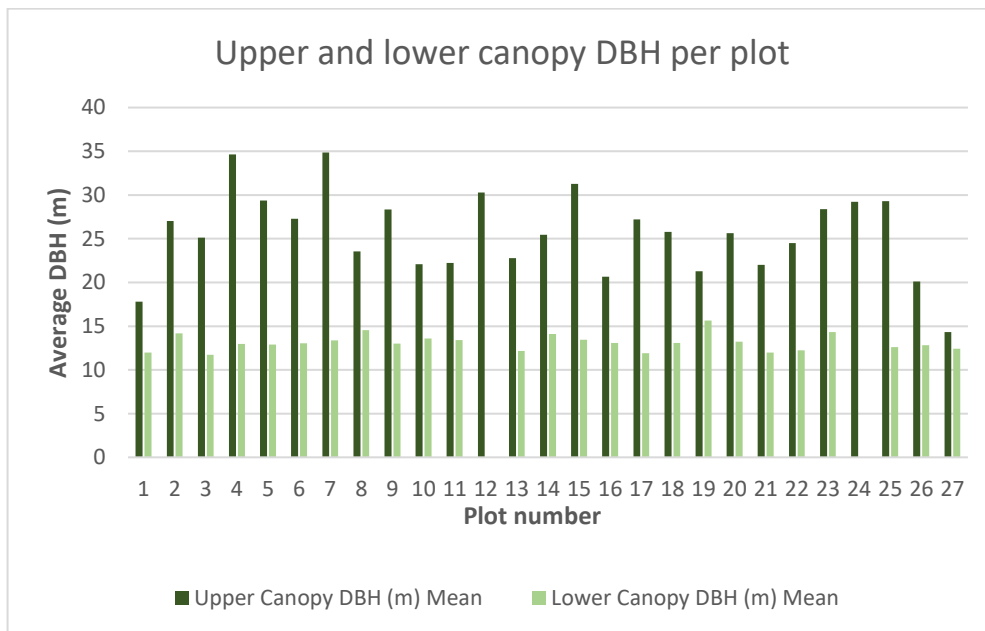


Figure 5.2: Comparison between upper and lower canopy average DBH per plot

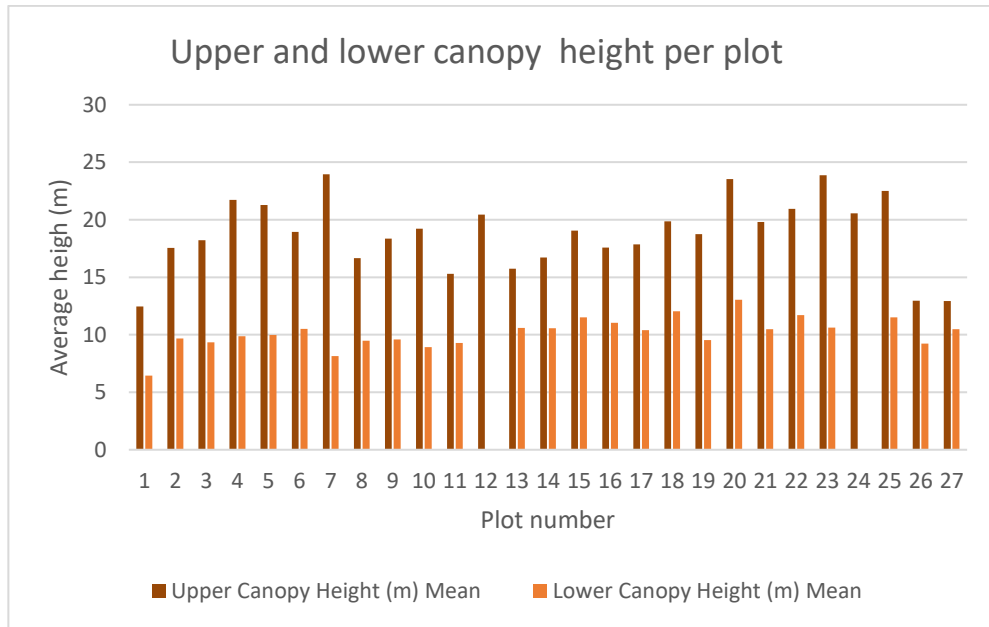


Figure 5.3: Comparison between upper and lower canopy average height per plot

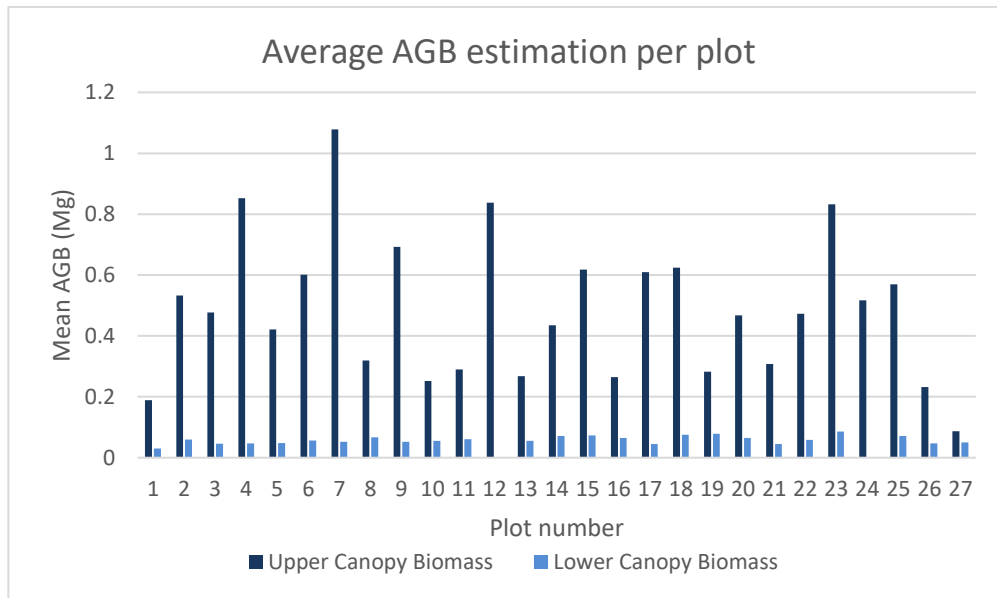


Figure 5.4: Comparison between upper and lower canopy biomass per plot

## 5.2. Linear and exponential relationship between VIs and AGB.

The research compared linear and exponential relationship between VIs and both upper canopy and total biomass. The results obtained showed that most VIs performed better with exponential relationship as compared to linear for both upper canopy and total biomass (Table 4.11 and Table 4.12) Also, the RMSE of the indices in all the tree categories reduced when using the exponential model than the linear relationship. Moreover, as seen in Figure 5.5, the linear relationship had negative residuals in Y axis while the exponential curve had no negative residuals in both the X and the Y axis, thus, showing that the linear model was not suitable.

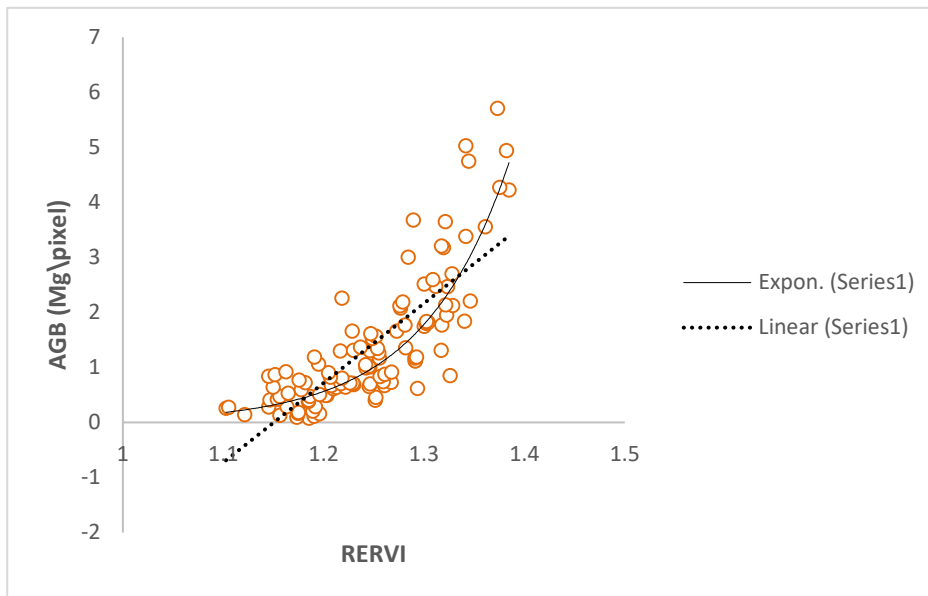


Figure 5.5: comparison between linear and exponential model: RERVI and AGB.

Furthermore, the Exponential model produced the best fit model with RERVI having the highest  $r^2$  of 0.66 and the least RMSE of 0.599Mg as compared to the linear model of the same index which had  $r^2$  of 0.63 and a RMSE of 0.689 Mg. The study finding is backed up by Wamunyima, (2005), who assessed the relationship between grass biomass and VIs using hyperspectral indices. The VIs were categorised into four categories which include: Normalized difference, Red-edge, three band and soil line hyperspectral indices. The study further compared the linear and the non-linear (exponential model) relationship between VIs and fresh grass biomass. The results obtained showed that the non-linear model performed better compared to the linear model with the  $r^2$  range increasing to 0.63- 0.78 from 0.60-0.75. This is because biomass has a nonlinear relationship with remote sensing variables when the vegetation reaches its maturity (Mauricio et al., 2016). In this case the biomass accumulation in the tree trunk continues to increase as the VIs values remain the same.

### 5.3. Relationship between VIs and AGB

The study groups the indices into three categories; the Narrow red-edge, broad band and canopy water content VIs. It was considered necessary for this research to study different categories of indices, since they had an influence on the performance of the AGB estimation depending the type of band used for the computation of the VIs. The spectral bands used were the Near Infrared (NIR), red, red-edge and Short Wave Infrared (SWIR) bands.

#### 5.3.1. Relationship between Narrow red-edge VIs and AGB

The Narrow red-edge indices were computed using the same formula as the broadband VIs. It was just that the red spectral band was replaced by the 740nm wavelength of red-edge spectral band which is band 6 for the Sentinel-2 image. The red edge VIs had the highest relationship with AGB for both upper canopy and total biomass. The highest  $r^2$  in this category was obtained from RERVI and RE-EVI2 explaining 66% of the variations in AGB. The indices in this category performed better than the broadband and the canopy water content VIs (Table 4.11 and Table 4.12). This is because the red-edge spectral band are located in between the red and the NIR regions, which are of high chlorophyll absorption and reflectance areas (Figure

5.6). Hence, it makes the red-edge spectral band more sensitive to the variations in the leaf properties and chlorophyll (Slonecker et al., 2009). Moreover, vegetation has a higher reflectance (around 60%) within the red-edge and NIR (700nm to 1300nm) portion of the electromagnetic spectrum compared red region (500nm to 700nm) which reflects less than 30% (Gitelson & Merzlyak, 1997). Furthermore, studies such as (Zhao et al., 2007; Chen et al., 2007) compared the performances of the VIs such as NDVI and SR in relation to biophysical properties such as LAI, using the red and the NIR bands with the red-edge bands, the findings were that modified red-edge indices had a better relationship by improving the  $r^2$  significantly than the standard indices using the red band.

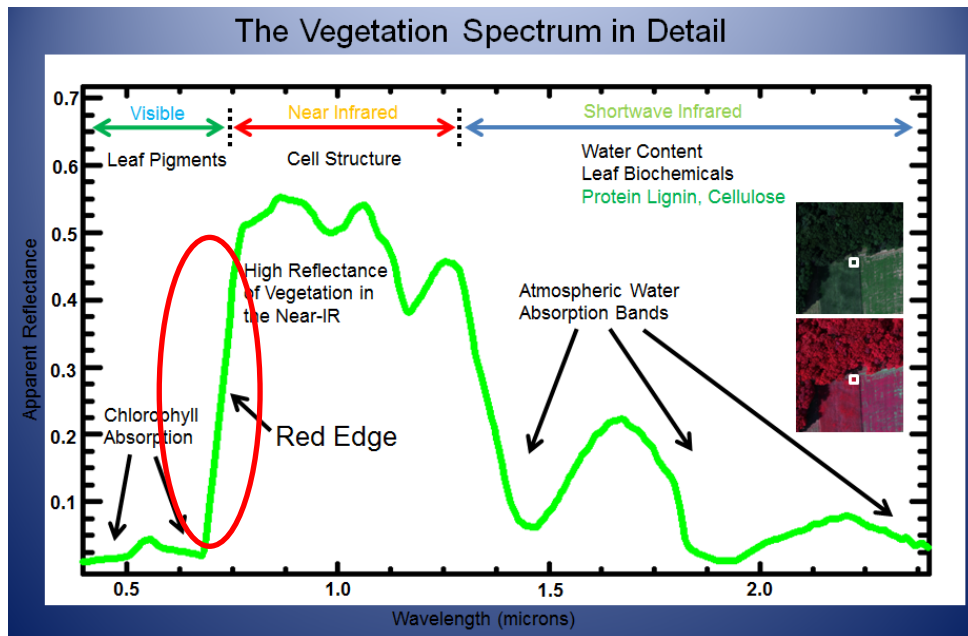


Figure 5.6: The position of the Red-edge along the electromagnetic spectrum.

Source: (Elowitz, 2016)

Winmore, (2012) examined the relationship between World-View 2 derived VIs to predict carbon stock in an indigenous forest in South Africa. The study compared the performance of the standard indices such as Simple ratio (SR), Soil Adjusted Vegetation index (SAVI) and NDVI, with the red-edge indices including the SR-RE, NDVI-RE, and SAVI-RE using simple linear regression. The result showed that the  $r^2$  increased when using the red-edge band in comparison to the red spectral band which achieved  $r^2$  was 0.62, 0.59 and 0.45 for the linear model. While for the non-linear model the  $r^2$  increased to 0.63, 0.61 and 0.58 for SR, NDVI, and SAVI respectively. However, when the red-edge band was used instead of the red spectral band for the linear model all the VIs achieved the same results with an  $r^2$  of 0.68, while the non-linear model yielded an  $r^2$  of 0.69, 0.70 and 0.68. Thus, the study concluded that the red-edge band improves the accuracy of the carbon stock estimation. Also, Mutanga et al., (2012) estimated biomass in a wetland ecosystem, which is characterized by mangrove, swamp forest, and coastal ecosystem by comparing the performance of the standard NDVI and the red-edge NDVI, the results obtained showed that the red-edge NDVI performed better with an  $r^2$  of 0.67 compared to the standard NDVI which obtain an  $r^2$  0.39. It is noted that the performance of the standard NDVI in these studies are slightly higher compared to the results obtained in this research since it used a Sentinel-2 medium resolution image of 10m. While the studies used World View-2 images which has a high spatial resolution of 2m, which based on previous studies have shown that the spatial resolution have an influence on the performance of the VIs in biomass estimation, since the higher the spatial resolution the better accuracy (Gara et al., 2016). Moreover, the studies analysed

a simple forest structure. Thus, the VIs were less saturated compared to the VIs used in this research which analysed a dense complex forest structure.

### **5.3.2. Relationship between canopy water content VIs and AGB**

The canopy water content index it had a weak relationship with AGB. Although it was better when compared to the broadband VIs, with values of the  $r^2$  ranging from 0.26 and 0.34 for NDII and NDWI respectively. This is because these indices were computed using SWIR bands, which has shown to be promising in biomass estimation in complex forest structure as compared to the broadband indices (Lu et al., 2004). The reason being that, the water content in the leaf continues to increase with the increase in the canopy cover. However, there is still limited studies on the potential of the canopy water content VIs in forest biomass estimation.

### **5.3.3. Relationship between broadband VIs and AGB**

The broadband indices had the weakest relationship with AGB for both upper canopy and total biomass (Table 4.11 and Table 4.12). The VIs included NDVI and EVI2. Even though EVI2 had a minimal improvement in the  $r^2$  by 0.05 compared to NDVI, the relationship with AGB was still poor. This result is backed up by Mcmorrow et al., (2001), the study's findings was that NDVI had a poor relationship with biomass in complex forest structure. Furthermore, Mganga et al., (2015), estimated AGB in Miombo woodlands in Kitwe and Mgaraganza forest areas in Tanzania by using Landsat TM derived NDVI. The study achieved  $r^2$  of 0.22 and 0.23 in both areas. This result is slightly higher than what was obtain in this study. This is because since the study area was not a complex forest structure as compared to Ayer Hitam forest. Also, Nugroho, (2006) obtained an  $r^2$  of 0.212 for EVI and 0.142 for NDVI when assessing the indices relationship between AGB the in tropical rainforest of Indonesia, the accuracy was low due to the problem of saturation.

Saturation occurs, especially when the vegetation reaches its maturity in cases of crops (Mutanga & Skidmore, 2004; Wang et al., 2016) while in this case it was because of the complex forest structure of the dense tropical rain forest (Lu et al., 2014; Das, 2012; Sinha et al., 2016). In such a situation the VIs cannot sense any more of the increase in biomass. This is because the saturation happens when vegetation cover the land fully or what is expressed sometimes by full leave area coverage. In this case the biomass continues to increase but the indices values does not change. VIs perform better in simple structure forest as compared to the dense forest (Lu et al., 2012). According to Wang et al., (2016) what contributes to saturation is the fact that the indices in this category are computed using the red spectral band (680nm) and the NIR. The red band tends to absorb radiation in the electromagnetic spectrum exponentially. In this case it does not continuously increase with an increase in the canopy cover, as the amount of red energy being absorb reaches its peak when the canopy closure is at 100%. While on the other hand, the NIR the reflectance increases due to multiple scattering as the canopy reach 100% (Thenkabail et al., 2000). Hence, it causes inequality in the ratio of the broad band indices such as NDVI and EVI2 due to the decrease is the red absorption band and the increase in the NIR. This will lead to poor estimation of biomass (Mutanga & Skidmore, 2004).

## **5.4. The combination of VIs with TLS.**

The total biomass estimated from combination of estimated upper canopy biomass from VIs and lower canopy biomass estimated from the TLS showed a good relationship with the total biomass estimated from combining ALS (upper canopy) and TLS (lower canopy) obtaining an  $r^2$  of 0.74 (Figure 4.13). This was better when compared to the results of using a single VI (Table 4.11 and Table 4.12). The upper canopy biomass estimated from the VIs was computed using the best VIs model which was RERVI. The idea

employed in this study of separating the canopy layers and integrating upper and lower canopy biomass, using different remote sensing sensors, is supported by Lawas, (2016) who combined ALS upper canopy biomass and TLS lower canopy biomass and obtained an  $r^2$  of 0.98. The accuracy obtained by Lawas, (2016) was higher compared to the one attained in this study. This is because LIDAR systems are capable of estimating canopy structure such as height and DBH, which enhances AGB computation (Popescu, 2007; Vaglio et al., 2016), but the optical medium resolution lacks this strength. Nonetheless optical satellite images have the ability to cover a larger area and they also have a high temporal resolution. The result has shown that integration of VIs and TLS improves the accuracy of biomass estimation. This means that VIs perform better when they are integrated with other remote sensing sensors. Moreover, the finding in this research has shown that the VIs have the potential of estimating upper canopy biomass hence they can be used as an alternative to ALS when estimating AGB at a larger scale.

### **5.5. Relevance of the Research for REDD+**

The REDD+ aim is to find an accurate method for biomass estimation which can also be cost effective. Based on the results obtained from this study. Sentinel-2 derived VIs have a potential in forest biomass estimation. Moreover, the image is freely available and it is also multi-spectral having 13 bands including the Red-edge and SWIR spectral bands. Moreover, it has a spatial resolution of 10m which is higher compared to other medium resolution satellite images. Furthermore, it also comes with the red-edge band which has shown to have a potential in reducing saturation. Also, the methods used in this study are feasible, in such a way that REDD+ can apply it at a larger scale including national and regional level. To top it up, since it has a high revisit time of 10 days, it will also enhance future monitoring of the forest biomass. Ultimately assisting REDD+ to be able to achieve its objective of reducing carbon dioxide emission in the atmosphere, which is in turn promoting sustainable forest management.

### **5.6. Limitations of the study.**

The use of the circular plot lead to some pixels being removed and considered as outliers since the plot area could not fit the square shaped pixels. Some trees that belong to the pixel that fell within the plot were left out since the pixel was not fully covered within the plot. Thus, they were considered not to be part of the sample.

All the Sentinel-2 spectral bands did not have the same resolution, some bands were 10m while others were 20m. Consequently, the 20m bands had to be resampled to 10m which might have affected the accuracy of the VIs in biomass estimation, due to the loss of spectral information.

The field samples collected had a shift due to the error of the GPS used. This made it difficult to match the trees with LIDAR data, especially the lower canopy trees. Thus, they had to be matched using the CHM extracted from the airborne LIDAR and UAV images.

The extraction of individual trees from the TLS was done manually through digitization, using the RiSCAN pro software. This was a very tedious process since some tree tags could not be identified and matched with the field data.

## 6. CONCLUSION AND RECOMMENDATION

### 6.1. Conclusion

The study shows that Sentinel-2 derived VIs have a potential in biomass estimation comparable to results achieved with other sensors. This study also shows that the exponential model including the red-edge improves the accuracy of biomass estimation. The broadband and the canopy water content VIs, have shown to have a poor estimation of AGB in complex forest structure due to saturation. The study reveals that VIs computed by using the red-edge spectral band are more suitable than VIs computed using the red spectral band in estimate tropical rainforest biomass. Also, the relationship between VIs and upper canopy biomass had the best fit model compared to the VIs relationship with the total biomass. Although there was a very minimal increase in the  $r^2$  of the total biomass, still it has a higher RMSE compared to the upper canopy biomass. Furthermore, the study has also shown that the nonlinear models are more suitable in assessing the relationship between VIs and AGB and combination of VIs with TLS improves the accuracy of the AGB estimation. The following are the conclusion remarks which are answering the research questions:

Is there a significant relationship between VIs and upper canopy biomass?

- The null hypothesis was rejected since P-Value of the regression model was  $< 0.05$  meaning that there was a significant relationship between VIs and upper canopy biomass. The best VI was RERVI with an  $r^2$  of 0.66.

Is there a significant relationship between VIs and total biomass?

- The null hypothesis was rejected since P-Value of the regression model were  $< 0.05$  meaning that there was a significant relationship between VIs and total biomass. The best VI was RERVI with an  $r^2$  of 0.66.

Is there a significant relationship between total biomass (VIs and TLS) and total biomass (ALS and TLS)?

- The null hypothesis was rejected since P-Value of the regression model were  $< 0.05$ . The combined VIs and TLS total biomass had a good relationship with total AGB obtained from TLS and ALS achieving an  $r^2$  of 0.74.

Which regression model best explains the relationship between the VIs and AGB?

- The exponential model was better compared to the linear model since almost all  $r^2$  of the VIs improved when using the exponential model. Also, the RMSE was lower for the nonlinear than the linear model.

### 6.2. Recommendation

- A more accurate GPS should be used for recording the coordinate of individual three to minimize the error when it comes to matching the biometric data with TLS and ALS point cloud data.
- Future research should also study the effect of topography on broadband VIs.
- Future research should use the red-edge VIs instead of the broadband VIs in large scale estimation of biomass in complex forest structure.

## LIST OF REFERENCES

---

- Abdel-rahman, E. M., Landmann, T., Kyalo, R., Ong, G., Mwalusepo, S., Sulieman, S., & Le, B. (2017). Predicting stem borer density in maize using RapidEye data and generalized linear models. *International Journal of Applied Earth Observations and Geoinformation*, 57, 61–74. doi.org/10.1016/j.jag.2016.12.008
- Adnan, I., Malek, A., Majid, N. M., & Alias, M. A. (2005). Mapping land use and decision support using remote sensing and geographical information system (GIS) at Ayer Hitam Forest Reserve (AHFR), Malaysia. *ResearchGate*, 79–89. Retrieved from <https://www.researchgate.net/publication/275337424>
- Alkama, R., & Cescatti, A. (2016). *Biophysical climate impacts of recent changes in global forest cover*. *Science* (Vol. 351). American Association for the Advancement of Science. Retrieved from <http://science.sciencemag.org/content/351/6273/600.abstract>
- Anderson, G. L., Hanson, J. D., & Haas, R. H. (1993). Evaluating landsat thematic mapper derived vegetation indices for estimating above-ground biomass on semiarid rangelands. *Remote Sensing of Environment*, 45(2), 165–175. doi.org/10.1016/0034-4257(93)90040-5
- AWF-WIKI. (Forest Inventory and Remote Sensing). (2016). Forest mensuration and remote sensing. Georg-August-Universität Göttingen, Germany. Retrieved on August 16, 2016 from [http://wiki.awf.forst.uni-goettingen.de/wiki/index.php/File:Terrestrial\\_laser\\_scanning.png](http://wiki.awf.forst.uni-goettingen.de/wiki/index.php/File:Terrestrial_laser_scanning.png)
- Badreldin, N., & Sanchez-Azofeifa, A. (2015). Estimating forest biomass dynamics by integrating multi-temporal Landsat satellite images with ground and airborne LiDAR data in the Coal Valley Mine, Alberta, Canada. *Remote Sensing*, 7(3), 2832–2849. doi.org/10.3390/rs70302832
- Baillarin, S. J., Meygret, A., Dechoz, C., Petrucci, B., Lacherade, S., Tremas, T., ... Spoto, F. (2012). Sentinel-2 level 1 products and image processing performances. *International Geoscience and Remote Sensing Symposium (IGARSS)*, 39(B1), 197-202. doi.org/10.1109/IGARSS.2012.6351959
- Baral, S. (2011). *Mapping Carbon Stock Using High Resolution Satellite Images In Sub-Tropical Forest Of Nepal*. Msc.Thesis. University of Twente, Faculty of Geo-Information Science and Earth Observation (ITC), Enschede, The Netherlands. Retrieved from [http://www.itc.nl/Pub/Home/library/Academic\\_output/AcademicOutput.html?p=11&y=11&l=20](http://www.itc.nl/Pub/Home/library/Academic_output/AcademicOutput.html?p=11&y=11&l=20)
- Basuki, T. M., van Laake, P. E., Skidmore, A. K., & Hussin, Y. A. (2009). Allometric equations for estimating the above-ground biomass in tropical lowland Dipterocarp forests. *Forest Ecology and Management*, 257(8), 1684–1694. doi.org/10.1016/j.foreco.2009.01.027
- Bienert, A., Scheller, S., Keane, E., Mullooly, G., & Mohan, F. (2006). Application of terrestrial laser scanner for the determination of forest inventory parameters. *International Archives of Photogrammetry, Remote Sensing and Spatial Information Science*, 36(5). Retrieved from [http://www.isprs.org/proceedings/XXXVI/part5/paper/1270\\_Dresden06.pdf](http://www.isprs.org/proceedings/XXXVI/part5/paper/1270_Dresden06.pdf)
- Breu, F., Guggenbichler, S., & Wollmann, J. (2012). *Manual for building tree volume and biomass allometric equations: from field measurement to prediction*. Rome, Italy: Food and Agriculture Organization of the United Nations (FAO). Retrieved from <http://www.fao.org/docrep/018/i3058e/i3058e.pdf>
- Calders, K., Newnham, G., Burt, A., Murphy, S., Raunonen, P., Herold, M., ... Kaasalainen, M. (2015). Nondestructive estimates of above-ground biomass using terrestrial laser scanning. *Methods in Ecology and Evolution*, 6(2), 198–208. doi.org/10.1111/2041-210X.12301
- Cao, Q., Miao, Y., Shen, J., Yu, W., Yuan, F., Cheng, S., ... Liu, F. (2016). Improving in-season estimation of rice yield potential and responsiveness to topdressing nitrogen application with Crop Circle active crop canopy sensor. *Precision Agriculture*, 17, 136–154. doi.org/10.1007/s11119-015-9412-y
- Ceccato, P., Flasse, S., Tarantola, S., Jacquemoud, S., & Grégoire, J.-M. (2001). Detecting vegetation leaf water content using reflectance in the optical domain. *Remote Sensing of Environment*, 77(1), 22–33. doi.org/10.1016/S0034-4257(01)00191-2
- Chave, J., Rejou-Mechain, M., Burquez, A., Chidumayo, E., Colgan, M. S., Delitti, W. B. C., ... Vieilledent, G. (2014). Improved allometric models to estimate the aboveground biomass of tropical trees. *Global Change Biology*, 20(10), 3177–3190. doi.org/10.1111/gcb.12629
- Chavez, P. S. (1988). An improved dark-object subtraction technique for atmospheric scattering

- correction of multispectral data An Improved Dark-Object Subtraction Technique for Atmospheric Scattering Correction of Multispectral Data \*. *Remote Sensing of Environment*, 24(3), 459–479. doi.org/10.1016/0034-4257(88)90019-3
- Chavez, P. S. (1996). Image-Based Atmospheric Corrections - Revisited and Improved. *Photogrammetric Engineering and Remote Sensing*, 62(9), 1025–1036. Retrieved from <http://www.unc.edu/courses/2008spring/geog/577/001/www/Chavez96-PERS.pdf>
- Chen, J., Yang, C., Wu, S., Chung, Y., Linton, A., & Chen, C. (2007). Leaf chlorophyll content and surface spectral reflectance of tree species along a terrain gradient in Taiwan 's Kenting National Park. *Botanical Studies*, 48, 71–77. Retrieved from <http://ejournal.sinica.edu.tw/bbas/content/2007/1/Bot481-08.pdf>
- CLOUDBRIDGE nature reserve. (2016). Tropical Rainforest. Retrieved August 16, 2016, from <http://www.cloudbridge.org/the-project/about-tropical-forests/>
- Collins, M. B. (2015). *Quantifying environmental indicators and assessing performance in tropical forest management*. Phd.Thesis. London School of Economics and Political Science (University of London). Retrieved from <http://etheses.lse.ac.uk/3073/>
- Das, S., & Singh, T. P. (2012). Correlation analysis between biomass and spectral vegetation indices of forest ecosystem. *International Journal of Engineering Research & Technology (IJERT)*, 1(5), 1–13. Retrieved from <http://www.ijert.org/view-pdf/532/correlation-analysis-between-biomass-and-spectral-vegetation-indices-of-forest-ecosystem>
- Das, S., & Singh, T. P. (2016). Forest Type, Diversity and Biomass Estimation in Tropical Forests of Western Ghat of Maharashtra Using Geospatial Techniques. *Small-Scale Forestry*, 15( 4), 517-532. doi.org/10.1007/s11842-016-9337-y
- Dassot, M., Constant, T., & Fournier, M. (2011). The use of terrestrial LiDAR technology in forest science: Application fields, benefits and challenges. *Annals of Forest Science*, 68(5), 959–974. doi.org/10.1007/s13595-011-0102-2
- Delegido, J., Verrelst, J., Alonso, L., & Moreno, J. (2011). Evaluation of sentinel-2 red-edge bands for empirical estimation of green LAI and chlorophyll content. *Sensors*, 11(7), 7063–7081. doi.org/10.3390/s110707063
- Dong, T., Liu, J., Qian, B., Zhao, T., Jing, Q., Geng, X., ... Shang, J. (2016). Estimating winter wheat biomass by assimilating leaf area index derived from fusion of Landsat-8 and MODIS data. *International Journal of Applied Earth Observation and Geoinformation*, 49, 63–74. doi.org/10.1016/j.jag.2016.02.001
- Elowitz, M. R. (2016). Imaging Spectroscopy (Hyperspectral Imaging). Retrieved February 10, 2017, from <http://www.markelowitz.com/Hyperspectral.html>
- EO. (2016). Earth Observation Portal Directory. Retrieved August 7, 2016, from <https://directory.eoportal.org/web/eoportal/satellite-missions/c-missions/copernicus-sentinel-2>
- ESA. (2015). *SENTINEL-2 User Handbook*. Paris, France: European Commission. Retrieved from [https://sentinel.esa.int/documents/247904/685211/Sentinel-2\\_User\\_Handbook](https://sentinel.esa.int/documents/247904/685211/Sentinel-2_User_Handbook)
- Fernández-Manso, A., Fernández-Manso, O., & Quintano, C. (2016). Sentinel-2A red-edge spectral indices suitability for discriminating burn severity. *International Journal of Applied Earth Observation and Geoinformation*, 50, 170–175. doi.org/10.1016/j.jag.2016.03.005
- Fernández-Manso, O., Fernández-Manso, A., & Quintano, C. (2014). Estimation of aboveground biomass in Mediterranean forests by statistical modelling of ASTER fraction images. *International Journal of Applied Earth Observation and Geoinformation*, 31(1), 45–56. doi.org/10.1016/j.jag.2014.03.005
- Frampton, W. J., Dash, J., Watmough, G., & Milton, E. J. (2013). Evaluating the capabilities of Sentinel-2 for quantitative estimation of biophysical variables in vegetation. *ISPRS Journal of Photogrammetry and Remote Sensing*, 82, 83–92. doi.org/10.1016/j.isprsjprs.2013.04.007
- Gao, B. (1996). NDWI -A Normalized Difference Water Index for Remote Sensing of Vegetation Liquid Water From Space. *Remote Sensing of Environment*, 58(3), 257–266. doi.org/10.1016/S0034-4257(96)00067-3
- Gara, T. W., Murwira, A., Dube, T., Sibanda, M., Donald, T., Ndaimani, H., ... Hatendi, C. M. (2016). Estimating forest carbon stocks in tropical dry forests of Zimbabwe : exploring the performance of high and medium spatial-resolution multispectral sensors. *Southern Forests: A Journal of Forest Science*,

- 1–10. doi.org/10.2989/20702620.2016.1233751
- Ghebremichael, Z. M. (2016). *Airborne LiDAR and Terrestrial laser scanner in assessing above ground biomass/carbon of Ayer Hitam forest reserve, Malaysia*. Msc.Thesis.University of Twente faculty of Geo-Information Science and Earth Observation. Retrieved from [http://www.itc.nl/library/papers\\_2016/msc/nrm/ghebremichael.pdf](http://www.itc.nl/library/papers_2016/msc/nrm/ghebremichael.pdf)
- Gisel Reyes, Sandra Brown, Jonathan Chapman, and A. E. L. (1992). *Wood Densities of Tropical Tree Species*. New Orleans, Louisiana. Retrieved from [https://www.srs.fs.usda.gov/pubs/gtr/gtr\\_so088.pdf](https://www.srs.fs.usda.gov/pubs/gtr/gtr_so088.pdf)
- Gitelson, A. ., & Merzlyak, M. . (1997). Remote estimation of chlorophyll content in higher plant leaves. *International Journal of Remote Sensing*, 18(12), 2691–2697. Retrieved from [http://calmit.unl.edu/people/agitelson2/pdf/28\\_IJRS\\_1997\\_Remote\\_estimation\\_chl\\_leaves.pdf](http://calmit.unl.edu/people/agitelson2/pdf/28_IJRS_1997_Remote_estimation_chl_leaves.pdf)
- Gizachew, B., Solberg, S., Næsset, E., Gobakken, T., Bollandsås, O. M., Breidenbach, J., ... Mauya, E. W. (2016). Mapping and estimating the total living biomass and carbon in low - biomass woodlands using Landsat 8 CDR data. *Carbon Balance and Management*, 11(1), 13. doi.org/10.1186/s13021-016-0055-8
- Gunlu, A., Ercanli, Baskent, E. Z., & Cakir, G. (2014). Estimating aboveground biomass using landsat TM imagery: A case study of Anatolian Crimean pine forests in Turkey. *Annals of Forest Research*, 57(2), 289–298. Retrieved from <http://afrjournal.org/index.php/afr/article/view/278>
- Guo, B. Bin, Qi, S. L., Heng, Y. R., Duan, J. Z., Zhang, H. Y., Wu, Y. P., ... Zhu, Y. J. (2017). Remotely assessing leaf N uptake in winter wheat based on canopy hyperspectral red-edge absorption. *European Journal of Agronomy*, 82, 113–124. doi.org/10.1016/j.eja.2016.10.009
- Hasmadi, I. M., Pakhriazad, H. Z., & Mohamad, F. S. (2010). Geographic Information System-Allocation Model for Forest Path: A Case Study in Ayer Hitam Forest Reserve, Malaysia. *American Journal of Applied Sciences*, 7(3), 376–380. doi.org/10.3844/ajassp.2010.376.380
- Heiskanen, J. (2006). Estimating aboveground tree biomass and leaf area index in a mountain birch forest using ASTER satellite data. *International Journal of Remote Sensing*, 27(6), 1135–1158. Retrieved from <http://www.tandfonline.com/doi/abs/10.1080/01431160500353858>
- Hudak, A. T., Evans, J. S., & Stuart Smith, A. M. (2009). LiDAR Utility for Natural Resource Managers. *Remote Sensing*, 1(4), 934–951. doi.org/10.3390/rs1040934
- Hunt, E. R., & Qu, J. J. (2013). Remote sensing of fuel moisture content from canopy water indices and normalized dry matter index. *Journal of Applied Remote Sensing*, 6(1), 1-10. doi.org/10.1117/1.JRS.6.061705
- IPCC. (1996). LUCF Sector for good practice guidance. In D. K. Jim Penman, Michael Gytarsky, Taka Hiraishi, Thelma Krug, T. N. Riitta Pipatti, Leandro Buendia, Kyoko Miwa, & K. T. and F. Wagner (Eds.), *Good Practice Guidance for Land Use, Land-Use Change and Forestry* (pp. 11–22). Kanagawa Japan: Institute for Global Environmental Strategies (IGES). Retrieved from [http://www.ipcc-nggip.iges.or.jp/public/gpplulucf/gpplulucf\\_files/Chp3/Chp3\\_1\\_Introduction.pdf](http://www.ipcc-nggip.iges.or.jp/public/gpplulucf/gpplulucf_files/Chp3/Chp3_1_Introduction.pdf)
- IPCC. (2006). *2006 IPCC Guidelines for National Greenhouse Gas Inventories Volume 4: Agriculture, Forestry and Other Land Use* (Vol. 4). Retrieved from <https://www.ipcc.ch/meetings/session25/doc4a4b/vol4.pdf>
- Jiang, Z., Huete, A. R., Didan, K., & Miura, T. (2008). Development of a two-band enhanced vegetation index without a blue band. *Remote Sensing of Environment*, 112(10), 3833–3845. doi.org/10.1016/j.rse.2008.06.006
- Jung, S.-E., Kwak, D.-A., Park, T., Lee, W.-K., & Yoo, S. (2011). Estimating Crown Variables of Individual Trees Using Airborne and Terrestrial Laser Scanners. *Remote Sensing*, 3(11), 2346–2363. doi.org/10.3390/rs3112346
- Kankare, V., Holopainen, M., Vastaranta, M., Puttonen, E., Yu, X., Hyypä, J., ... Alho, P. (2013). Individual tree biomass estimation using terrestrial laser scanning. *ISPRS Journal of Photogrammetry and Remote Sensing*, 75, 64–75. doi.org/10.1016/j.isprsjprs.2012.10.003
- Karna, Y. K., Hussin, Y. A., Gilani, H., Bronsveld, M. C., Murthy, M. S. R., Qamer, F. M., ... Baniya, C. B. (2015). Integration of WorldView-2 and airborne LiDAR data for tree species level carbon stock mapping in Kayar Khola watershed, Nepal. *International Journal of Applied Earth Observation and Geoinformation*, 38, 280–291. doi.org/10.1016/j.jag.2015.01.011
- Kociuba, W., Kubisz, W., & Zagorski, P. (2014). Use of terrestrial laser scanning (TLS) for monitoring and

- modelling of geomorphic processes and phenomena at a small and medium spatial scale in Polar environment (Scott River - Spitsbergen). *Geomorphology*, 212, 84–96. doi.org/10.1016/j.geomorph.2013.02.003
- Kumar, L., Sinha, P., Taylor, S., & Alqurashi, A. F. (2015). Review of the use of remote sensing for biomass estimation to support renewable energy generation. *Journal of Applied Remote Sensing*, 9(1), 1–15. <http://doi.org/10.1117/1.JRS.9.097696>
- Lawas, C. J. C. (2016). *Complementary use of Airborne LiDAR and Terrestrial laser scanner to assess above ground biomass/carbon in Ayer Hitam tropical rain forest reserve*. Msc. Thesis. University of Twente faculty of Geo-Information Science and Earth Observation. Retrieved from [http://www.itc.nl/library/papers\\_2016/msc/nrm/lawas.pdf](http://www.itc.nl/library/papers_2016/msc/nrm/lawas.pdf)
- Lefsky, M. A., Cohen, W. B., Parker, G. G., & Harding, D. J. (2002). Lidar remote sensing for ecosystem studies. *BioScience*, 52(1), 19–30. Retrieved from <http://www.fsl.orst.edu/rna/Documents/publications/Lidar%20remote%20sensing%20for%20ecosystem%20studies%20pub2813.pdf>
- Liang, X., Kankare, V., Hyypä, J., Wang, Y., Kukko, A., Haggren, H., ... Vastaranta, M. (2016). Terrestrial laser scanning in forest inventories. *ISPRS Journal of Photogrammetry and Remote Sensing*, 115, 63–77. doi.org/10.1016/j.isprsjprs.2016.01.006
- Lu, D. (2005). Aboveground biomass estimation using Landsat TM data in the Brazilian Amazon. *International Journal of Remote Sensing*, 26(12), 2509–2525. doi.org/10.1080/01431160500142145
- Lu, D., Chen, Q., Wang, G., Liu, L., Li, G., & Moran, E. (2014). A survey of remote sensing-based aboveground biomass estimation methods in forest ecosystems. *International Journal of Digital Earth*, 9(1), 63–105. doi.org/10.1080/17538947.2014.990526
- Lu, D., Chen, Q., Wang, G., Moran, E., Batistella, M., Zhang, M., ... Saah, D. (2012). Aboveground Forest Biomass Estimation with Landsat and LiDAR Data and Uncertainty Analysis of the Estimates. *International Journal of Forestry Research*, 1–16. doi.org/10.1155/2012/436537
- Lu, D., Mausel, P., Brondizio, E., & Moran, E. (2002). Above-Ground Biomass Estimation of Successional and Mature Forests Using TM Images in the Amazon Basin. In *Advances in Spatial Data Handling* (pp. 183–196). Berlin, Heidelberg: Springer Berlin Heidelberg. doi.org/10.1007/978-3-642-56094-1\_14
- Lu, D., Mausel, P., Brondizio, E., & Moran, E. (2004). Relationships between forest stand parameters and Landsat TM spectral responses in the Brazilian Amazon Basin. *Forest Ecology and Management*, 198(1), 149–167. doi.org/10.1016/j.foreco.2004.03.048
- Maas, H.-G., Bienert, A., Scheller, S., & Keane, E. (2008). Automatic Forest Inventory Parameter Determination from Terrestrial Laser Scanner Data. *International Journal of Remote Sensing*, 29(5), 1579–1593. doi.org/10.1080/01431160701736406
- Maltamo, M., Næsset, E., & Vauhkonen, J. (2014). *Forestry Applications of Airborne Laser Scanning*. (K. vonTimo P. T. Gadow, Ed.) Springer (Vol. 27). New York London: Springer Heidelberg. Retrieved from <http://link.springer.com/book/10.1007/978-94-017-8663-8>
- Mauricio, J., Pizaña, G., Manuel, J., & Hernández, N. (2016). Remote Sensing-Based Biomass Estimation. In M. Marghany (Ed.), *Environmental Applications of Remote Sensing* (pp. 3–40). InTech. doi.org/10.5772/61813
- Mauya, E. W., Hansen, E. H., Gobakken, T., Bollandsås, O. M., Malimbwi, R. E., & Næsset, E. (2015). Effects of field plot size on prediction accuracy of aboveground biomass in airborne laser scanning-assisted inventories in tropical rain forests of Tanzania. *Carbon Balance and Management*, 10(10), 1–14. doi.org/10.1186/s13021-015-0021-x
- Mcmorrow, J., Pelz, D., & Boyd, D. S. (2001). Mapping the biomass of Bornean tropical rain forest from remotely sensed data Mapping the biomass of Bornean tropical rain forest from remotely sensed data. *Global Ecology and Biogeography*, 10(4), 379–387. doi.org/10.1046/j.1466-822X.2001.00248.x
- Mermoz, S., Bouvet, A., Le Toan, T., & Mathieu, R. (2015). Under-estimation of biomass loss with REDD+ standard reporting method. In *2015 IEEE International Geoscience and Remote Sensing Symposium (IGARSS)* (pp. 3882–3885). IEEE. doi.org/10.1109/IGARSS.2015.7326672
- Mganga, N. D., & Lyaruu, H. V. M. (2015). Applicability of Satellite Remote Sensing in Accounting Above- Ground Carbon in Miombo Woodlands. *International Journal of Advanced Remote Sensing and GIS*, 4(1), 1334–1343. Retrieved from <http://technical.cloud-journals.com/index.php/IJARSG/article/view/Tech-457>

- Michael, G. (2001). Rainforest Biomes. Retrieved February 10, 2017, from <http://www.blueplanetbiomes.org/rainforest.htm>
- Mohd, A., Yaman, A. R., & Jamaludin, M. A. (1999). Recreational opportunities for public use in Ayer Hitam Forest: Setting the stage and park management approach. *Pertanika Journal Tropical Agricultural Science*, 22(2), 161–166. Retrieved from <https://core.ac.uk/download/files/452/12223084.pdf>
- Mutanga, O., Adam, E., & Azong, M. (2012). High density biomass estimation for wetland vegetation using WorldView-2 imagery and random forest regression algorithm. *International Journal of Applied Earth Observations and Geoinformation*, 18(August), 399–406. doi.org/10.1016/j.jag.2012.03.012
- Mutanga, O., & Skidmore, A. K. (2004). Hyperspectral band depth analysis for a better estimation of grass biomass (*Cenchrus ciliaris*) measured under controlled laboratory conditions. *International Journal of Applied Earth Observation and Geoinformation*, 5(2), 87–96. doi.org/10.1016/j.jag.2004.01.001
- Mutanga, O., & Skidmore, A. K. (2004). Narrow band vegetation indices overcome the saturation problem in biomass estimation. *International Journal of Remote Sensing*, 25(19), 3999–4014. doi.org/10.1080/01431160310001654923
- Muukkonen, P., & Heiskanen, J. (2005). Estimating biomass for boreal forests using ASTER satellite data combined with standwise forest inventory data. *Remote Sensing of Environment*, 99(4), 434–447. doi.org/10.1016/j.rse.2005.09.011
- Næsset, E., Ørka, H. O., Solberg, S., Bollandsås, O. M., Hansen, E. H., Mauya, E., ... Gobakken, T. (2016). Mapping and estimating forest area and aboveground biomass in miombo woodlands in Tanzania using data from airborne laser scanning, TanDEM-X, RapidEye, and global forest maps: A comparison of estimated precision. *Remote Sensing of Environment*, 175, 282–300. doi.org/10.1016/j.rse.2016.01.006
- NASA. (2016). Climate Change: Vital Signs of the Planet: Causes. Retrieved May 31, 2016, from <http://climate.nasa.gov/causes/>
- Njoku, E. G. (2013). Encyclopedia of Remote Sensing. *Journal of Chemical Information and Modeling*, 53(9), 1689–1699. Retrieved from [http://staff.washington.edu/dushaw/epubs/Tomography\\_Ency\\_Remote\\_Sense\\_Springer\\_2014.pdf](http://staff.washington.edu/dushaw/epubs/Tomography_Ency_Remote_Sense_Springer_2014.pdf)
- Nugroho, N. P. (2006). *Estimating Carbon Sequestration in Tropical Rainforest using Intergrated Remote Sensing and Ecosystem Productivity Modelling*. Msc. Thesis. University of Twente Faculty of Geo-information Science and Earth observation, . Retrieved from [http://www.itc.nl/library/papers\\_2006/msc/nrm/nugroho.pdf](http://www.itc.nl/library/papers_2006/msc/nrm/nugroho.pdf)
- Padilla, F. M., Pe, M. T., Gallardo, M., & Thompson, R. B. (2017). Determination of sufficiency values of canopy reflectance vegetation indices for maximum growth and yield of cucumber. *European Journal of Agronomy*, 84, 1–15. doi.org/10.1016/j.eja.2016.12.007
- Peters, A. J. (2007). Performance evaluation of spectral vegetation indices using a statistical sensitivity function. *Remote Sensing of Environment*, 106 (1), 59–65. doi.org/10.1016/j.rse.2006.07.010
- Petrie, G., & Toth, C. K. (2008). Terrestrial Laser Scanner. In J. Shan & C. K. Toth (Eds.), *Topographic Laser Ranging and Scanning Principles and Processing* (pp. 87–128). Boca Raton, United States of America: Taylor & Francis Group. Retrieved from <http://citeseerx.ist.psu.edu/viewdoc/download?doi=10.1.1.112.9793&rep=rep1&type=pdf>
- Phua, M., Ling, Z., Wong, W., Korom, A., Ahmad, B., & Besar, N. A. (2014). Estimation of Above-Ground Biomass of a Tropical Forest in Northern Borneo Using High-resolution Satellite Image. *Journal of Forest and Environmental Science*, 30(2), 233–242. doi.org/10.7747/JFS.2014.30.2.233
- Popescu, S. C. (2007). Estimating biomass of individual pine trees using airborne lidar. *Biomass and Bioenergy*, 31(9), 646–655. doi.org/10.1016/j.biombioe.2007.06.022
- Prasad, O. P., Hussin, Y. A., Weir, M. J. C., & Karna, Y. K. (2016). Derivation of Forest Inventory Parameters for Carbon Estimation using Terrestrial Lidar. *International Archives of Photogrammetry, Remote Sensing and Spatial Information Science*, 41(B8). doi.org/10.5194/isprsarchives-XLI-B8-677-2016
- Saari, N. S., M, W. R. W., Kamzaih, & K., F.-H. (2014). Community structure of trees in Ayer Hitam Forest Reserve, Puchong, Selangor, Malaysia. *ResearchGate*, 77(1), 73–86. Retrieved from <https://www.researchgate.net/publication/270106458>
- Sadadi, O. (2016). *Accuracy of measuring tree height using Airborne LiDAR and Terrestrial Laser Scanner and its effect on estimating forest biomass and carbon stock in Ayer Hitam tropical rain forest, Malaysia*. Msc.thesis.University of Twente Faculty of Geo-Information and Earth observation. Retrieved from <http://www.itc.nl/>

- library/papers\_2016/msc/nrm/ojoatre.pdf
- Satellite Imaging Corporation (SIC). (2016). Sentinel-2A Satellite Sensor (10m). Retrieved August 7, 2016, from <http://www.satimagingcorp.com/satellite-sensors/other-satellite-sensors/sentinel-2a/>
- Sibanda, M., Mutanga, O., & Rouget, M. (2017). Testing the capabilities of the new WorldView-3 space-borne sensor's red-edge spectral band in discriminating and mapping complex grassland management treatments. *International Journal of Remote Sensing*, 38(1), 1–22. doi.org/10.1080/01431161.2016.1259678
- Silleos, N. G., Alexandridis, T. K., Gitas, I. Z., & Perakis, K. (2006). Vegetation Indices: Advances Made in Biomass Estimation and Vegetation Monitoring in the Last 30 Years. *Geocarto International*, 21(4), 21–28. doi.org/10.1080/10106040608542399
- Sinha, S., Jeganathan, C., Sharma, L. K., & Nathawat, M. S. (2016). Developing synergy regression models with space-borne ALOS PALSAR and Landsat TM sensors for retrieving tropical forest biomass. *Journal of Earth System Science*, 125(4), 725–735. doi.org/10.1007/s12040-016-0692-z
- Sium, M. T. (2015). *Application of Very high resolution imagery and Terrestrial Laser Scanning for estimating carbon stock in tropical rain forest of Royal Belum, Malaysia*. Msc.Thesis.University of Twente Faculty of Geo-Information Science and Earth Observation. Retrieved from [http://www.itc.nl/library/papers\\_2015/msc/nrm/sium.pdf](http://www.itc.nl/library/papers_2015/msc/nrm/sium.pdf)
- Slonecker, T., Haack, B., & Price, S. (2009). Spectroscopic Analysis of Arsenic Uptake in Pteris Ferns. *Remote Sensing*, 1(4), 644–675. doi.org/10.3390/rs1040644
- Sousa, A. M. O., Gonçalves, A. C., Mesquita, P., & Marques da Silva, J. R. (2015). Biomass estimation with high resolution satellite images: A case study of Quercus rotundifolia. *ISPRS Journal of Photogrammetry and Remote Sensing*, 101, 69–79. doi.org/10.1016/j.isprsjprs.2014.12.004
- Srinivasan, S., Popescu, S. C., Eriksson, M., Sheridan, R. D., & Ku, N. W. (2015). Terrestrial laser scanning as an effective tool to retrieve tree level height, crown width, and stem diameter. *Remote Sensing*, 7(2), 1877–1896. doi.org/10.3390/rs70201877
- Thenkabail, P. S., Smith, R. B., & Pauw, E. De. (2000). Hyperspectral Vegetation Indices and Their Relationships with Agricultural Crop Characteristics. *Remote Sensing of Environment*, 71(2), 158–182. doi.org/10.1016/S0034-4257(99)00067-X
- Tsendbazar, N. (2011). *Object Based Image Analysis Of Geo-Eye VHR Data To Model Above Ground Carbon Stock In Himalayan Mid-Hill Forests, Nepal*. Msc.Thesis. University of Twente, Faculty of Geo-Information Science and Earth Observation (ITC), Enschede, The Netherlands. Retrieved from [http://www.itc.nl/Pub/Home/library/Academic\\_output/AcademicOutput.html?p=11&y=11&l=20](http://www.itc.nl/Pub/Home/library/Academic_output/AcademicOutput.html?p=11&y=11&l=20)
- Vaglio Laurin, G., Puletti, N., Chen, Q., Corona, P., Papale, D., & Valentini, R. (2016). Above ground biomass and tree species richness estimation with airborne lidar in tropical Ghana forests. *International Journal of Applied Earth Observation and Geoinformation*, 52, 371–379. doi.org/10.1016/j.jag.2016.07.008
- Van Laar, A., & Akca, A. (2007). *Forest Mensuration*. (M. T. Klaus Von Gadow, Timo Pukkala, Ed.) Springer (Vol. 13). Dordrecht, The Netherlands: Springer Netherlands. doi.org/10.1126/science.24.624.760
- Vashum, K. T., & Jayakumar, S. (2012). Methods to Estimate Above-Ground Biomass and Carbon Stock in Natural Forests - A Review. *Journal of Ecosystem and Ecography*, 2(4), 116. [https://www.researchgate.net/profile/S\\_Jayakumar/publication/285880298\\_Methods\\_to\\_estimate\\_above-ground\\_biomass\\_and\\_carbon\\_stock\\_in\\_natural\\_forests\\_A\\_review/links/56b99d6c08ae9d9ac67e0b25.pdf](https://www.researchgate.net/profile/S_Jayakumar/publication/285880298_Methods_to_estimate_above-ground_biomass_and_carbon_stock_in_natural_forests_A_review/links/56b99d6c08ae9d9ac67e0b25.pdf)
- Wamunyima, S. (2005). *Estimating Fresh Grass Biomass at Landscape Level Using Hyperspectral Remote Sensing*. Msc.Thesis. University of Twente faculty of Geo-Information Science and Earth Observation. Retrieved from [http://www.itc.nl/library/papers\\_2005/msc/nrm/wamunyima.pdf](http://www.itc.nl/library/papers_2005/msc/nrm/wamunyima.pdf)
- Wang, C., Feng, M., Yang, W., Ding, G., Sun, H., Xie, Y., & Qiao, X. (2016). Impact of spectral saturation on leaf area index and aboveground biomass estimation of winter wheat. *Spectroscopy Letters*, 49(4), 241–248. doi.org/10.1080/00387010.2015.1133652
- Weiß, J. (2009). Application and statistical analysis of terrestrial laser scanning and forest growth simulations to determine selected characteristics of Douglas-Fir stands. *Folia Forestalia Polonica, Series A*, 51(2), 123–137. Retrieved from <https://zenodo.org/record/30883/files/weiss9-2-1.pdf>
- Wiegand, C. L., Richardson, A. J., Escobar, D. E., & Gerbermann, A. H. (1991). Vegetation indices in

- crop assessment. *Remote Sensing of Environment*, 35(2-3), 105–119. Retrieved from <http://www.sciencedirect.com/science/article/pii/S003442579190004P>
- Winmore, G. T. (2012). *Modelling spatial variations in wood volume and forest carbon stocks in dry forests of Southern Africa using remotely sensed data*. Msc.Thesis. University of Zimbabwe.
- Wulder, M. A., White, J. C., Nelson, R. F., Næsset, E., Ørka, H. O., Coops, N. C., ... Gobakken, T. (2012). Lidar sampling for large-area forest characterization: A review. *Remote Sensing of Environment*, 121, 196–209. doi.org/10.1016/j.rse.2012.02.001
- Zhang, X., Friedl, M. A., Schaaf, C. B., Strahler, A. H., Hodges, J. C. F., Gao, F., ... Huete, A. (2003). Monitoring vegetation phenology using MODIS. *Remote Sensing of Environment*, 84(3), 471–475. doi.org/10.1016/S0034-4257(02)00135-9
- Zhang, X., & Ni-meister, W. (2014). *Biophysical Applications of Satellite Remote Sensing*. (Jonathan M. Hanes, Ed.) *Springer Remote Sensing/Photogrammetry*. New York Dordrecht London Library: Springer Heidelberg. Retrieved from <http://link.springer.com/book/10.1007/978-3-642-25047-7>
- Zhao, D., Huang, L., Li, J., & Qi, J. (2007). A comparative analysis of broadband and narrowband derived vegetation indices in predicting LAI and CCD of a cotton canopy. *ISPRS Journal of Photogrammetry and Remote Sensing*, 62(1), 25–33. doi.org/10.1016/j.isprsjprs.2007.01.003
- Zhao, P., Lu, D., Wang, G., Wu, C., Huang, Y., & Yu, S. (2016). Examining Spectral Reflectance Saturation in Landsat Imagery and Corresponding Solutions to Improve Forest Aboveground Biomass Estimation. *Remote Sensing*, 8(6), 469. doi.org/10.3390/rs8060469

## APPENDICES

Appendix 1: Regression statistics summary; RE-EVI and upper canopy biomass

### RE-EVI2

Regression Statistics	
Multiple R	0.787377503
R Square	0.619963333
Adjusted R Square	0.616508454
Standard Error	0.735918464
Observations	112

ANOVA					
	df	SS	MS	F	Significance F
Regression	1	97.1835115	97.1835115	179.4457547	7.45E-25
Residual	110	59.57335844	0.541575986		
Total	111	156.7568699			

	Coefficients	Std.Error	t Stat	P-value
Intercept	2.383017026	0.290419879	-8.205419809	4.77E-13
X Variable 1	22.42757085	1.674232018	13.39573644	7.44955E-25

Appendix 2: Regression statistics summary; RERVI and upper canopy biomass

### RERVI

Regression Statistics	
Multiple R	0.794001307
R Square	0.630438076
Adjusted R Square	0.627078422
Standard Error	0.725705741
Observations	112

ANOVA					
	df	SS	MS	F	Significance F
Regression	1	98.82549943	98.82549943	187.6497111	1.59E-25
Residual	110	57.93137051	0.526648823		
Total	111	156.7568699			

	Coefficients	Std.Error	t Stat	P-value
Intercept	-16.63547009	1.317961095	-12.62212531	4.01E-23
X Variable 1	14.46081977	1.055647597	13.69852952	1.5885E-25

Appendix 3: Regression statistics summary; RENDVI and upper canopy biomass.

### RENDVI

<i>Regression Statistics</i>	
Multiple R	0.769914064
R Square	0.592767666
Adjusted R Square	0.589065554
Standard Error	0.731465178
Observations	112

ANOVA					
	<i>df</i>	<i>SS</i>	<i>MS</i>	<i>F</i>	<i>Significance F</i>
Regression	1	85.66871432	85.66871432	160.1160756	3.40811E-23
Residual	110	58.85454372	0.535041307		
Total	111	144.523258			

	<i>Coefficients</i>	<i>Std.Error</i>	<i>t Stat</i>	<i>P-value</i>
Intercept	-2.126523351	0.294846422	-7.212308493	7.41002E-11
X Variable 1	32.85871551	2.596767779	12.6536981	3.40811E-23

Appendix 4: Regression statistics summary; RE-EVI2 and total biomass.

### RE-EVI2

<i>Regression Statistics</i>	
Multiple R	0.792653083
R Square	0.62829891
Adjusted R Square	0.624919809
Standard Error	0.722113177
Observations	112

ANOVA					
	<i>df</i>	<i>SS</i>	<i>MS</i>	<i>F</i>	<i>Significance F</i>
Regression	1	96.95622469	96.95622469	185.9367162	2.18559E-25
Residual	110	57.35921841	0.52144744		
Total	111	154.3154431			

	<i>Coefficients</i>	<i>Std.Error</i>	<i>t Stat</i>	<i>P-value</i>
Intercept	-2.283428813	0.284971816	-8.01282332	1.28472E-12
X Variable 1	22.40132939	1.642824661	13.6358614	2.18559E-25

Appendix 5: Regression statistics summary; RERVI and total biomass.

**RERVI**

Regression Statistics	
Multiple R	0.799143698
R Square	0.638630649
Adjusted R Square	0.635345473
Standard Error	0.712006585
Observations	112

ANOVA					
	df	SS	MS	F	Significance F
Regression	1	98.55057164	98.55057164	194.3977023	4.6003E-26
Residual	110	55.76487146	0.506953377		
Total	111	154.3154431			

	Coefficients	Std.Error	t Stat	P-value
Intercept	-16.51520512	1.293081927	-12.7719712	1.84702E-23
X Variable 1	14.44069111	1.035720124	13.94265765	4.6003E-26

Appendix 6: Regression statistics summary; RENDVI and total biomass

**RENDVI**

Regression Statistics	
Multiple R	0.770427243
R Square	0.593558136
Adjusted R Square	0.58986321
Standard Error	0.727429997
Observations	112

ANOVA					
	df	SS	MS	F	Significance F
Regression	1	85.00411	85.00411	160.6414123	3.06071E-23
Residual	110	58.20698	0.529154		
Total	111	143.2111			

	Coefficients	Std.Error	t Stat	P-value
Intercept	-2.31867696	0.29898	-7.75529	4.79577E-12
X Variable 1	34.04031657	2.685745	12.67444	3.06071E-23

Appendix 7: Regression statistics summary; NDWI and upper canopy biomass

**NDWI**

<i>Regression Statistics</i>	
Multiple R	0.557978368
R Square	0.31133986
Adjusted R Square	0.305079313
Standard Error	0.959159407
Observations	112

ANOVA

	<i>df</i>	<i>SS</i>	<i>MS</i>	<i>F</i>	<i>Significance F</i>
Regression	1	45.75136	45.75136381	49.73046	1.64329E-10
Residual	110	101.1985	0.919986767		
Total	111	146.9499			

	<i>Coefficients</i>	<i>Std.Error</i>	<i>t Stat</i>	<i>P-value</i>
Intercept	-3.363037256	0.680147	-4.944575613	2.76E-06
X Variable 1	17.51114235	2.483152	7.051982598	1.64E-10

Appendix 8: Regression statistics summary; NDII and upper canopy biomass

**NDII**

<i>Regression Statistics</i>	
Multiple R	0.475009154
R Square	0.225633697
Adjusted R Square	0.218594003
Standard Error	1.019234928
Observations	112

ANOVA

	<i>df</i>	<i>SS</i>	<i>MS</i>	<i>F</i>	<i>Significance F</i>
Regression	1	33.29651602	33.29651602	32.05163567	1.2111E-07
Residual	110	114.2723822	1.038839839		
Total	111	147.5688983			

	<i>Coefficients</i>	<i>Std.Error</i>	<i>t Stat</i>	<i>P-value</i>
Intercept	-9.238245967	1.879582541	-4.91505202	3.11961E-06
X Variable 1	17.6159163	3.11157404	5.661416401	1.2111E-07

Integrating Sentinel-2 derived Vegetation Indices and Terrestrial Laser Scanner to estimate Above-ground biomass/Carbon in Ayer Hitam tropical forest

Appendix 9: Regression statistics summary; NDWI and total biomass

NDWI

<i>Regression Statistics</i>	
Multiple R	0.559498946
R Square	0.313039071
Adjusted R Square	0.306793972
Standard Error	0.947089032
Observations	112

ANOVA					
	<i>df</i>	<i>SS</i>	<i>MS</i>	<i>F</i>	<i>Significance F</i>
Regression	1	44.96150172	44.96150172	50.12555494	1.43082E-10
Residual	110	98.66753985	0.896977635		
Total	111	143.6290416			

	<i>Coefficients</i>	<i>Std.Error</i>	<i>t Stat</i>	<i>P-value</i>
Intercept	-3.217316055	0.671587606	-4.790612609	5.23004E-06
X Variable 1	17.35932605	2.451902878	7.079940321	1.43082E-10

Appendix 10: Regression statistics summary; NDII and total biomass

NDII

<i>Regression Statistics</i>	
Multiple R	0.477235797
R Square	0.227754006
Adjusted R Square	0.220733588
Standard Error	1.004490126
Observations	112

ANOVA					
	<i>df</i>	<i>SS</i>	<i>MS</i>	<i>F</i>	<i>Significance F</i>
Regression	1	32.73364668	32.73364668	32.44165833	1.03704E-07
Residual	110	110.9900455	1.009000414		
Total	111	143.7236922			

	<i>Coefficients</i>	<i>Std.Error</i>	<i>t Stat</i>	<i>P-value</i>
Intercept	-9.03931547	1.852391487	4.879808362	3.61404E-06
X Variable 1	17.46638532	3.066560333	5.695757924	1.03704E-07

Appendix 11: Regression statistics summary, EVI2 and upper canopy biomass

**EVI2**

<i>Regression Statistics</i>	
Multiple R	0.381033686
R Square	0.14518667
Adjusted R Square	0.137415639
Standard Error	1.118822102
Observations	112

ANOVA					
	<i>df</i>	<i>SS</i>	<i>MS</i>	<i>F</i>	<i>Significance F</i>
Regression	1	23.38677	23.3867685	18.68306576	3.40229E-05
Residual	110	137.6939	1.251762896		
Total	111	161.0807			

	<i>Coefficients</i>	<i>Std.Error</i>	<i>t Stat</i>	<i>P-value</i>
Intercept	-5.075207312	1.50311	-3.376471845	0.001015617
X Variable 1	5.199850348	1.203003	4.322391208	3.40229E-05

Appendix 12: Regression statistics summary, NDVI and upper canopy biomass

**NDVI**

<i>Regression Statistics</i>	
Multiple R	0.319412839
R Square	0.102024562
Adjusted R Square	0.093861148
Standard Error	1.1049199
Observations	112

ANOVA					
	<i>df</i>	<i>SS</i>	<i>MS</i>	<i>F</i>	<i>Significance F</i>
Regression	1	15.25789265	15.25789265	12.49778255	0.000597362
Residual	110	134.2932784	1.220847985		
Total	111	149.551171			

	<i>Coefficients</i>	<i>Std.Error</i>	<i>t Stat</i>	<i>P-value</i>
Intercept	-5.537784359	1.96406851	-2.81954745	0.005705313
X Variable 1	11.06681431	3.130445455	3.535220297	0.000597362

Integrating Sentinel-2 derived Vegetation Indices and Terrestrial Laser Scanner to estimate Above-ground biomass/Carbon in Ayer Hitam tropical forest

---

Appendix 13: Regression statistics summary, EVI2 total biomass

EVI2

<i>Regression Statistics</i>	
Multiple R	0.38315
R Square	0.146804
Adjusted R Square	0.139048
Standard Error	1.101787
Observations	112

ANOVA					
	<i>df</i>	<i>SS</i>	<i>MS</i>	<i>F</i>	<i>Significance F</i>
Regression	1	22.97615	22.97615	18.92701	3.05E-05
Residual	110	133.5328	1.213934		
Total	111	156.5089			

	<i>Coefficients</i>	<i>Std. Error</i>	<i>t Stat</i>	<i>P-value</i>
Intercept	-4.90472	1.480175	-3.31361	0.001247
X Variable 1	5.15384	1.18465	4.350518	3.05E-05

Appendix 14: Regression statistics summary, NDVI and total biomass

NDVI

<i>Regression Statistics</i>	
Multiple R	0.321431
R Square	0.103318
Adjusted R Square	0.095167
Standard Error	1.093789
Observations	112

ANOVA					
	<i>df</i>	<i>SS</i>	<i>MS</i>	<i>F</i>	<i>Significance F</i>
Regression	1	15.16345	15.16345	12.67451	0.000549
Residual	110	131.6011	1.196374		
Total	111	146.7646			

	<i>Coefficients</i>	<i>Std. Error</i>	<i>t Stat</i>	<i>P-value</i>
Intercept	-5.39028	1.937026	-2.78276	0.006345
X Variable 1	10.98916	3.086731	3.560128	0.000549

Appendix 15: Downloading site of Sentinel-2 satellite image

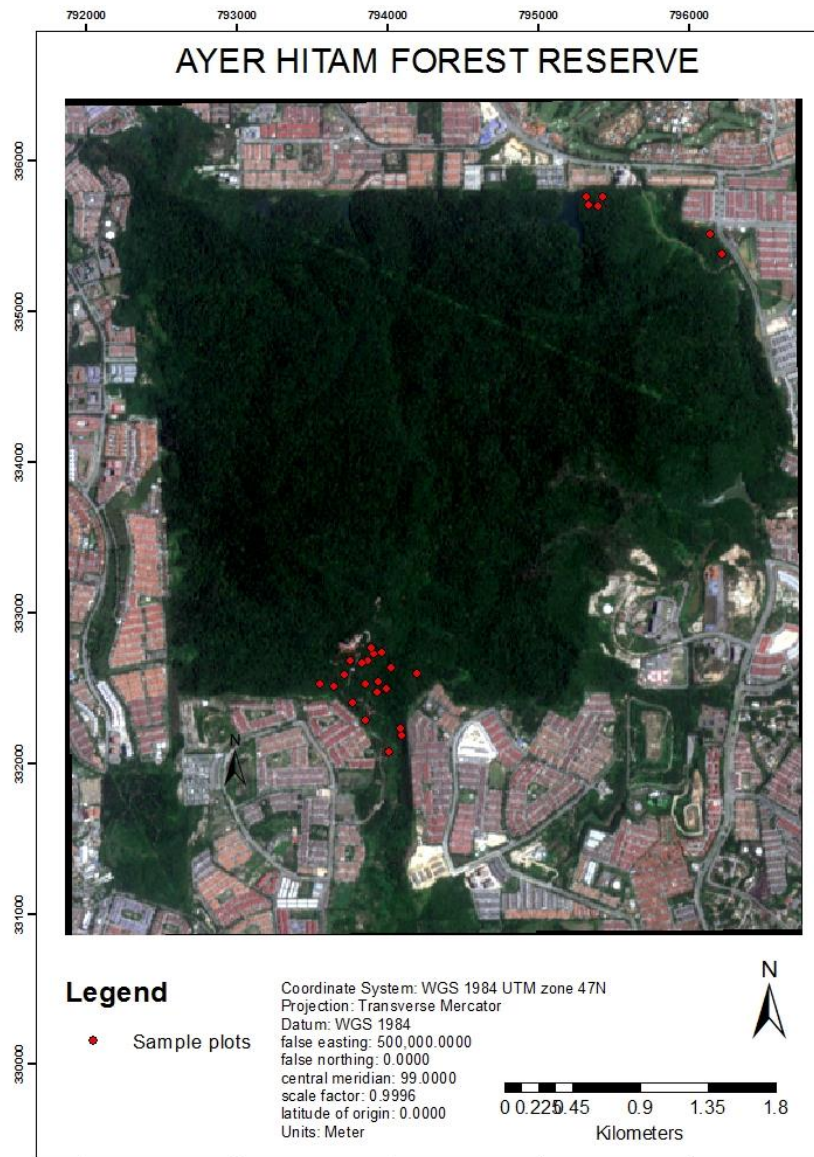
The screenshot displays the Sentinel Scientific Data Hub interface. At the top, the ESA and Copernicus logos are visible, along with the text "Sentinels Scientific Data Hub". The main content area is titled "S2A\_MSIL1C\_20170203T032931\_N0204\_R018\_T47NQD\_20170203T034408" and includes the URL: [https://scihub.copernicus.eu/dhus/odata/v1/Products\('172a3001-e70c-4601-adba-8a9e3c5e6c1e'\)/\\$value](https://scihub.copernicus.eu/dhus/odata/v1/Products('172a3001-e70c-4601-adba-8a9e3c5e6c1e')/$value).

The interface is divided into several sections:

- Footprint:** A map showing the satellite's footprint over a region in Southeast Asia, including cities like Kuala Lumpur, Singapore, and Jakarta.
- Quicklook:** A thumbnail image of the satellite data.
- Attributes:** A section containing a **Summary** with the following details:
  - Date:** 2017-02-03T03:29:31.026Z
  - Filename:** S2A\_MSIL1C\_20170203T032931\_N0204\_R018\_T47NQD\_20170203T034408.SAFE
  - Identifier:** S2A\_MSIL1C\_20170203T032931\_N0204\_R018\_T47NQD\_20170203T034408
  - Instrument:** MSI
- Inspector:** A list of files included in the SAFE package:
  - AUX\_DATA
  - DATASTRIP
  - GRANULE
  - HTML

The interface also features a search bar, a list of products on the left, and navigation controls at the bottom.

Appendix 16: Sample plots analysed in the study area



Appendix 17: Airborne Lidar DTM and the drainage pattern

